Order Number 9329153

Interactions and orientation in concentrated suspensions of rigid rods: Theory and experiment

Sandstrom, Chad Richard, Ph.D.

University of Illinois at Urbana-Champaign, 1993

U·M·I
300 N. Zeeb Rd.
Ann Arbor, MI 48106

INTERACTIONS AND ORIENTATION IN CONCENTRATED SUSPENSIONS OF RIGID RODS: THEORY AND EXPERIMENT

BY

CHAD RICHARD SANDSTROM

B.S., University of Illinois, 1988
M.S., University of Illinois, 1990

THESIS

Submitted in partial fulfillment of the requirements
for the degree of Doctor of Philosophy in Mechanical Engineering
in the Graduate College of the
University of Illinois at Urbana-Champaign, 1993

Urbana, Illinois

UNIVERSITY OF ILLINOIS AT URBANA-CHAMPAIGN

THE GRADUATE COLLEGE

May 1993

WE HEREBY RECOMMEND THAT THE THESIS BY

Chad Richard Sandstrom

ENTITLED Interactions and Orientation in Concentrated Suspensions of Rigid Rods: Theory and Experiment

BE ACCEPTED IN PARTIAL FULFILLMENT OF THE REQUIREMENTS FOR THE DEGREE OF Doctor of Philosophy

Charles L. Tucker III
Director of Thesis Research

A. L. Addy
Head of Department

Committee on Final Examination†

Charles L. Tucker III
Chairperson

Christopher J. Lawrence

John A. Walker

Barclay G. Jones

† Required for doctor's degree but not for master's.

O-517

INTERACTIONS AND ORIENTATION IN CONCENTRATED SUSPENSIONS OF RIGID RODS: THEORY AND EXPERIMENT

CHAD RICHARD SANDSTROM

Department of Mechanical and Industrial Engineering

University of Illinois at Urbana-Champaign, 1992

Charles L. Tucker III, Thesis Advisor

ABSTRACT

A theory for the processing-induced fiber orientation and stress in fiber reinforced-polymer composites is presented. Short-fiber-reinforced polymer composites are represented by concentrated suspensions of rigid rods. In concentrated suspensions, fiber-fiber contact is likely and affects the fiber orientation state and suspension rheology. Fiber orientation is given as a function of the strain in the continuum and the probable effects of physical inter-fiber contact. Continuum stress is calculated from the stress in the fluid and fibers, where fiber stress is a result of the local disturbance in the fluid velocity field and of the inter-fiber contact forces. Fiber orientation is described via probability density function whose transport equation has the form of a generalized advection-diffusion equation with a orientation dependent diffusion. This equation is solved using a finite difference scheme and the results are presented versus experiments with suspensions with planar orientation in planar stretching flow. Experiments and simulation agree that increasing concentrations result in increased interaction-based diffusion.

to my family.

ACKNOWLEDGMENTS

Thanks go first and foremost to my friend and advisor Dr. Charles L. Tucker III, and to his wife Laurie Tucker. For guidance, for wisdom, for good conversation and wonderful dinners I will always remember them fondly. Without the support and cajoling and love of my wife Julia, I certainly would never have made it through, thanks will be lavished daily upon her. My friend Alex Arzoumanidis played a key role in the design and execution of the experiments.

This research was funded by GenCorp Research Division, by Shell Development Co., and by Norsolor. The author was supported in part by the Department of Mechanical and Industrial Engineering of the University of Illinois through a Graduate Teaching Fellowship.

I am indebted also to the members of my dissertation committee for their input and the members of the Polymer Processing Laboratory for their comraderie. The staff of the Department of Mechanical and Industrial Engineering were invaluable throughout the course of this research.

TABLE OF CONTENTS

LIST OF TABLES

LIST OF FIGURES

1. INTRODUCTION

1.1 Polymer Composites and Concentrated Suspensions

Composite materials created by adding short reinforcing fibers to a polymeric matrix have been one of the most important new classes of materials of the last twenty years. These materials are important because short fiber reinforcement adds stiffness and strength to a material that can still be easily processed. Processing of short-fiber-reinforced composites is generally defined by the matrix material. Polymers in an unfilled state can be formed through fluid deformation and solidified in the desired shape. Compression molding, extrusion, and injection molding are some of the processes often used, and the fibers travel with the matrix material. The fiber reinforcement is also subject to designer choice; spun glass, carbon fibers, drawn polymers or vegetable fibers are all in service. The addition of *short* fibers that can flow with the matrix creates a composite material with superior properties that can retain many of the processing characteristics of the unfilled matrix.

The mechanical properties of composites reinforced by short fibers depend on the amount of reinforcing fibers and the orientation of the fibers. Fibers may add stiffness or strength to a compliant thermoplastic, or toughness to a brittle thermoset. The reinforcing qualities of a fiber are anisotropic; the strong, stiff fiber contributes more to mechanical properties (particularly strength and stiffness) in the axial direction than in the transverse directions. The orientation state of the finished composite is of crucial importance to the designer who expects optimum performance from a short-fiber reinforced polymer composite.

The orientation state of a short fiber composite is determined by the rheology of the composite melt, the orientation of the fibers before processing and the kinematics of mold flow. The fibers in the melt can travel and strain with the matrix. This process-induced strain changes the spatial and orientation distributions of the

fibers in the material. Several useful theories exist for the orientation behavior of solid particles in dilute suspensions undergoing deformation. Other researchers have attempted to extend these theories to high concentration domains while ignoring the effects of particle interaction.

In practice, fiber volume concentrations in short fiber reinforced composites exist in the range of 10-50%. This figure lies well above the dilute range for fibers with of aspect ratios 10^2-10^5. Therefore, physical fiber-fiber contact in these composite melts is likely. These contacts introduce inter-fiber interaction forces that affect the rheology and orientation behavior in the composite during flow.

1.2 Goal of Research

Short fiber reinforced composites in the processing stage can be modeled as concentrated suspensions of fibers. We seek to develop a model for the flow of such suspensions. This model will capture the essential physics of particle-particle interaction inherent in a concentrated suspension. We will examine the orientation behavior of the model in simple flows and compare its results against experimental results and numerical simulation. The result of this work will yield transport equations for suspension momentum, fiber dispersion and fiber orientation.

1.3 Organization of Thesis

The following chapter reviews the research pertinent to this study. Here we discuss general background of composites design emphasizing the need for an understanding of the orientation phenomena in the composite material. General results for suspension rheology and hydrodynamics are given in the latter part of Chapter Two. These results are the key to the fiber orientation during processing.

Chapter Three details the new analytical theory of a concentrated suspension of rigid rods. "Concentrated" implies that the fibers experience several contacts from neighboring fibers. These contacts introduce a mechanical fiber-fiber

interaction force that affects the orientation development and the rheology of the suspension. Inclusion of this effect is the cornerstone of this work. A numerical solution to the theory is implemented in Chapter Four. Results of a finite-difference solution are also presented.

Chapter Five examines orientation and fiber-fiber contact in concentrated suspensions undergoing planar stretching flow through a set of experiments..

Chapter Six shows a comparison of the experimental results with the numerical solution of Chapter Four. It also demonstrates a simplification of the theory of Chapter Three into an easily implemented diffusion function. Herein is a discussion of the theory in comparison to the existing stochastic and diffusive models of fiber orientation.

The final chapter summarizes the work, briefly recaps the discussions of Chapters Six and Seven and offers recommendations future research.

2. COMPOSITE MATERIALS AND SUSPENSION RHEOLOGY

Composite materials made of polymer reinforced with short stiff fibers have significant importance and growing potential as engineering materials. Yet processing these materials and controlling the reinforcement microstructure remains a complicated enterprise. Short fiber composites have been studied for several years and processing research has been linked to particle suspension rheology. This chapter reviews the research in these fields with an emphasis on the importance of the fiber orientation.

2.1 Short-Fiber Reinforced Polymer Composites

While composite materials posess great potential, the inherent inhomogeneity of the polymer/fiber combination requires more careful treatment than common materials. This section shows why the promise of short-fiber reinforced polymer composites presents a complicated challenge.

2.1.1 Fiber Orientation Defines Mechanical Properties

The mechanical properties of these materials are enhanced by the existence of short reinforcing fibers. Typically the fibers are spun from glass, but carbon fibers are also often used. In more exotic applications one may find boron or ceramic fibers. The diameter of the reinforcement is usually on the order of ten micrometers and the length may range from a fraction of a millimeter to two centimeters. Therefore, length-to-diameter ratios are typically large, 10-1000. The reinforcing qualities of the fiber parallel the geometric dimensions; they are a far more effective reinforcement in the axial direction than in the transverse direction. Furthermore, heat conduction will occur at different rates along the fiber length as opposed to across the fibers. Toughness is augmented by fibers that arrest cracks propagating in the transverse direction. Therefore, the orientation of each fiber is a critical quantity for many of the composite's mechanical and thermal properties.

Experimental evidence of the relationship between fiber orientation and mechanical properties can be found in the published research. Darlington, McGinley and Smith [1] tested discs of glass reinforced polypropylene from an edge-gated injection mold. They found that regions of higher fiber alignment corresponded to increases in tensile strength and modulus. Other researchers [2,3,4,5] show many similar qualitative results for different matrix materials, fiber materials and geometries, and molding processes. Schwarz, Fischer, and Eyerer [6] have attempted to correlate measured mechanical properties against measured fiber orientation. In the following paragraphs, theoretical work relating fiber orientation and fiber volume fraction is reviewed. Theoretical studies are more abundant and more precise than the existing experimental work, and yet both indicate that materials of high fiber orientation will show high strength and stiffness in the fiber direction, and markedly lower values in the transverse directions.

Overall mechanical behavior of the composite is dependent upon the aggregate orientation of all the fibers. There are several theories for calculation of composite material properties. All approach the problem in two steps. First, one calculates the properties for a completely aligned composite. This requires a knowledge of the volume fraction and the aspect ratios of the reinforcement. Second, the properties of the aligned composite are used to create a weighted average for all possible orientation directions. This step requires a knowledge of the orientation state of the finished composite.

Hill [7] was among the first to calculate the properties of the aligned composite. He considered a cylinder of material comprised of continuous, perfectly-aligned fibers embedded in another homogeneous material. The fibers were regularly spaced throughout the composite. The matrix was isotropic, the fibers were transversely isotropic, and consequently the resulting composite was transversely isotropic. That is, mechanical properties were uniform in all directions

$$P_c = P_m \frac{1 + \xi x c}{1 - x c}$$

$$x = \frac{P_f - P_m}{P_f + \xi P_m}$$

P_c	ξ
E_{11}	$2r_e$
$E_{22} = E_{33}$	2
$G_{12} = G_{23}$	1

Table 2.1 The Halpin-Tsai Equations for the moduli of a fibrous composite material.

in the plane perpendicular to the fiber direction. The fibers and matrix then were assumed to strain equally and the Hooke's law was written for the composite.

The Halpin-Tsai equations [8] are a refinement of Hill's method. They allow the composite designer a simple means of estimating the mechanical properties of an aligned composite from the properties of the matrix and fibers, the fiber aspect ratio and volume fraction. Table 2.1 recaps the Halpin-Tsai equations for stiffness. P_c represents a composite property, and P_m and P_f indicate the corresponding properties of the matrix and fiber, respectively. r_e is the aspect ratio of the fibers $\frac{L}{d}$, and c is the volume fraction of the fibers. Inspection of these equations show that the fiber direction modulus E_{11} is dominated by the properties of the fibers, while the transverse directions are dominated by the properties of the matrix.

Once the contribution of the aligned fibers is understood, the next step entails determination of the effects of a distribution of fiber orientation in the composite. Much of the original research in this area involved the "laminate analogy." The composite material was idealized as many layers of uniformly oriented fibers. Classical laminated plate theory would then be used to predict the properties of the idealized composite. The thickness and orientation of the each layer would be manipulated until the orientation state of the laminate matched that of the composite material. Halpin and Pagano [9] showed that the moduli of a composite with

random in-plane oriented short fiber reinforcement could be well predicted by a quasi-isotropic laminate of equal fiber volume fraction and fiber aspect ratio.

More recently, the effect of fiber orientation distribution in composite materials has been accounted for by the use of orientation averaging techniques [10,11]. The method requires knowing the functional dependence of the mechanical property of interest upon the orientation. In this case the orientation must be a variable that can be quantitatively expressed. Next, the function is integrated over all possible values of the orientation and the integrand weighted by the fraction of fibers at that particular value of the orientation. Therefore, if the property of the composite is some function of a unit vector p indicating fiber orientation i.e. $P_c(\mathbf{p})$, then for some distribution of orientation the composite property is found through an orientation average.

$$\langle P_c \rangle = \oint \psi(\mathbf{p})\, P_c(\mathbf{p})\, d\mathbf{p} \tag{2.1}$$

$\psi(\mathbf{p})$ in Eq. 2.1 is the orientation distribution function; it gives information about the fraction of fibers at every possible value of p. The angle brackets about P_c indicate that it is an ensemble average of the contributions from all possible fiber orientations, and it is no longer a function of a specific p, but a macroscopic average property of the composite. This method has been used successfully to predict composite elastic moduli, bending stiffness, thermal expansion, and thermal and electrical conductivity.

This section has briefly shown that the mechanical properties of the short fiber reinforced materials are strongly influenced by the orientation of the reinforcing fibers. Furthermore, through the use of classical continuum mechanics principles, those mechanical properties can be predicted given a knowledge of the

matrix properties, the fiber properties and volume fraction present, *and* the orientation state of the reinforcement.

2.1.2 *Processing Induces Fiber Orientation*

The previous section has shown that the fiber orientation state is a critical consideration for sound design decisions. In a short fiber reinforced composite, the advantage of easy processing is accompanied by the disadvantage of a mutable orientation. The fibers in the composite melt travel and rotate with the liquid matrix. This process-induced motion changes the spatial and orientational distributions of the fibers in the material.

The trends and details of fiber motion during processing have been investigated by many researchers. One of the most basic observations is that converging flows aligned fibers in the flow direction, while diverging flows align the fibers perpendicular to the streamlines [12,13,14]. The alignment grows with the intensity of the flow field, the duration of the flow, and the aspect ratio of the particles. Converging and diverging flows are stretching flows and the fibers align themselves in the direction of positive strain. Shearing flow also orients fibers; in this case the fibers are rotated into the plane of shear leaving most fibers axes pointed along the streamlines. It has been observed though that the orienting strength of a shear flow was not as strong as that of a stretching flow [13]

Many researchers have observed a layered microstructure of fibers in injection molded engineering composites [14,15,16,17]. depending on the processing conditions and the researchers interpretation, these composites have been proclaimed to contain from three to seven layers. Consistently mentioned is a 'core' region whose fibers are oriented nearly random in-plane. In the case of a radial flow spreading from the gate or from a constriction in the part, the fibers in the core will be oriented perpendicular to the streamlines by the stretching flow in this region.

Also typically observed are two 'shell' layers found above and below the core wherein the fibers lie in the streamline direction. The fibers in the shell have been oriented by the stronger shear flow near the wall. Other observed layers include core-shell transition layers and a 'skin' layer at the surface of the part. The skin layer is made up of polymer and fibers that have traveled through and been oriented by the fountain flow at the flow front and then quickly frozen at the mold wall [16,18].

The presence of this complicated structure is due to the changing combinations of stretching and shearing flows found in even the simplest of molds. The thickness of each layer is strongly dependent on such processing parameters as the Graetz number, the Brinkman number and the Pearson number, which compare injection time scales, heat transfer, and temperature scales respectively. Layer thicknesses are also dependent upon the rheology of the suspension which in turn is generally a function of the fiber orientation.

From the discussion in this subsection it is apparent that fiber orientations or thicknesses of layers in injection moldings are critically linked to the processing conditions of the composite, and cannot be known *a priori*. Tucker [19] discusses several regimes which delineate the degree of coupling of fiber orientation to flow kinematics. Rarely can one confidently completely neglect the fiber contribution to the flow. Rather, flow, extra stress, and fiber orientation typically are closely coupled.

2.1.3 *Composite Rheology*

The presence of solid reinforcing fibers in the composite creates a material that is difficult to characterize rheologically. During processing, the fibers and polymer will flow together. Fibers reorient in response to the rotational component of the strain, while at the same time the fibers resist the fluid straining along their

axes. The fiber-polymer suspension therefore shows rheological behaviors that are not typically seen in homogeneous fluids.

The fibers affect fluid properties in the same fashion as they affect mechanical properties such as stiffness and strength. That is, the fibers increase the viscosity in the flowing composite because they resist stretching along their axes. When fibers lie down along the streamlines of a shear flow, their contribution to the viscosity is lessened. Dinh [20] showed this in experiments with randomly dispersed fibers that resulted in high shear viscosity in comparison to that of suspensions with fibers oriented only in the planes of shear.

In series of experiments, Barone and Caulk [21] studied compression mold flow of fiber reinforced thermosets. They found that the composite material traveled in plug flow as it spread through the mold, the gapwise velocity gradients being nearly zero. They reasoned that the material was slipping at the mold surface or that the shearing was confined to a very small region near the mold wall. In either event, the mold fills in biaxial elongation which yields very different flow front shapes when compared to that of typical Hele-Shaw or shear-dominated flow. Flow front progression is a critical aspect of controlled polymer processing, and the rheological contribution of the fiber reinforcement cannot be neglected.

The combination of orientation-dependent viscosity with the knowledge that fibers reorient within the processing flow indicates that polymer composites are complicated materials that require careful process modeling. The rheology of short fiber reinforced composites has been linked to the rheology of suspensions, and that body of research is surveyed in Section 2.4.

2.2 Description of Orientation in Fibrous Composites

The previous section asserts that fiber orientation is a critical factor in the rheological and mechanical properties of the short-fiber reinforced composite. Also

apparent is a lack in quantitative relations between orientation and rheology. Quantitative relations for rheology or mechanical calculations require precise and economical representation of the orientation state of the composite. This section discusses several methods for characterizing fiber orientation.

2.2.1 *Orientation of a Single Fiber*

Consider first a *single* fiber immersed in the composite. The orientation of that fiber is described by the unit vector p pointing along the axis of the fiber. Alternately, the orientation of the fiber can be described by a pair of Eulerian angles θ and ϕ. Figure 2.1 shows the fiber with its orientation in terms of the unit vector and the Eulerian angles. The components of p are related to ϕ and θ.

$$p_1 = \cos\phi \sin\theta \tag{2.2a}$$

$$p_2 = \sin\phi \sin\theta \tag{2.2b}$$

$$p_3 = \cos\theta \tag{2.2c}$$

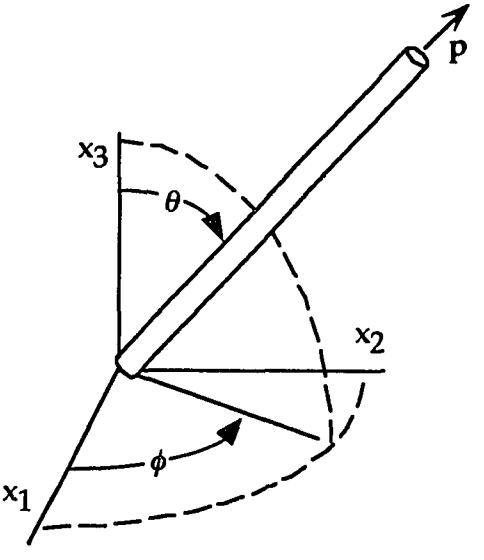

Figure 2.1 A single reinforcing fiber with an orientation specified both by the unit vector p and by the Eulerian angles θ and ϕ.

Furthermore, since p is a unit vector,

$$\mathbf{p}\cdot\mathbf{p} = 1 \tag{2.3}$$

In generalized terms, the orientation of fibers in the composite is a random variable. The integral over all possible orientations of the fiber describes a unit sphere.

$$\oint_{\mathbf{p}} d\mathbf{p} = \int_0^{\pi}\int_0^{2\pi} \sin\theta\, d\theta d\phi = 4\pi \tag{2.4}$$

In the composite, the orientation of a single fiber on the unit sphere is actually of no practical value. Hundreds of thousands of fibers will typically be found in a short-fiber reinforced composite. Keeping track of all individual orientations would require far too many degrees of freedom for any modern computer. Therefore, a simpler description of fiber orientation state, one that conveys the statistical nature the orientation of a fiber, is given in the next sub-section.

2.2.2 *Probability Distribution Function*

The orientation of a single fiber can be expressed only as a probability of existence somewhere on the unit sphere. We use a *probability distribution function* $\psi(\mathbf{p})$ to describe the likelihood that a fiber can be found near some particular orientation (say $\mathbf{p}_1$ or θ_1 & ϕ_1). This probability P can be expressed in terms of the probability distribution function (PDF) and a small orientation range ($d\mathbf{p}$ or $\sin\theta\, d\theta d\phi$) as

$$P(\mathbf{p}_1 \le \mathbf{p} \le \mathbf{p}_1 + \mathbf{dp}) = \psi(\mathbf{p}_1)\,\mathbf{dp} \tag{2.5a}$$

and alternately as

$$P(\theta_1 \le \theta \le \theta_1 + d\theta,\ \phi_1 \le \phi \le \phi_1 + d\phi) = \psi(\theta,\phi)\sin\theta_1\, d\theta d\phi \tag{2.6b}$$

This is equivalent to saying that the PDF describes the fraction of the fibers in the composite near a particular orientation.

There are a number of stipulations associated with the PDF. First, since the ends of a fiber are indiscernible,

$$\psi(\mathbf{p}) = \psi(-\mathbf{p}) \tag{2.7}$$

$$\psi(\theta,\phi) = \psi(\pi - \theta,-\phi) \tag{2.8}$$

Furthermore, the orientation of any fiber is certain to lie *somewhere* within the unit sphere. Therefore, the integral of the PDF over the entire domain is equal to unity.

$$1 = \oint_{\mathbf{p}} \psi(\mathbf{p})\,\mathbf{dp} = \int_0^{\pi}\int_0^{2\pi} \psi(\theta,\phi)\sin\theta\, d\theta d\phi \tag{2.9}$$

This is also considered as a normalization condition [11].

2.2.3 *Orientation Tensors*

A more compact description of the orientation state of a composite (or of a suspension of elongated particles) can be given by a truncated set of moments of the distribution function. Advani and Tucker [11] call these moments the "orientation

tensors." The first moment $\mathbf{a}_1$ of the orientation probability distribution function is the ensemble average of the fibers in the material

$$\mathbf{a}_1 = \oint \mathbf{p}\psi(\mathbf{p})\, d\mathbf{p} = \langle \mathbf{p} \rangle = 0 \tag{2.10}$$

This representation of the first order orientation tensor follows Gibbs notation; it is written in boldface and the order of the tensor is indicated by the numeral in the subscript. The average of the orientation of all the fibers in the composite is the "ensemble average" and is denoted by the angle brackets. Orientation tensors can be calculated at every order and the next three are as follows.

$$\mathbf{a}_2 = \oint \mathbf{pp}\psi(\mathbf{p})\, d\mathbf{p} = \langle \mathbf{pp} \rangle \tag{2.11}$$

$$\mathbf{a}_3 = \oint \mathbf{ppp}\psi(\mathbf{p})\, d\mathbf{p} = 0 \tag{2.12}$$

$$\mathbf{a}_4 = \oint \mathbf{pppp}\psi(\mathbf{p})\, d\mathbf{p} = \langle \mathbf{pppp} \rangle \tag{2.13}$$

Since the PDF is even, only the even order tensors are non-zero, and there are infinitely many. Typically, only the lower order tensors are used (first, second, fourth).

In Cartesian tensor notation[1], the orientation tensors look like,

$$a_{jk} = \oint p_j p_k \psi(\mathbf{p})\, d\mathbf{p} \tag{2.14}$$

---

[1]In Cartesian tensor notation, the number of indices indicate the order of the tensor. Following convention, a repeated index implies summation over all possible values of that index.

$$a_{jklm} = \oint p_j p_k p_l p_m \psi(\mathbf{p})\, d\mathbf{p} \tag{2.15}$$

From their construction, one can see that the orientation tensors are completely symmetric.

$$a_{jk} = a_{kj} \tag{2.16}$$

$$a_{jklm} = a_{jkml} = a_{kjml} = a_{kmjl} = a_{kmlj} = \text{...etc.} \tag{2.17}$$

and that the higher order tensors contain all information about the lower order tensors.

$$a_{jkll} = a_{jk} \tag{2.18}$$

$$a_{jklmnn} = a_{jklm} \tag{2.19}$$

The orientation tensors are functions of the probability distribution function and so it follows that the PDF can be reconstructed from the orientation tensors.

$$\psi(\mathbf{p}) = \frac{1}{4\pi} + \frac{15}{8\pi} b_{jk} f_{jk}(\mathbf{p}) + \frac{315}{32\pi} b_{jklm} f_{jklm}(\mathbf{p}) + \ldots \tag{2.20}$$

In Eq. (2.20) the deviatoric versions of the orientation tensors are used.

$$b_{jk} = a_{jk} - \frac{1}{3}\delta_{jk}$$

$$b_{jklm} = a_{jklm} - \frac{1}{7}(\delta_{jk}a_{lm} + \delta_{jl}a_{km} + \delta_{jm}a_{kl} + \delta_{kl}a_{jm} + \delta_{km}a_{jl} + \delta_{lm}a_{jk})$$

$$+ \frac{1}{35}(\delta_{jk}\delta_{lm} + \delta_{jl}\delta_{km} + \delta_{jm}\delta_{kl}) \qquad (2.21)$$

and the tensors f_{jk} and f_{jklm} etc. are "tensor basis functions" defined as follows by Onat and Leckie [22]

$$f_{jk} = p_j p_k - \frac{1}{3}\delta_{jk}$$

$$f_{jklm} = p_j p_k p_l p_m - \frac{1}{7}(\delta_{jk}p_l p_m + \delta_{jl}p_k p_m + \delta_{jm}p_k p_l + \delta_{kl}p_j p_m$$

$$+ \delta_{km}p_j p_l + \delta_{lm}p_j p_k) + \frac{1}{35}(\delta_{jk}\delta_{lm} + \delta_{jl}\delta_{km} + \delta_{jm}\delta_{kl}) \qquad (2.22)$$

The right-hand-side of Eq. (2.20) is the expansion of the PDF into its spherical harmonics. The use of a finite number of orientation tensors to represent ψ is equivalent to truncating the harmonic series. Some information will be lost in the truncation, but the economy of the orientation tensors is often an acceptable trade-off for the accuracy and large size of the full PDF.

2.2.4 *Conservation of Orientation Probability*

The orientation will change due to motion in the suspension. The orientation in a suspension is a convected quantity which will change as the suspension flows. Thus, we need the material derivative to fully describe changes in the distribution function.

$$\frac{D}{Dt} = \frac{\partial}{\partial t} + \mathbf{v}\cdot\nabla = \frac{\partial}{\partial t} + v_j\frac{\partial}{\partial x_j} \qquad (2.23)$$

In orientation space (a unit sphere), orientation is conserved. Therefore, the equation of conservation of orientation looks similar to that for conservation of mass.

$$\frac{D\psi}{Dt} = -\nabla\cdot(\psi\dot{\mathbf{p}}) \tag{2.24}$$

On the surface of the unit sphere, the gradient operator reduces from generalized spherical coordinates to $\nabla = \frac{\partial}{\partial \mathbf{p}}$. The equation of change for the distribution function is simply

$$\frac{D\psi}{Dt} = -\frac{\partial}{\partial \mathbf{p}}\cdot(\psi\dot{\mathbf{p}}) \tag{2.25}$$

The term in the parenthesis is an orientation flux. The time-rate-of-change of the orientation vector $\dot{\mathbf{p}}$ is a function of the kinematics within the suspension. This is discussed in Section 2.4.3, and Chapter Three details a theory that involves a new expression for $\dot{\mathbf{p}}$. Equation (2.25) may be written in terms of the Eulerian angles by using the following relations.

$$\nabla = \frac{\partial}{\partial \mathbf{p}} = \mathbf{d}_\theta\frac{\partial}{\partial\theta} + \mathbf{d}_\phi\frac{1}{\sin\theta}\frac{\partial}{\partial\phi} \tag{2.26}$$

$$\dot{\mathbf{p}} = \dot{\theta}\,\mathbf{d}_\theta - \sin\theta\,\dot{\phi}\,\mathbf{d}_\phi \tag{2.27}$$

This gives

$$\frac{D\psi}{Dt} = -\frac{\partial}{\partial\theta}(\dot{\theta}\,\psi) - \frac{\partial}{\partial\phi}(\dot{\phi}\,\psi) \tag{2.28}$$

Similar lengthy manipulations carried out by Advani [23] yield the conservation equation for the orientation tensors. The total derivative of the second order orientation tensor is shown here.

$$\frac{Da_2}{Dt} = -\frac{1}{2}(\omega \cdot a_2 - a_2 \cdot \omega) + \frac{1}{2}(\dot{\gamma} \cdot a_2 - a_2 \cdot \dot{\gamma} - 2\dot{\gamma} \cdot a_4) + 2D_r(\delta - \beta a_2) \tag{2.29}$$

Equation (2.29) is expressed as a function of the vorticity tensor $\omega = (\nabla v - \nabla v^t)$, the strain rate tensor $\dot{\gamma} = (\nabla v + \nabla v^t)$, an isotropic diffusivity D_r, and β, which equals 3 for three-dimensional orientation and 2 for planar orientation. Furthermore, the fourth rank orientation tensor a_4 appears in the equation of change for the second rank tensor a_2. Likewise, a_6 appears in $\frac{Da_4}{Dt}$ and so on. Orientation tensors are moments of the probability distribution function and individually contain an incomplete amount of information about orientation state. The appearance of higher rank tensors in the equations of change is pervasive and presents a closure problem. This type of closure problem has been discussed by other researchers [11,24,25,26] and none could develop a closure that is suitable for all manifestations of the distribution function (i.e. nearly aligned vs. near random). The closure problem in the governing equation for the orientation tensors is the price that is paid for their economy.

Suspensions of elongated particles such as short-fiber-reinforced composite materials include a structural variable such as the distribution function or a set of orientation tensors. Therefore, in addition to the standard conservation equations for mass, momentum, energy, etc., an equation is required that describes the

transport mechanism for the structure, the orientation state. Orientation probability must be conserved.

2.3 Regimes of Suspension Concentration

When discussing suspensions, the volumetric ratio of solid to fluid is a critical quantity whose magnitude dominates much of the fluid mechanics. Typically the concentration c is separated into three distinct regimes; dilute, semi-dilute or semi-concentrated, and concentrated. We will consider these regimes for suspensions of rigid fibers of length L and diameter D.

The dilute regime is characterized by particles whose motions affect no other particles in the suspension. The mean minimum separation distance between fibers is greater than L. A single fiber in suspension will be completely free to rotate without interference from other fibers. This single fiber must be insulated from neighboring particles by a sphere of fluid of minimum diameter L; if n is the number of fibers per unit volume, $n < \frac{1}{L^3}$. This corresponds to a concentration $c < \frac{d^2}{L^2}$.

When fibers are on average separated by distances less than a fiber length yet more than a fiber diameter, one can expect non-negligible hydrodynamic interaction between particles. This is the semi-dilute regime. The disturbances to the flow field due to fluid motion around one particle affect the flow field around its neighbors, and occasional close mechanical contact is possible. In this case $\frac{1}{L^3} < n < \frac{1}{dL^2}$ and $\frac{d^2}{L^2} < c < \frac{d}{L}$.

The concentrated regime is characterized by each fiber having numerous neighbors within a distance of d. Interactions between fibers become a significant factor in the force balance on each fiber. When the number volume fraction $n > \frac{1}{dL^2}$, and the concentration $c > \frac{d}{L}$, the suspension is concentrated. For a suspension of fibers with a typical aspect ratio (say $\frac{L}{d} = 100$), the concentrated regime begins at 1%

volume fraction of fibers. Typical volume fractions in commercially viable short fiber reinforced composites lie in the range of 10-50%.

2.4 Rheology of Suspensions

The flowing composite material comprised of fibers and molten polymer may be considered a suspension. The behavior of solids immersed in fluids have been extensively studied and this section reviews those results.

2.4.1 Single Particles in Dilute Suspension

Einstein [27] was the first to apply the results of hydrodynamics the flow around a spherical solid. His calculations include the force on the particle surface and from that he derives the effective viscosity η of the dilute suspension.

$$\eta = \mu(1 + 2.5c) \tag{2.30}$$

The right-hand-side of Eq. (2.30) requires μ, the viscosity of the Newtonian suspending fluid and c, the volume fraction of spheres in the dilute suspension. "Dilute" here signifies that the spheres remain so far separated in the suspension that hydrodynamic perturbations due to the presence of any one are felt by no other particle.

The classical solution of the hydrodynamics around an ellipsoid was provided by Jeffery [28]. A neutrally buoyant ellipsoid immersed in a simple shear flow will exhibit a rotation caused by the fluid. His result for the rotation rate is typically referred to as a *Jeffrey orbit*.

$$\frac{d\phi}{dt} = \dot{\phi} = \dot{\gamma}\frac{(a^2 - b^2)}{(a^2 + b^2)}(\sin 2\phi \sin 2\theta) \tag{2.31}$$

$$\frac{d\theta}{dt} = \dot{\theta} = \frac{\dot{\gamma}}{(a^2 + b^2)} (a^2 \cos^2\phi + b^2 \sin^2\phi) \tag{2.32}$$

θ and ϕ are defined in Figure 2.1 and a and b are the major and minor axes of the ellipsoid. In a shear flow, the ellipsoid will rotate about an axis in the shear plane perpendicular to the streamlines. The rotation rate will be very high when the particle is oriented perpendicular to the plane of shear and very low when the particle lies in the plane of shear. The rotation rate expressions can be integrated twice with respect to time to yield the period of rotation T_r of a particle in a shear flow. This is the time required for one Jeffrey orbit.

$$T_r = \frac{2\pi(a^2 + b^2)}{ab\,\dot{\gamma}} \tag{2.33}$$

The work of Burgers [29] follows Jeffrey's result for a 'slender body,' an ellipsoid with an infinitely large aspect ratio, $a/b >> 1$. In that case the orientation behavior is given as

$$\dot{\phi} = \dot{\gamma} \sin2\phi \sin2\theta \tag{2.34}$$

$$\dot{\theta} = \dot{\gamma} \cos^2\phi \tag{2.35}$$

Slender body theory will be covered more thoroughly in the first section of Chapter Three.

2.4.2 Behavior of Interacting Particles

The preceding results for motions and suspension viscosity are valid only for dilute suspensions of particles. When two or more particles approach one another

they will interact. The interactions studied in the literature include hydrodynamic interaction, mechanical interaction, and Brownian motion of larger rod-like macromolecules.

Mason and coworkers have conducted an extensive research program on the behavior of interacting particles in suspension. Spheres, rods, and discs are included in their literature, which is concerned with the motions of individual particles, collision kinematics, steady state behavior, and reversibility and dispersion of particle interactions.

Two- and three-body collisions of non-Brownian spherical particles have been studied by Karnis, Goldsmith, and Mason [30], and Anczurowski and Mason [31]. When two spheres approach, their paths curve about the other, and the particles will rotate as a rigid dumbbell in an mutual orbit. Eventually the pair will separate, and upon reversal the phenomenon will be repeated exactly backwards. Anczurowski, Cox, and Mason [32] have demonstrated reversibility in a small collection of rods in suspension.

Studies of larger rod suspensions [32,33] have shown steady state orientation, losses in suspension memory (i.e. irreversibility) and permanent changes in the orbital constants. These effects result from long- and short-range particle interactions and Brownian disturbances in dilute suspension. Mason and Manley [34] have postulated that slender rods affect a suspension volume up to 100 times that of the particle volume. This large *effective volume* causes particle interaction to be more frequent as the aspect ratio grows and leads to a restriction of free rotation for rods in suspensions.

Cox [35] has done an asymptotic analysis of the forces, moments, and resultant motions of suspension particles nearly in contact with each other and with walls. In a Newtonian fluid of viscosity μ at a minimum separation distance h, forces and torques are of the order of $O(\mu \ln(h))$.

In a dilute suspension, the interaction volume may be very large because the hydrodynamic disturbances decay slowly, proportional to the inverse of the separation distance. Shaqfeh and Koch [36] investigated hydrodynamic interactions of rigid rods in suspension with a fixed bed of spheres. They cite that particle shielding or "Brinkman screening" can significantly damp the long range hydrodynamic fluctuations, allowing a simplification in non-dilute suspensions that permits the researcher to consider only short range interactions.

2.4.3 *Experimental Suspension Rheology*

Short fiber reinforced composites are processed in a liquid state. Therefore, controlled mold filling is a rheological undertaking. This section discusses the kinematics, stress and viscosity characteristics observed in experiments with fiber suspensions particularly as related to polymer composites.

Reviews of non-dilute suspension rheology have been completed by Kamal and Mutel [37], Dinh and Armstrong [38] and by Maschmeyer and Hill [39]. Among the first observations to be made in all of these reviews: the addition of elongated particles to a Newtonian suspending fluid creates a non-Newtonian suspension. Also, as one might expect, an increase in the fiber concentration or aspect ratio will increase the viscosity.

Many different non-Newtonian characteristics are cited in the literature. Consistently cited is a shear thinning behavior. At low shear rates many suspensions show a Newtonian plateau. As the shear rate grows, viscosity decreases, and often another Newtonian plateau is established at high shear rates. This shear thinning behavior is more prominent as the volume fraction is increased. In the literature of liquid crystal rheology [40,41] this same shear thinning is also often noted. The reviews of non-dilute suspension rheology also cite numerous examples of yield stresses and normal stress effects like Weissenberg rod climbing.

Several experimental non-dilute suspensions have displayed plug flow behavior in shear. This is related to extensional viscosities measured to be orders of magnitude higher than the Newtonian result of 3μ. Though only a few phenomena are consistently reported for all suspensions, and results occasionally contradict one another, all researchers emphasize that fiber orientation is a critical quantity and that curious transient results were dependent upon the rotations of the fibers in the non-dilute suspensions.

The introduction of solid fibers will affect viscosity and stress while at the same time altering the flow kinematics. A study of a dilute suspension flow through a 4:1 contraction by Libscomb, Denn, Hur and Boger [42] shows a pronounced increase in the size of the recirculation zone ahead of the contraction. This is again related to the extensional flow in the contraction and the suspension's increased viscosity of extension. Furthermore, Libscomb *et al.* successfully modeled their experimental flow by incorporating the fiber orientation and the resistance to elongation in a finite element calculation.

Theories like that of Jeffery [28] and Burgers [29] predict that fibers will always align in the direction of largest positive strain rate in elongational flow, or in the case of shearing flow, lie predominately in plane of shear rotating with periodic Jeffery orbits. These trends are qualitatively exhibited in all suspension orientation studies, but *perfect* alignment or *perfect* orbit behavior is never present. Stover, Koch and Cohen [43] and Folgar and Tucker [44] have observed a diffusive behavior in the orientation of fibers sheared in a Couette device.

The addition of solid rod-like particles to a Newtonian fluid creates a suspension that shows many curious phenomena. All of these rheological behaviors are a result of the interplay between straining fluid and solid particles moving and rotating in the mixture. The following section reviews the research into the

theoretical examinations of suspension rheology and the physics that govern their behavior.

2.4.4 *Theoretical Suspension Rheology*

Theoretical treatment of suspension begins with the work of Einstein [27] and Jeffery [28] and has recently seen a growth in research interest. Work aimed at extending the viscosity expression from a dilute suspension of spheroids has been reviewed by Frish and Simha [45]. Within their findings one sees that as the concentration is increased, hydrodynamic interactions and two-body collisions must be accounted for. This approach yields a viscosity that takes the form of an asymptotic expansion in concentration.

$$\eta = \mu(1 + \alpha_1(c)c + \alpha_2(c^2)c^2 + O(c^3)) \tag{2.36}$$

The α terms are basis functions all of O(1) in magnitude. Recall that for a dilute suspension with no interactions, $\alpha_1 = 2.5$ and all others equal zero. There is little agreement over the form of the basis functions.

Similarly, continued analysis of the behavior of suspensions of ellipsoidal particles have produced corrections to the viscosity worked out by Jeffrey. His expression for dilute suspension viscosity parallels that for spheroids (spheroids are simply a special case of ellipsoids). The expressions are again dependent on the Newtonian viscosity of the suspending medium and the aspect ratio and volume fraction of ellipsoids. The basis functions in this case are a function of concentration *and* of the ratio of major to minor axes of the ellipse. Mutel [46] reviews much of the research aimed at these basis functions for ellipsoids, which are affected by not only the flow fields but also Brownian motion and hydrodynamic disturbances from neighboring fibers.

An increase in the number density of the suspended fibers complicates the motion of the particles in the semi-concentrated suspension. Flow field disruptions and mechanical interactions begin to affect neighboring particles. Multi-body interactions will affect the orientation of all involved fibers; often this is irreversible. This has been shown through many of the experiments discussed in Sections 2.4.2-3.

Where physics is uncertain, a phenomenological approach can prove useful. The particles in suspension create a material with an internal structure. The first objective description of a generalized fluid with a built-in direction is the *Transversely Isotropic Fluid* developed by Ericksen [47]. A suspension of elongated particles has a directional nature by virtue of the presence of the particles. By including only the first order functions of the fluid director, **p**, the orientation vector in the instance of ellipsoidal suspensions, he derived the following equation for extra stress τ.

$$\tau = \mu\dot{\gamma} + \mu_1 + \frac{1}{2}\mu_2\dot{\gamma}:\mathbf{pp} + \mu_3(\dot{\gamma}\cdot\mathbf{pp} + \mathbf{pp}\cdot\dot{\gamma}) \tag{2.37}$$

The constants μ_i are viscosities which can be calculated from theories such as Jeffrey's equations or may be left to the experimentalist to determine. Barthés-Biesel and Acrivos [48] have shown that nearly all constitutive equations derived for spheres, ellipsoids, and droplets conform to this empirical form.

Theoretical approaches to rheology of non-dilute suspensions of long fibers have only recently seen much interest in the literature. Among the first, Batchelor [49] extended early work on these systems and calculated bulk rheological properties of suspensions of fully aligned ellipsoids in a Newtonian fluid. The extra stress in a suspension of ellipsoids is given as

$$\tau = \mu \dot{\gamma} + c \Sigma \sigma_p \tag{2.38}$$

σ_p is the stress in a single particle calculated via integration of the fluid forces over the ellipsoid surface. The summation is performed over all the particles in the suspension. In his theory Batchelor assumes an elongational flow and the uniform stretching direction orientation that would accompany such a flow. This theory uses a *cell model* approach, reducing the suspension problem to that of a single particle in an effective continuum comprised of fluid and fibers. Once the stress on the single fiber in the cell is derived, the sum is carried out over all particles in the suspension.

Dinh and Armstrong [50] followed Batchelor's work and developed a rheological model for semi-concentrated fiber suspensions. Their model is created by focusing again on a 'test fiber' in the suspension. Dinh and Armstrong use *slender-body theory* established by Burgers [28] to describe the fluid forces on a rigid cylinder in a moving fluid. The surrounding Newtonian fluid and fibers make up an effective medium that influences the hydrodynamics of the test fiber. The fiber in this effective medium will travel and rotate affinely with the bulk excepting that it cannot stretch. The presence of the fibers produce an extra term in the stress after that of Batchelor.

$$\tau = \mu \dot{\gamma} + \frac{nL^2}{12} \zeta_a \kappa : \langle pppp \rangle \tag{2.39}$$

Here $\kappa = (\nabla v)^T = \frac{\partial v_i}{\partial x_j}$ is the velocity gradient tensor and $\langle pppp \rangle$ is the ensemble average of the fourth order dyadic product of the unit orientation vector p. ζ is the fluid drag coefficient tensor and has the form

$$\zeta = \zeta_p \mathbf{pp} + \zeta_t(\boldsymbol{\delta} - \mathbf{pp}) \tag{2.40}$$

where ζ_p and ζ_t are the coefficients describing the drag on the cylinder from axial and transverse fluid motion respectively. For a dilute suspension of cylinders in a Newtonian fluid, $\zeta_p = \zeta_t/2 \cong \mu L$. Dinh and Armstrong give an estimate for the axial drag coefficient as a function of lateral fiber spacing h in a non-dilute suspension.

$$\zeta_p = \frac{2\pi\mu L}{\ln(2h/D)} \tag{2.41}$$

Orientation behavior from Dinh and Armstrong's theory is equivalent to Burger's [28] and to Jeffrey's equation [27] with an infinite axis ratio for the rigid rods.

$$\dot{\mathbf{p}} = \boldsymbol{\kappa}\cdot\mathbf{p} - \boldsymbol{\kappa}:\mathbf{ppp} \tag{2.42}$$

Equation (2.42) shows that the rods will follow the straining fluid ($\boldsymbol{\kappa}\cdot\mathbf{p}$) but will not stretch ($-\boldsymbol{\kappa}:\mathbf{ppp}$). Dinh and Armstrong's theory predicts perfect alignment of the fibers in steady shear and in elongation. Experiments with typical extrusion and injection molding materials, and laboratory suspensions, show this qualitative relationship between flow and orientation. Fibers will lie down in the plane of shear or will rotate into the direction of stretching. But, contrary to theory, *perfect* alignment is rare. Dinh and Armstrong's theory also predicts no fiber contribution to suspension viscosity in steady shear flow. A small amount of out-of-plane tilt in orientation can significantly affect resistance to steady shear.

Hinch and Leal [51] have studied the diffusive effect of Brownian disturbances on the orientation state of small elongated particles. Brownian motion affects the stress in the suspension both through orientation perturbations and through added stresses in the particles from the collisions. Doi and Edwards [52] have also developed a rheological theory for Brownian rod-like particles in suspension (liquid crystals). They include an observation that the rods are caged or 'entangled' by neighboring rods, and from a calculation of the average interparticle spacing, they can write an expression for diffusivities of the particle. Doi and Edwards surmise that axial diffusion is unaffected by caging and that transverse and rotational diffusion will be restricted by interparticle spacing.

Other researchers have developed theories that result in a diffusivity in the particle translation and rotation. Dilute polymer solutions have been studied for many years using Hookean dumbbells. Wedgewood and Öttinger [53] have shown that even in dilute solution, flow about one dumbbell can cause a hydrodynamic interaction that effects the neighboring particles. Furthermore, they have shown that preaveraging the configuration-dependent terms in the hydrodynamic drag tensor nullifies the effects of interactions between particles. That is, the interaction-induced diffusion is only present when the hydrodynamic fluctuations are included in the flow field around each particle.

Hydrodynamic interactions have also been studied in suspensions of rigid rods. Shaqfeh and Koch [36] use "multiple reflection expansions" of hydrodynamic interactions and neglect longer range interactions on the basis of what they cite as 'hydrodynamic screening'. This makes the orientation averaging techniques tractable and is essentially an extended use of Batchelor's cell model approach that includes several fibers in the cell. They found that the orientational diffusivity for the rods would increase due to interactions as concentration grew within the dilute regime, and then diffusivity would begin to decrease in the semi-concentrated

regime due to hydrodynamic screening. The hydrodynamic screening essentially reduces the relative variance of interaction effects between fibers.

One of the earliest and most basic theories for fiber suspensions that include an orientational diffusivity was proposed by Folgar and Tucker [44]. This theory includes an empirical diffusion term that is derived from no particular mechanism. The rationale behind including a diffusion term was to model mechanical interaction effects in the suspension. This gives an expression for fiber orientation behavior that looks like that of Dinh and Armstrong [51] with one addition.

$$\dot{\mathbf{p}} = \boldsymbol{\kappa}\cdot\mathbf{p} - \boldsymbol{\kappa}:\mathbf{ppp} - \frac{C_I \dot{\gamma}}{\psi}\frac{\partial \psi}{\partial \mathbf{p}} \tag{2.43}$$

The third term of the right-hand-side of Eq. (2.43) is a phenomenological diffusion term. C_I is the interaction coefficient, and $\dot{\gamma}$ is the scalar magnitude of the strain rate. This combination simulates a strain rate dependent diffusion, appropriate for particles whose motion is driven by the suspension strain. Otherwise, this term acts in a fashion similar to rotary Brownian diffusion, disorienting fibers aligned by the motion of the fluid. Numerical and experimental work by Bay, Tucker and Davis [54] using this interaction coefficient with injection molding flows show that inclusion of interaction effects in Eq. (2.43) captures more of the physics of fiber orientation, but procedures for choosing an appropriate C_I are not well established.

2.5 Stochastic Geometry and Statistics

The fibers within a composite form a network whose geometry is crucial to the rheology of the suspension. Yet this geometry cannot be specified explicitly. The orientation of a particular fiber or the aggregate orientation in a particular position

can only be expressed as a probability. Often the fibers are small and numerous enough and the scale of the flow sufficiently large to provide small variances in statistical quantities that rely on the orientation. If this is true, the material may be modeled with a continuum theory with orientation as a state variable. If a suspension property P is reliant upon the fiber orientation $\mathbf{p}$, the bulk property is calculated from an average of the quantity over orientation space which is weighted by the probability distribution function.

$$E(P) = \langle P \rangle = \oint \psi(\mathbf{p})\, P(\mathbf{p})\, d\mathbf{p} \tag{2.44}$$

In statistical terms this is the expected value of P created from the ensemble average of the contributions of the fibers. This is the method of determining the stiffness properties of fiber-reinforced composites discussed in Section 2.1.3. The actual result of P may often not be exactly the expected value. Variance gives an indication of the size of the deviation possible. The variance of this property is the squared expected deviation from the mean.

$$\mathrm{Var}(P) = \langle (P - \langle P \rangle)^2 \rangle = \oint \psi(\mathbf{p})\, (P(\mathbf{p}) - E(P))^2\, d\mathbf{p} \tag{2.45}$$

As time advances, the orientation state will change. Therefore, the value of P is a function of time as well as the random variable $\mathbf{p}$. The correlation function measures the degree to which $P(t_1)$ is related to $P(t_2)$, $(t_2 \geq t_1)$.

$$C(t_2 - t_1) = \frac{\langle (P(t_2) - \langle P \rangle)\, (P(t_1) - \langle P \rangle) \rangle}{\langle (P(t_2) - \langle P \rangle)^2 \rangle} \tag{2.46}$$

This function is identically equal to one (1) when $t_2 = t_1$. As $t_2 - t_1$ goes to infinity, the correlation function goes to zero. The two terms in the numerator will become uncorrelated.

The time scale over which orientation states are uncorrelated is the correlation time. This quantity is essentially the area under the curve of correlation as a function of time difference.

$$\varepsilon = \int_{t_1}^{\infty} C(t_2 - t_1)\, dt_2 \tag{2.47}$$

Fiber networks have long been studied in the paper-making industry, and Kalmes and Corte have published a series of work on the stochastic geometry of fiber networks [55,56]. Crucial to the strength of paper sheets is the number of crossings experienced by each fiber in the material. Fiber crossing will also serve to generate interaction forces in wet suspensions of polymer composites. Kalmes and Corte calculate the average number of crossings N_I experienced by a fiber of length L in a 2 dimensional sheet having n_A fibers per unit area to be

$$N_I = \frac{2\, n_A\, L^2}{\pi} \tag{2.48}$$

If the orientations of fibers in a polymer composite are nearly all in-plane as often seen in compression molding and thin injection molds, n_A can be approximated as $n_A \approx nd$. This results in an equation for the number of fiber crossings or number of fibers that pass within d of a particular fiber.

$$N_I = \frac{2c}{\pi}\frac{L}{d} \tag{2.49}$$

For a typical composite with a fiber volume fraction of 10% and a fiber aspect ratio of 100, the expected number of crossings will be 6.4. This suggests that interactions due to fiber crossings are not a negligible factor in composite material suspensions.

2.6 Summary and Conclusions

The mechanical performance of short fiber reinforced composites are heavily dependent upon the orientation of the reinforcing fibers. Generally, each fibers acts only as reinforcement along the axis direction. Processing of these materials creates the orientation in the final part, while simultaneously the orientation influences rheology and mold filling.

Most polymer composite materials may be considered concentrated suspensions of fibers in polymer melt or pre-polymer. Theoretical and experimental studies of fiber suspensions have made progress towards describing the concentrated regime. The behavior of a single fiber in a straining fluid is well established and researchers have calculated the orientation dependent rheological properties of these suspensions. As concentration is increased, fiber-fiber collisions become a factor in the both the orientation behavior of the fibers and in the rheological properties of the flowing material. Interactions have been accounted for in phenomenological and hydrodynamic models, and the results of these suggests that dispersion due to interactions is important for many industrial applications involving fiber-laden flows.

In suspensions of fibers representative of short-fiber reinforced composites, direct fiber-fiber contact is highly probable. Theories that include hydrodynamic and Brownian interactions show an orientational dispersion. A theory that includes mechanical particle-particle interaction in concentrated suspensions is needed to

model the coupled elements of orientation and rheology in commercially viable short-fiber reinforced composite materials.

3. A THEORY FOR MODELING CONCENTRATED FIBER SUSPENSIONS

The preceding chapter has demonstrated the need for a model of concentrated fiber suspensions that can be used to model the processing behavior of short-fiber reinforced polymer composites. This chapter details the development of an analytical model that will serve that need by including the probability that fibers in the suspension will be subject to mechanical interaction with neighboring fibers. This rheological model combines ideas from slender body theory [29] with a statistical description of the mechanical interactions that occur during processing of short-fiber-reinforced polymer composites.

3.1 Definitions

The continuum theory is built by considering a single fiber immersed in the suspension. This single fiber will be called the 'test fiber.' The surrounding fluid and fiber suspension will be considered an homogenous entity, referred to as the effective medium.

Figure 3.1 shows the test fiber and its geometry in the suspension. The

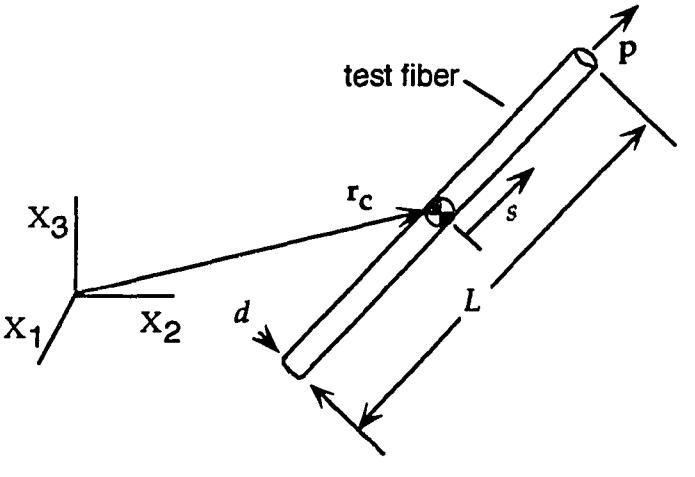

Figure 3.1 The test fiber of length L and diameter d at position $\mathbf{r}_c$ with orientation $\mathbf{p}$. The coordinate s is measured along the axis in the $\mathbf{p}$ direction.

position of the centroid of the fiber is given by a vector $\mathbf{r}_c$ measured from a fixed Cartesian coordinate frame X_1, X_2, X_3. The orientation of the fiber is described by the unit vector p pointing along the axis of the fiber. The orientation can also be described by a pair of Eulerian angles ϕ and θ. The components of p are related to ϕ and θ. These relations are given in Eq. (2.2a-c). The orientation of the test fiber in the suspension is a random variable which can be described with a probability distribution function $\psi(\mathbf{p}) = \psi(\phi,\theta)$. The probability of finding a fiber oriented in a range p to p+dp is given by the product $\psi(\mathbf{p})d\mathbf{p}$.

The test fiber is likely to experience several contacts from neighboring fibers in the suspension. The number and position of these contacts and the orientations of the "interacting fibers" are all random variables. Figure 3.2 shows the test fiber and the i^{th} of N possible interacting fibers. The contact point lies at position s_i along the test fiber and position s_i' along the interacting fiber. The exact location of the contact point within the suspension can be specified by the position and orientation vectors of either fiber in conjunction with its axial coordinate.

$$\mathbf{r}^{contact} = \mathbf{r}_c + s_i\mathbf{p} = \mathbf{r}_{ci}' + s_i'\mathbf{p}_i' \tag{3.1}$$

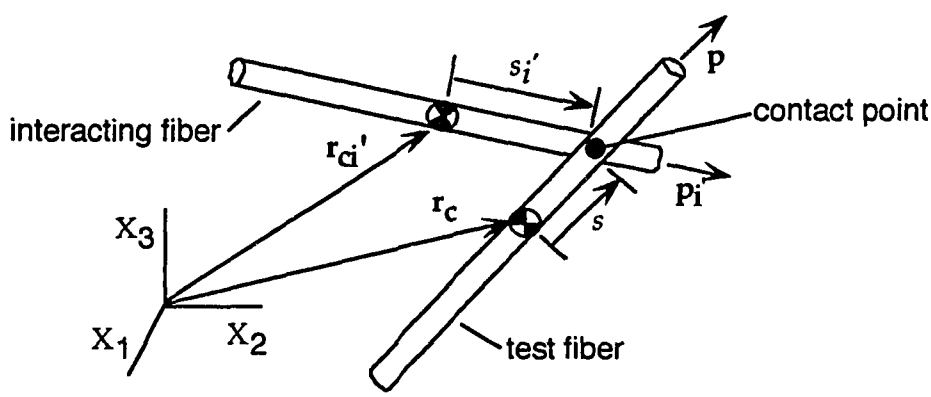

Figure 3.2 Test fiber and the i^{th} interacting fiber.

The test fiber serves as a representative of all fibers in the suspension. It will rotate and translate and contribute to suspension stress in response to the stress applied by the effective medium and whatever interaction forces are present.

3.2 Assumptions

Several assumptions are used to create a model for the non-dilute suspension of rigid rods.

- The suspending medium is a Newtonian fluid
- Inertia and gravity effects are negligible.
- Suspended particles are slender, rigid rods of uniform length and diameter
- The bulk flow field is homogeneous.

$$\mathbf{v} = \boldsymbol{\kappa} \cdot \mathbf{r} \quad \text{where } \kappa_{jk} = \frac{\partial v_j}{\partial x_k}$$

- Particle-particle interaction force is linear in relative velocity (hydrodynamic friction)
- Fibers are shielded from all but nearest-neighbor interactions

3.3 Slender Body Results for a Single Fiber in a Straining Fluid

The stress in the test fiber is partly due to the strain in the effective medium surrounding the fiber. The differential hydrodynamic force $d\mathbf{F}_h$ on an infinitesimal segment of the fiber ds is, according to slender body theory, proportional to the velocity difference between the effective medium and the fiber segment.

$$d\mathbf{F}_h = \frac{1}{L}\boldsymbol{\zeta} \cdot [\mathbf{v}^{\text{medium}} - \mathbf{v}^{\text{segment}}]\, ds \tag{3.2}$$

The factor of proportionality ζ is the *hydrodynamic drag tensor,* and has the following form

$$\zeta = \zeta_a(2\delta - pp) \tag{3.3}$$

ζ_a is the scalar axial drag coefficient that depends on the fiber dimensions and the viscosity of the liquid. Equation (3.3) describes a transversely isotropic hydrodynamic drag. The drag is twice as strong in the transverse direction as in the axial direction.

The velocity of the effective medium $\mathbf{v}^{medium}$ at a position $\mathbf{r}$ in a continuum experiencing a homogeneous deformation is

$$\mathbf{v} = \kappa \cdot \mathbf{r} \tag{3.4}$$

neglecting any solid body translation or choosing an appropriate origin for $\mathbf{r}$. Replacing $\mathbf{r}$ in Eq. (3.4) with the position of *ds* on the fiber will give the effective velocity of the continuum at the segment. The differential force of Eq. (3.2) can be expressed in terms of the vectors $\mathbf{r}_c$ and $\mathbf{p}$, their timewise derivatives, and the coordinate *s*.

$$dF_h = \frac{1}{L}\zeta \cdot [\, \kappa \cdot (r_c + sp) - (\dot{r_c} + s\dot{p}) \,]\, ds \tag{3.5}$$

Total hydrodynamic force on the fiber results from integrating Eq. (3.5) over the entire fiber length, $-L/2 \le s \le +L/2$.

$$\mathbf{F_h} = \zeta \cdot [\, \kappa \cdot \mathbf{r_c} - \dot{\mathbf{r}}_c \,] \tag{3.6}$$

Equation (3.6) indicates that the force of the straining medium on the fiber is independent of $\dot{\mathbf{p}}$, the rotation of the fiber. In the absence of inertia effects and fiber-fiber interactions, fiber centroid motion is found by setting $\mathbf{F_h} = 0$.

$$\dot{\mathbf{r}}_c = \kappa \cdot \mathbf{r_c} \tag{3.6}$$

The fiber centroid will travel affinely with the effective medium in the absence of any other forces besides those imparted by the suspending fluid.

The moments exerted on the fiber due to the fluid motion can be determined by again considering a small element of the fiber at a distance s from the centroid. The force at that point is $d\mathbf{F_h}$, and the differential moment on the segment is

$$d\mathbf{M_h} = s\mathbf{p} \times d\mathbf{F_h} \tag{3.7}$$

Integrating as before yields the moment on the rigid fiber from the straining fluid.

$$\mathbf{M_h} = \mathbf{p} \times \frac{L^2}{12} \{ \zeta \cdot [\, \kappa \cdot \mathbf{p} - \dot{\mathbf{p}}] \} \tag{3.8}$$

The hydrodynamic moment exerted on the fiber is independent of the translation of the fiber.

The motion of the orientation vector in the absence of other moments can be calculated now by setting the hydrodynamic moment on the fiber equal to zero.

$$\mathbf{p} \times \frac{L^2}{12} \{ \boldsymbol{\zeta} \cdot [\boldsymbol{\kappa} \cdot \mathbf{p} - \dot{\mathbf{p}}] \} = 0 \tag{3.9}$$

This equation implies that p is collinear with the vector on the right of the cross-product symbol. The collinear relationship between the terms in the cross product can be expressed in another fashion.

$$g(t)\,\mathbf{p} = \frac{L^2}{12} \{ \boldsymbol{\zeta} \cdot [\boldsymbol{\kappa} \cdot \mathbf{p} - \dot{\mathbf{p}}] \} \tag{3.10}$$

The orientation vector multiplied by some unknown scalar function of time is equal to the vector on the right. To solve for the unknown scalar function $g(t)$ it is useful to substitute the expression for the tensor drag coefficient in Eq. (3.3)

$$g(t)\mathbf{p} = \frac{L^2}{12} \{ \zeta_a [2\boldsymbol{\delta} \cdot \boldsymbol{\kappa} \cdot \mathbf{p} - \mathbf{pp} \cdot \boldsymbol{\kappa} \cdot \mathbf{p} - 2\boldsymbol{\delta} \cdot \dot{\mathbf{p}} + \mathbf{pp} \cdot \dot{\mathbf{p}}] \} \tag{3.11}$$

Since the orientation vector is a unit vector (i.e. p is inextensible), the derivative $\dot{\mathbf{p}}$ must be normal to p. Use of this fact and rearrangement yields

$$g(t)\mathbf{p} = \frac{L^2}{12}\left\{\zeta_a\left[2\boldsymbol{\kappa}\cdot\mathbf{p} - \boldsymbol{\kappa}:\mathbf{ppp} - 2\dot{\mathbf{p}}\right]\right\} \tag{3.12}$$

Taking the dot product of both sides with **p** will yield an expression for $g(t)$ will eliminate the **p** dependence on the left hand side and the $\dot{\mathbf{p}}$ on the right hand side.

$$g(t) = \frac{L^2\zeta_a}{12}\left[\boldsymbol{\kappa}:\mathbf{pp}\right] \tag{3.13}$$

Substitution of this relation back into Eq. (3.12) and rearrangement will give an expression for slender-body-theory fiber rotation.

$$\dot{\mathbf{p}} = \boldsymbol{\kappa}\cdot\mathbf{p} - \boldsymbol{\kappa}:\mathbf{ppp} \tag{3.14}$$

This is equivalent to the fiber rotation used by Dinh and Armstrong [38] in their theory, or to Jeffrey's equation [27] in the limit of infinite aspect ratio. It is derived via slender body theory for suspension dynamics that include no fiber-fiber interactions.

3.4 Force and Torque from Mechanical Fiber-Fiber Interaction

Chapter Two demonstrated that interactions between fibers will contribute significant effects to concentrated suspension rheology. Furthermore, it confirmed that mechanical interactions (defined as particle separation distances less than d) are not only possible but are probable. This section extends the slender body theory for fiber suspensions to include interaction forces from nearby fibers.

3.4.1 *Forces from a Single Interacting Fiber*

Inclusion of the effects of interacting fibers begins by considering a single additional fiber approaching within one diameter of the test fiber. The position and orientation of the interacting fiber is described like that of the test fiber with the addition of a prime, $\mathbf{r_c}'$ and $\mathbf{p}'$. Equation (3.1) for the contact position is valid as the fiber diameter goes to zero in the slender body limit. Figure 3.3 shows the geometrical relationship of the test fiber and the interacting fiber.

The force exerted on the test fiber by the second fiber shall be called *a priori* $\mathbf{f}$. The force on the interacting fiber will be equal and opposite, $\mathbf{f} = -\mathbf{f}'$. A constitutive equation is required to describe the interaction force in terms of the kinematic variables. This development is left to a following section and for the present f is assumed to be known.

The total force on the fiber now is the sum of the hydrodynamic force and the interaction force.

$$\mathbf{F} = \zeta \cdot [\, \kappa \cdot \mathbf{r_c} - \dot{\mathbf{r}}_c \,] + \mathbf{f} \tag{3.15}$$

The motion of the centroid is found by setting the total force equal to zero.

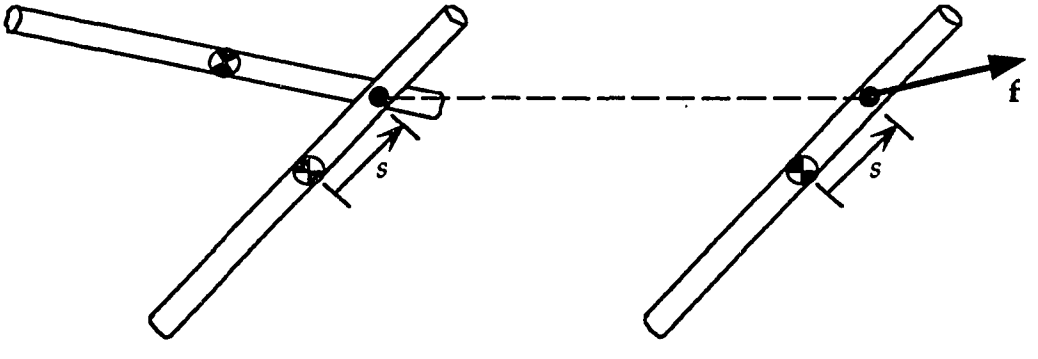

Figure 3.3 Interacting fiber action resolved into interaction force $\mathbf{f}$ at contact point s.

$$\dot{\mathbf{r}}_c = \boldsymbol{\kappa}\cdot\mathbf{r}_c + \boldsymbol{\zeta}^{-1}\cdot\mathbf{f} \tag{3.16}$$

The inverse of the hydrodynamic drag tensor is shown in Appendix A to be

$$\boldsymbol{\zeta}^{-1} = \frac{1}{2\zeta_a}(\boldsymbol{\delta} + \mathbf{pp}) \tag{3.17}$$

Equation (3.16) then becomes

$$\dot{\mathbf{r}}_c = \boldsymbol{\kappa}\cdot\mathbf{r}_c + \frac{1}{2\zeta_a}(\boldsymbol{\delta} + \mathbf{pp})\cdot\mathbf{f} \tag{3.18}$$

The centroid motion will be affected by the presence of the interaction force. Note that the tensor $(\boldsymbol{\delta} + \mathbf{pp})$ allows forces in the $\mathbf{p}$ direction to be doubly effective at moving the fiber.

The interaction force induces a translational dispersion velocity to both fibers $\mathbf{v}_d$ and $\mathbf{v}_d'$.

$$\mathbf{v}_d = \frac{1}{2\zeta_a}(\boldsymbol{\delta} + \mathbf{pp})\cdot\mathbf{f} \tag{3.19}$$

The dispersion velocity of the interacting fiber will be equal and opposite.

$$\mathbf{v}_d' = \frac{1}{2\zeta_a}(\boldsymbol{\delta} + \mathbf{pp})\cdot(-\mathbf{f}) \tag{3.20}$$

The moments on the test fiber can also be summed, yielding an expression for the rotation of the fiber in the presence of the interaction force. The interaction moment is simply the moment arm crossed with the applied force.

$$\mathbf{M}_I = s\mathbf{p} \times \mathbf{f} \tag{3.21}$$

Summation of hydrodynamic and interaction moments give the total moment on the test fiber.

$$\mathbf{M} = \mathbf{p} \times \left\{ \frac{L^2}{12} \zeta \cdot [\, \boldsymbol{\kappa} \cdot \mathbf{p} - \dot{\mathbf{p}}\,] + s\mathbf{f} \right\} \tag{3.22}$$

When the moment is set to zero it is again apparent that the term in the curly brackets of Eq. (3.22) must be collinear with $\mathbf{p}$. Therefore the orientation behavior of the test fiber is found in the manner described in Eq. (3.14).

$$\dot{\mathbf{p}} = \boldsymbol{\kappa} \cdot \mathbf{p} - \boldsymbol{\kappa} : \mathbf{ppp} + \frac{6s}{L^2 \zeta_a} \mathbf{f} \cdot (\boldsymbol{\delta} - \mathbf{pp}) \tag{3.23}$$

Again, the interaction force alters the motion of the fiber from the dilute response. The tensor $(\boldsymbol{\delta} - \mathbf{pp})$ selects forces perpendicular to $\mathbf{p}$; these are the only components that can change the orientation. The fluid drag coefficient inhibits the rotational effect of the interaction force.

3.4.2 Forces from Several Interacting Fibers

One interacting fiber on the test fiber is easily conceptualized, but the step to several interacting fibers is required. Consider N interacting fibers each denoted by the subscript i, i = 1,N. The total force on the test fiber can be written in manner similar to Eq. (3.15)

$$\mathbf{F} = \zeta \cdot [\, \kappa \cdot \mathbf{r}_c - \dot{\mathbf{r}}_c \,] + \sum_{i=1}^{N} \mathbf{f}_i \tag{3.24}$$

The motion of the test fiber can be expressed as a function of the hydrodynamic motion and the interaction forces.

$$\dot{\mathbf{r}}_c = \kappa \cdot \mathbf{r}_c + \frac{1}{2\zeta_a} (\delta + \mathbf{pp}) \cdot \sum_{i=1}^{N} \mathbf{f}_i \tag{3.25}$$

The total moment on the test fiber includes the moments due to the forces $\mathbf{f}_i$ applied at positions s_i.

$$\mathbf{M} = \mathbf{p} \times \left\{ \frac{L^2}{12} \zeta \cdot [\, \kappa \cdot \mathbf{p} - \dot{\mathbf{p}} \,] + \sum_{i=1}^{N} s_i \mathbf{f}_i \right\} \tag{3.26}$$

The test fiber will rotate in response to the moments applied. Equating the total applied moment to zero, the orientation behavior of the test fiber is determined for multiple interactions with neighboring fibers in the suspension.

$$\dot{\mathbf{p}} = \kappa \cdot \mathbf{p} - \kappa : \mathbf{ppp} + \frac{6}{L^2 \zeta_a} \sum_{i=1}^{N} s_i \mathbf{f}_i \cdot (\, \delta - \mathbf{pp} \,) \tag{3.27}$$

3.5 Continuum Stress

Presuming that the contact forces and geometry are known, calculation of the stress in the continuum is possible. The stress in the continuum is the sum of the stress in the fluid phase plus the stress in the solid fiber phase, as shown by Batchelor [50]. His *cell model* approach involves considering a small volume of the suspension containing only one fiber surrounded by the effective medium. The volume of this cell will be $(1/n)$, where n is the number density of the fibers. Figure 3.4 shows the representative cell of the test fiber surrounded by effective medium.

Random samples of the stress along the length of the representative volume will yield a stress contribution due to the average force carried by the fiber in the p direction on the p face and a stress contribution from the surrounding medium. $\frac{1}{nL}$ is the area transverse to the fiber, and $\overline{F}$ is defined as the average force carried by the fiber. The slender fiber will not contribute to the any shear stress nor any normal stress not in the p direction. The stress in the

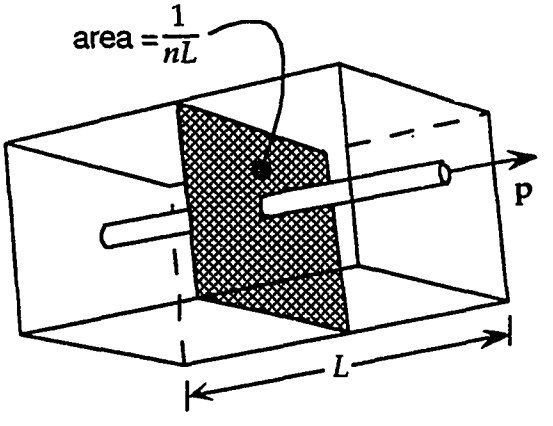

Figure 3.4 Representative volume of suspension with stress contribution from the single test fiber.

test fiber cell is given by the following equation.

$$\tau(\mathbf{p}) = \mu\dot{\gamma} + nL\,\bar{\mathbf{F}}\,\mathbf{p} \tag{3.28}$$

This stress is a function of the orientation of the test fiber **p** because the cell is built about that particular fiber. A continuum expression for the stress in the suspension is found by averaging the effects of the microstructure of fibers, by performing an orientation average over all possible fiber directions.

The average force carried in the test fiber remains to be found. The fiber load as a function of the axial coordinate s can be found *via* a force balance on a segment of the fiber. This process gives an expression for the force carried by the fiber as a function of s. Figure 3.5 shows the fiber segment with associated forces.

$$\Sigma\,\mathbf{F} = 0 = \mathbf{f}^{\text{medium}} + \mathbf{f}^{\text{interactions}} + \mathbf{F}(s) \tag{3.29}$$

The internal load at any position s is balanced by the integral of the continuous suspension forces on the fiber and the sum of the contact forces.

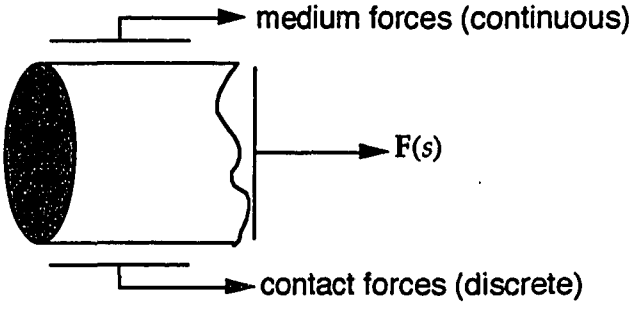

Figure 3.5 Free-body diagram of fiber segment.

$$\mathbf{F}(s) = -\int_{-L/2}^{s} \frac{1}{L}\boldsymbol{\zeta}\cdot[\,\boldsymbol{\kappa}\cdot\mathbf{r}_c + s\boldsymbol{\kappa}\cdot\mathbf{p} - \dot{\mathbf{r}}_c - s\dot{\mathbf{p}}\,]\,ds + \sum_{i=1}^{N} \mathbf{f}_i u(s-s_i) \tag{3.30}$$

In this equation, $u(s-s_i)$ is the unit step function, equal to zero if $s < s_i$ and equal to one otherwise. The boundary condition on the end of the slender fiber is force equal to zero. Carrying out the integral gives the force in the test fiber as a function of s.

$$\mathbf{F}(s) = -\left(s+\frac{L}{2}\right)\frac{1}{L}\boldsymbol{\zeta}\cdot[\boldsymbol{\kappa}\cdot\mathbf{r}_c - \dot{\mathbf{r}}_c] - \left(\frac{s^2}{2}-\frac{L^2}{8}\right)\frac{1}{L}\boldsymbol{\zeta}\cdot[\,\boldsymbol{\kappa}\cdot\mathbf{p}-\dot{\mathbf{p}}\,] - \sum_{i=1}^{N}\mathbf{f}_i u(s-s_i) \tag{3.31}$$

The average force is then is found through integration of Eq. (3.31) with respect to s and division by L.

$$\overline{\mathbf{F}} = \frac{1}{L}\int_{-L/2}^{+L/2} \mathbf{F}(s)\,ds \tag{3.32}$$

The result of this integration after substitution of the terms for fiber motion from Eq. (3.24) and Eq. (3.27) yields a simple expression for fiber load.

$$\overline{\mathbf{F}} = \frac{L}{12}\,\boldsymbol{\zeta}\cdot\boldsymbol{\kappa}:\mathbf{ppp} + \sum_{i=1}^{N}\frac{s_i}{L}\mathbf{f}_i\cdot\mathbf{pp} \tag{3.33}$$

Note that the average force in the fiber, a product of straining medium and random interaction forces, will always lie in the fiber axis direction. This is consistent with the assumptions of slender body theory.

Substitution of average fiber force into Eq. (3.28) gives bulk stress in the immediate vicinity of the test fiber.

$$\mathbf{t}(\mathbf{p}) = \mu\dot{\boldsymbol{\gamma}} + \frac{nL^2}{12}\,\boldsymbol{\zeta}\cdot\boldsymbol{\kappa}:\mathbf{pppp} + n\sum_{i=1}^{N} s_i\mathbf{f}_i\cdot\mathbf{ppp} \tag{3.34}$$

The fiber contribution to the stress is a normal stress along the fiber axis (manifested in the tensor **pp**). Moreover, if $\mathbf{f}_i$ is set to zero, Eq. (3.34) reduces to the result of Dinh and Armstrong [38], which is consistent with their assumption of no fiber-fiber interactions. An orientation average of the stress performed in order to determine the aggregate affect of the microstructure on the suspension is not truly valid yet, as the interaction forces in Eq. (3.34) will very likely be a function of orientation. That functional dependence is unkown at this point but will be developed in the next sections.

3.6 A Constitutive Relation for Interaction Force

The continuum stress contains a term for the forces applied by the interacting fibers and the positions of contact. Interaction force cannot be known *a priori,* and therefore we require a constitutive relation that will give the interaction force in terms of the kinematic variables of the effective medium.

Using the assumption that this interaction force is hydrodynamic in nature, a simple expression can be written.

$$\mathbf{f}_i = \mathbf{f}_I\cdot\left[\,\dot{\mathbf{r}}_c' + s_i'\dot{\mathbf{p}}' - \dot{\mathbf{r}}_c - s_i\dot{\mathbf{p}}\,\right] \tag{3.35}$$

This gives the contact force as some tensor f_I multiplied by the relative velocity of the interacting fiber at the point of contact with the test fiber. The hydrodynamic friction is given with a tensorial form to produce different forces for different configurations and relative velocities of the fibers.

The translation and rotation of the test fiber are given by Eqs. (3.24) and (3.27). These equations also describe the motion of the interacting fibers. Substitution of these equations into the constitutive relation gives

$$\begin{aligned} f_i = f_I \cdot \Big[\quad & \{ \kappa \cdot r_c' + \frac{1}{2\zeta_a} (\delta + p_i' p_i') \cdot \sum_{j=1}^{N_i'} f_j' \} \\ & + s_i' \{ \kappa \cdot p_i' - \kappa : p_i' p_i' p_i' + \frac{6}{L^2 \zeta_a} \sum_{j=1}^{N_i'} s_j' f_j' \cdot (\delta - p_i' p_i') \} \\ & - \{ \kappa \cdot r_c + \frac{1}{2\zeta_a} (\delta + pp) \cdot \sum_{i=1}^{N} f_i \} \\ & - s_i \{ \kappa \cdot p - \kappa : ppp + \frac{6}{L^2 \zeta_a} \sum_{i=1}^{N} s_i f_i \cdot (\delta - pp) \} \quad \Big] \end{aligned} \tag{3.36}$$

The summations within the first two terms in curly brackets are over all interactions on the i^{th} interacting fiber. Several terms on the right-hand side will cancel due to geometric factors associated with the contact point.

$$\begin{aligned} f_i = f_I \cdot \Big[\quad & \{ s_i \kappa : ppp - s_i' \kappa : p_i' p_i' p_i' \} \\ & + \frac{1}{2\zeta_a} (\delta + p_i' p_i') \cdot \sum_{j=1}^{N_i'} f_j' \\ & + s_i' \frac{6}{L^2 \zeta_a} \sum_{j=1}^{N_i'} s_j' f_j' \cdot (\delta - p_i' p_i') \end{aligned}$$

$$-\frac{1}{2\zeta_a}(\delta+\mathbf{pp})\cdot\sum_{i=1}^{N}\mathbf{f}_i$$

$$-s_i\frac{6}{L^2\zeta_a}\sum_{i=1}^{N}s_i\mathbf{f}_i\cdot(\delta-\mathbf{pp})\ ] \tag{3.37}$$

One can see that each individual interaction force $\mathbf{f}_i$ on the test fiber is dependent on the motion of the test fiber and *all* interacting fibers on both the test fiber and the i^{th} interacting fiber. Fiber contact forces and fiber motions are therefore interdependent. Shaqfeh and Koch [36] solve a similar difficulty involving hydrodynamic interactions using a multiple reflection expansion technique.

As a closure approximation, we will use the dilute motion of the fibers involved in interaction to determine the interaction force. This approximation could serve as a first step in an iteration scheme, or the hydrodynamic friction coefficient tensor may be modified to accommodate higher order effects of interaction motion. Using this assumption for the fiber motion, Eq. (3.37) is simplified to include only the terms in the curly brackets.

$$\mathbf{f}_i = \mathbf{f}_I\cdot[\,s_i\boldsymbol{\kappa}:\mathbf{ppp}-s_i'\boldsymbol{\kappa}:\mathbf{p}_i'\mathbf{p}_i'\mathbf{p}_i'\,] \tag{3.38}$$

In this form, the interaction force is a function of the bulk velocity field, test and interacting fiber orientations, and contact position only. Substitution of Eq. (3.38) into the expression for stress in the neighborhood of the test fiber gives

$$\tau(\mathbf{p}) = \mu\dot{\gamma} + \frac{nL^2}{12}\zeta\cdot\kappa{:}\mathbf{pppp} + n\sum_{i=1}^{N} s_i\,\mathbf{f}_I\cdot\left[\,s_i\kappa{:}\mathbf{ppp} - s_i'\kappa{:}\mathbf{p}_i'\mathbf{p}_i'\mathbf{p}_i'\,\right]\cdot\mathbf{ppp} \tag{3.39}$$

The stress in the cell about the test fiber is a function of bulk strain rate, test fiber geometry and contact fiber geometry.

The interaction force coefficient tensor will be a function of the separation distance, the intervening fluid viscosity and the area of contact. Relative velocities of contacts in the transverse directions and in the axial direction on the test fiber *may* have different effects. This suggests a simple transversely isotropic form for the force coefficient tensor.

$$\mathbf{f}_I = f_p\mathbf{pp} + f_T(\boldsymbol{\delta} - \mathbf{pp}) \tag{3.40}$$

Other tensorial combinations of p and p' could be used to create the interaction drag coefficient tensor, but none are as simple as this form. Inserting Eq. (3.40) into the equations for fiber translation, rotation and cell stress yields interesting results. We begin first by inserting the relations for fiber interation force, including the transversely isotropic form of the interaction force coefficient.

$$\dot{\mathbf{r}}_c = \kappa\cdot\mathbf{r}_c + \frac{1}{2z_a}(\boldsymbol{\delta} + \mathbf{pp})\cdot\sum_{i=1}^{N}\left[f_p\mathbf{pp} + f_T(\boldsymbol{\delta} - \mathbf{pp})\right]\cdot\left[\,s_i\kappa{:}\mathbf{ppp} - s_i'\kappa{:}\mathbf{p}_i'\mathbf{p}_i'\mathbf{p}_i'\,\right] \tag{3.41}$$

The tensor dot product $(\boldsymbol{\delta} + \mathbf{pp})\cdot[f_p\mathbf{pp} + f_T(\boldsymbol{\delta} - \mathbf{pp})]$ can be completed first because the tensors are symmetric.

$$[f_p\mathbf{pp} + f_T(\boldsymbol{\delta} - \mathbf{pp})] \cdot (\boldsymbol{\delta} + \mathbf{pp}) = 2f_p\mathbf{pp} + f_T(\boldsymbol{\delta} - \mathbf{pp}) \tag{3.42}$$

Replacing this product in Eq. (3.41) gives

$$\dot{\mathbf{r}}_c = \boldsymbol{\kappa}\cdot\mathbf{r}_c + \frac{1}{2z_a}\sum_{i=1}^{N}[2f_p\mathbf{pp} + f_T(\boldsymbol{\delta} - \mathbf{pp})] \cdot [\, s_i\boldsymbol{\kappa}:\mathbf{ppp} - s_i'\boldsymbol{\kappa}:\mathbf{p}_i'\mathbf{p}_i'\mathbf{p}_i' \,] \tag{3.43}$$

Using the same procedure on the fiber orientation equation (3.27)

$$\dot{\mathbf{p}} = \boldsymbol{\kappa}\cdot\mathbf{p} - \boldsymbol{\kappa}:\mathbf{ppp} + \frac{6}{L^2z_a}\sum_{i=1}^{N} s_i[f_p\mathbf{pp} + f_T(\boldsymbol{\delta} - \mathbf{pp})] \cdot [\, s_i\boldsymbol{\kappa}:\mathbf{ppp} - s_i'\boldsymbol{\kappa}:\mathbf{p}_i'\mathbf{p}_i'\mathbf{p}_i' \,] \cdot (\boldsymbol{\delta} - \mathbf{pp}) \tag{3.44}$$

The dot product of the tensors $[f_p\mathbf{pp} + f_T(\boldsymbol{\delta} - \mathbf{pp})] \cdot (\boldsymbol{\delta} - \mathbf{pp})$ leaves only the transverse terms in the equation, a significant simplification.

$$\dot{\mathbf{p}} = \boldsymbol{\kappa}\cdot\mathbf{p} - \boldsymbol{\kappa}:\mathbf{ppp} + \frac{6}{L^2\zeta_a}\sum_{i=1}^{N} s_i f_T\, [\, s_i\boldsymbol{\kappa}:\mathbf{ppp} - s_i'\boldsymbol{\kappa}:\mathbf{p}_i'\mathbf{p}_i'\mathbf{p}_i' \,] \cdot (\boldsymbol{\delta} - \mathbf{pp}) \tag{3.45}$$

Furthermore, the stress equation is simplified through the same process to include only the axial term of the coefficient tensor.

$$\boldsymbol{\tau}(\mathbf{p}) = \mu\dot{\boldsymbol{\gamma}} + \frac{nL^2}{12}\,\boldsymbol{\zeta}\cdot\boldsymbol{\kappa}:\mathbf{pppp}$$

$$+ n\sum_{i=1}^{N} s_i f_p\,[\,s_i\boldsymbol{\kappa}:\mathbf{ppp} - s_i'\boldsymbol{\kappa}:\mathbf{p}_i'\mathbf{p}_i'\mathbf{p}_i'\,]\cdot\mathbf{ppp} \tag{3.46}$$

In the case of the orientation and the stress, the effect a transversely isotropic interaction force coefficient tensor is actually nil. The orientation uses only the scalar coefficient from the transverse motion, and the stress uses only the scalar coefficient from the axial motion. This is to be expected actually, since axial motion will not rotate a fiber and the slender body can bear loads only along the axis. Therefore a scalar version of the interaction force coefficient will be suitable in all following computations.

Another possibility for interactions is two fibers approaching in the direction perpendicular to the plane defined by their orientation vectors. This motion would have the effect of changing the separation distance between the solid particles, and the contribution to the interaction force tensor would include a term in the $\mathbf{p}\times\mathbf{p}'$ direction from relative motion in the $\mathbf{p}\times\mathbf{p}'$ direction which is proportional to the inverse of the changing separation distance.

The scalar interaction force coefficients will be a function of the relative orientation of the test fiber and the interacting fiber. When the fibers lie at right angle to one another, the area of the contact is approximately d^2. As the angle between two fibers decreases the area of contact increases. Therefore, the scalar interaction coeficient is proportional to the inverse of the sine of the angle between the test fiber and the interacting fiber.

3.7 Fiber-Fiber Contact from Geometric Probability

The contact geometry for interactions with fibers having orientations $\mathbf{p}_i'$ at positions s_i and s_i' cannot be expressly given for calculation of equations like Eq.

(3.39). Fiber network geometry in a suspension of small particles is a stochastic variable. Contacts on the test fiber can be given only in terms of probabilities. This section details a method of statistically accounting for fiber-fiber crossings in the suspension, and using that description to determine the fiber microstructure effects on the suspension rheology.

A discrete sum over i intersecting fibers is not applicable for a fiber in an actual suspension; instead an integral of the probability of contact over the length of the test fiber, over the length of the intersecting fiber, and over all possible orientations for the intersecting fiber must serve to represent discrete contacts. Intersection probability increases with fiber length, fiber number fraction and with the angle between the fibers. In a suspension containing n fibers per unit volume, the expected number of fibers in a volume V is simply nV. If we restrict fiber orientations to lie nearly in a single plane, a common occurrence in thinner injection and compression molds, the probability of contact becomes clear. Contact probability is the probability of finding a fiber in a volume of fluid adjacent to the test fiber segment.

Consider an infinitesimal segment of the test fiber. If there exists a crossing at that point, an intersecting fiber segment will reside in the portion of effective medium just above or below the test fiber segment. The volume of that

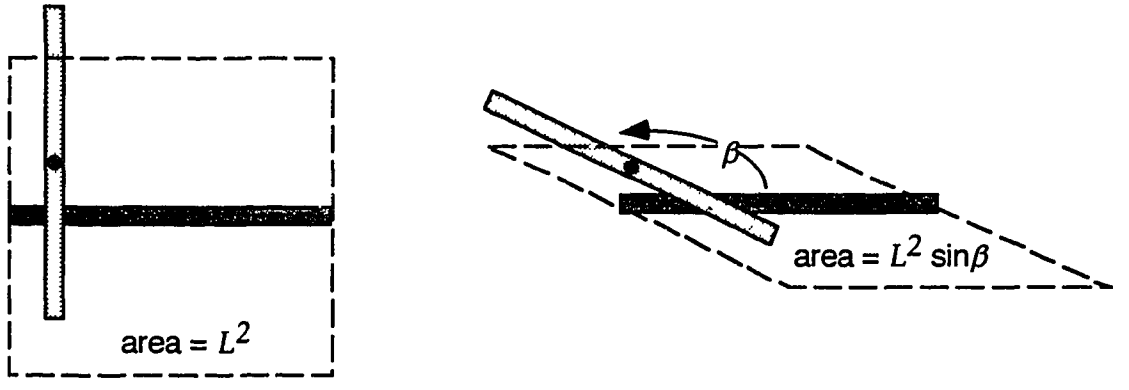

Figure 3.6 Two pairs of fibers with different relative orientations. Crossing is less likely as intersection angle leaves $\pi/2$.

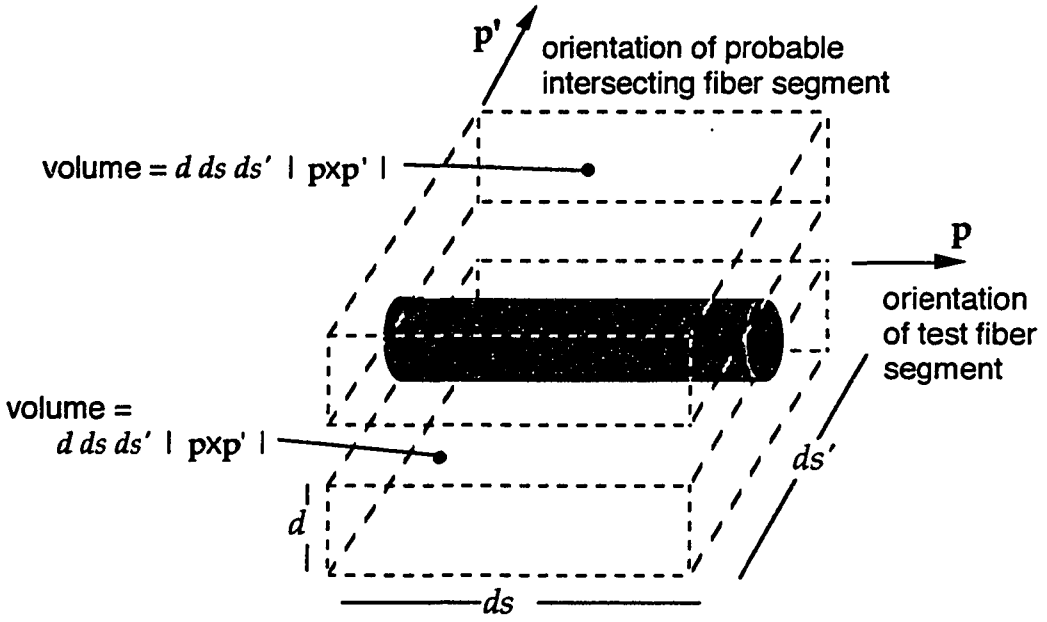

Figure 3.7 Test fiber segment. Crossing occurs if an interacting fiber segment lies in the volume of fluid above or below the test fiber segment.

portion will depend on the angle of intersection between the interacting fiber and the test fiber. Figure 3.6 demonstrates this geometrical relationship in a top view of the test fiber and an interacting fiber. The probability of contact with a fiber at 90° is higher than that for a fiber at some angle $\beta \neq \pi/2$. The area of the parallelogram that the interacting fiber centroid must lie in for crossing to occur is a maximum at $b = \pi/2$ and decreases to zero as β goes to zero or π.

Figure 3.7 shows the infinitesimal test fiber segment oriented at p. Above and below are volumes in the effective medium whose size are one fiber diameter thick by an area of $ds \times ds'$ multiplied by the absolute value of the sine of the angle between p and p'. The probability P of contact at a given segment on the test fiber equals that fluid volume multiplied by the number of fibers per unit volume times the fraction of fibers at the intersecting orientation.

$$P = 2n\,\psi(\mathbf{p})\,d\,ds\,ds'\;|\mathbf{p}\times\mathbf{p}'|\;d\mathbf{p}' \tag{3.47}$$

The total number of fiber interactions expected on the test fiber may be found by integrating this probability along the entire test fiber length, along the lengths of all possible interacting fibers and over all possible interaction orientations.

$$E(N) = \oint_{\mathbf{p}'}\int_{-L/2}^{+L/2}\int_{-L/2}^{+L/2} 2n\,\psi(\mathbf{p}')\,d\,ds\,ds'\;|\mathbf{p}\times\mathbf{p}'|\;d\mathbf{p}' \tag{3.48}$$

Equation (3.48) can be evaluated for random in-plane fiber orientation by using $\psi = \frac{1}{2\pi}$. The result of the integration gives the expected number of fiber-fiber crossings per fiber in a random in-plane fiber suspension.

$$E(N) = \frac{2c}{\pi}\frac{L}{d} \tag{3.49}$$

Equation (3.49) is identical to that of Kalmes and Corte [55] for 2D wood pulp networks (Eq. (2.49)).

3.8 Probabilistic Expressions for Fiber Motion and Suspension Stress

To this point, N had been assumed to be known for development purposes, but it is a random variable whose expected value can be calculated. The previous section showed how the probability of contact can predict the expected number of contacts on some test fiber of orientation p. All other functions of the random variables involving number and orientations of interacting fibers can be expressed in the same fashion, with integrals over the probability space of interaction replacing a sum of discrete interactions.

3.8.1 General Expressions

The probability integral can be substituted into the equation for fiber centroid translation. The integral is substituted for the sum in Eq. (3.24) to give the expected value of fiber translation.

$$E(\dot{\mathbf{r}}_c) = \boldsymbol{\kappa}\cdot\mathbf{r}_c + \frac{nd}{\zeta_a} \oint_{\mathbf{p}'} \int_{-L/2}^{+L/2} \int_{-L/2}^{+L/2} \psi(\mathbf{p}') \, |\mathbf{p}\times\mathbf{p}'| \, \mathbf{f}_I \cdot [\, s\boldsymbol{\kappa}:\mathbf{ppp} - s'\boldsymbol{\kappa}:\mathbf{p}'\mathbf{p}'\mathbf{p}' \,] \, ds \, ds' \, d\mathbf{p}' \cdot (\boldsymbol{\delta} + \mathbf{pp}) \tag{3.50}$$

Evaluation of this integral for any form of the distribution function yields a trivial result. The expected motion of the centroid is simply the dilute motion.

$$E(\dot{\mathbf{r}}_c) = \boldsymbol{\kappa}\cdot\mathbf{r}_c \tag{3.51}$$

All of the effects of interactions have been averaged out of the picture in Eq. (3.51). The same situation develops when evaluating the integral expression for fiber motion. The orientation behavior of the test fiber in the suspension is a function of random fiber interactions as well as straining fluid

$$E(\dot{\mathbf{p}}) = \boldsymbol{\kappa}\cdot\mathbf{p} - \boldsymbol{\kappa}:\mathbf{ppp} + \frac{12nd}{L^2\zeta_a} \oint_{\mathbf{p}'} \int_{-L/2}^{+L/2} \int_{-L/2}^{+L/2} \psi(\mathbf{p}') \, |\mathbf{p}\times\mathbf{p}'| \, \mathbf{f}_I \cdot [\, s^2\boldsymbol{\kappa}:\mathbf{ppp} - ss'\boldsymbol{\kappa}:\mathbf{p}'\mathbf{p}'\mathbf{p}' \,] \, ds \, ds' \, d\mathbf{p}' \cdot (\boldsymbol{\delta} - \mathbf{pp}) \tag{3.52}$$

This integral too is identically equal to zero for any distribution function.

$$E(\dot{\mathbf{p}}) = \boldsymbol{\kappa}\cdot\mathbf{p} - \boldsymbol{\kappa}:\mathbf{ppp} \tag{3.53}$$

The *expected* orientation behavior of a fiber in a suspension with multiple fiber-fiber interactions is simply the dilute motion.

The stress equation including the integral of probable interactions from neighboring fibers in the suspension is

$$E(\tau(\mathbf{p})) = \dot{\mu\gamma} + \frac{nL^2}{12}\,\boldsymbol{\zeta}\cdot\boldsymbol{\kappa}:\mathbf{pppp} + 2n^2d \oint_{\mathbf{p}'}\int_{-L/2}^{+L/2}\int_{-L/2}^{+L/2} \psi(\mathbf{p}')\,|\mathbf{p}\times\mathbf{p}'|\, \mathbf{f}_1\cdot[\, s^2\boldsymbol{\kappa}:\mathbf{ppp} - ss'\boldsymbol{\kappa}:\mathbf{p}'\mathbf{p}'\mathbf{p}'\,]\, ds\, ds'\, d\mathbf{p}'\cdot\mathbf{ppp} \tag{3.54}$$

The integral term in this equation is *not* identically equal to zero for any distribution function. Mechanical fiber-fiber interaction in non-dilute suspension will cause an increase in the stress in a non-dilute suspension.

3.8.2 Results for Random-in-Plane Orientation

As a means of examining these expressions for suspension stress and fiber motion analytically, we now consider the special case where fibers are randomly distributed in space and randomly oriented parallel to a single plane. Furthermore, in order to extract an analytical expression for expected stress about the test fiber, we will simplify the hydrodynamic inter-fiber friction tensor to a scalar constant f_1. The expected values for test fiber motion remain the same as

that seen in Eq.s (3.53) and (3.51). Yet with these stipulations, the equation for stress simplifies to a more elucidating form.

$$E(\tau(p)) = \mu\dot{\gamma} + \frac{nL^2}{12}\zeta\cdot\kappa{:}pppp + \frac{n^2dL^4f_1}{12}\kappa{:}pppp \tag{3.55}$$

Two observations can be made regarding this equation. One, the inclusion of mechanical interactions produces a new term in the stress expression (third of the right-hand side of Eq. (3.55)), a term that is second order in fiber number fraction. In that respect, this result is analogous to constitutive equations for non-dilute suspensions of interacting spheres. Two, the interaction term has the same functionality with respect to suspension kinematics and test fiber orientation (κ:pppp) as the fiber-fluid term. Therefore, simplified theories like those of Dinh and Armstrong [38] or Batchelor [50] could accommodate fiber-fiber contact through a modified hydrodynamic fluid drag tensor ζ.

3.8.3 Orientation Averaging for Suspension Stress

This theory for non-dilute suspensions including fiber-fiber interactions was developed using a cell model or test fiber approach. To this point we have concerned ourselves only with the behavior of the test fiber and the suspension in its immediate vicinity. In order to predict the stress in the continuum which represents the macroscopic behavior of the suspension, Eq. (3.47) for stress in the cell about the test fiber must be integrated over all possible orientations of the generalized "test fiber."

$$E(\tau) = \oint_p \psi(p)\, E(\tau(p))\, dp \tag{3.56}$$

For a random in-space distribution and random in-plane orientation the result for stress is

$$E(\tau(p)) = \mu\dot{\gamma} + \frac{nL^2}{12}\zeta\cdot\kappa:\langle pppp\rangle + \frac{n^2dL^4f_1}{12}\kappa:\langle pppp\rangle \qquad (3.57)$$

In Eq. (3.57) the angle brackets indicate an ensemble average over all possible values for the fourth-order dyadic product of the orientation vector. This is the fourth order orientation tensor of the suspension as described by Advani and Tucker [11].

Discussion of the macroscopic behavior of the individual fiber motion is not meaningful. Test fiber rotation and translation is only pertinent at the microscopic level, at the level of the fiber, not at the macroscopic level of the continuum representation of the suspension. Rather, the orientation distribution function and the fiber number fraction are macroscopic variables which will change with respect to time and position. These require their own conservation equations which are discussed in the following section.

3.9 Conservation Equation for Orientation Probability

The work discussed thus far demonstrated expressions for the expected values of the stress state and fiber motion in suspension. These were derived from the averaged quantities for interaction, and produced trivial results for fiber motion. The effects of interaction simply averaged out. But, no single fiber in the network will experience precisely the average interaction effect. The stochastic nature of the fiber network will introduce variance in the interactions upon a fiber. This will lead to variance in the dependent quantities of stress, fiber orientation and fiber translation.

Variance in the factors that influence fiber orientation are the mechanistic basis for what Folgar and Tucker [44] proposed as *orientational diffusion.* Fiber orientation is a stochastic variable, given in terms of a probability distribution function ψ. The evolution of a stochastic variable is described by the Fokker-Planck equation (e.g. Reif [55]).

$$\frac{D\psi}{Dt} = -\frac{\partial}{\partial \mathbf{p}} \cdot [\mathbf{A}(\mathbf{p})\psi(\mathbf{p})] + \frac{1}{2}\frac{\partial^2}{\partial \mathbf{p}^2} : [\mathbf{D}(\mathbf{p})\psi(\mathbf{p})]. \tag{3.58}$$

In this equation, A(p) and D(p) are defined as follows.

$$\mathbf{A}(\mathbf{p}) = \lim_{\tau \to 0} \frac{E(\Delta \mathbf{p})}{\tau} \tag{3.59}$$

$$\mathbf{D}(\mathbf{p}) = \lim_{\tau \to 0} \frac{E(\Delta \mathbf{p}^2)}{\tau} \tag{3.60}$$

Here $\Delta \mathbf{p}$ represents the random orientational change of a fiber over a time t. In Eq. (3.52), the expected value of the orientation change in a small time is the expected value of $\dot{\mathbf{p}}$ (as in Eq. (3.46)). A(p) is therefore named the advection vector. D(p) is the expected value of the square of the angle change possible in τ. It is called the diffusion tensor, and can be expressed as $\varepsilon \mathrm{Var}(\dot{\mathbf{p}})$, where ε is a time scale over which the interaction geometry (number and position of contacts) is uncorrelated. Appendix B details the derivation of $\mathbf{D}(\mathbf{p}) = \varepsilon \mathrm{Var}(\dot{\mathbf{p}})$. A(p) has already been calculated in Eq. (3.46), and $\mathrm{Var}(\dot{\mathbf{p}})$ is derived similarly according to the definition of statistical variance. The diffusion function is given as the integral

$$\mathbf{D(p)} = \frac{72\varepsilon nd}{L^2\zeta_a^2} \oint_{\mathbf{p}'} \int_{-L/2}^{+L/2} \int_{-L/2}^{+L/2} \psi(\mathbf{p}') \, |\mathbf{p}\times\mathbf{p}'| \, \{ \mathbf{f_1} \cdot [s^2\boldsymbol{\kappa}:\mathbf{ppp} - ss'\boldsymbol{\kappa}:\mathbf{p}'\mathbf{p}'\mathbf{p}'] \cdot (\boldsymbol{\delta} - \mathbf{pp}) \}^{II} ds \, ds' \, \mathbf{dp}' \tag{3.61}$$

Here the superscript ^{II} indicates a dyadic product of the vector term in the curly brackets with itself. Using this particular form of the advection-diffusion equation, the time evolution of the orientation state ψ can be solved for any given suspension kinematics.

The random variables of interaction will influence fiber orientation, and they will fluctuate over small time increments. The correlation time e is a measure of those small time scales of fluctuation. It is calculated from the correlation function (Eq. 2.46) for orientation behavior.

$$C(t_2 - t_1) = \frac{\langle (\dot{\mathbf{p}}(t_2) - \langle \dot{\mathbf{p}} \rangle)(\dot{\mathbf{p}}(t_1) - \langle \dot{\mathbf{p}} \rangle) \rangle}{\langle (\dot{\mathbf{p}}(t_1) - \langle \dot{\mathbf{p}} \rangle)^2 \rangle} \tag{3.62}$$

Initially, the correlation function is equal to one and it decreases to zero as t_2 goes to infinity. The correlation time measures speed at which the correlation function shrinks to zero. e is the integral of the correlation function over time from $t_2 = t_1$ to $t_2 = \infty$.

$$\varepsilon = \int_{t2=t1}^{t2=\infty} C(t_2 - t_1) \, dt_2 \tag{3.63}$$

This integral is not evaluated explicitly for concentrated suspensions of rigid rods. The magnitude of the correlation time is proportional to the inverse of the scalar magnitude of the strain rate. Faster motion in the suspension means shorter times over which interaction geometries change. Furthermore, correlation time is proportional to the inverse of the number of fibers in the neighborhood of the test fiber. More fibers nearby mean more opportunities for the interaction geometry to be altered. Therefore, the correlation time used in the diffusion function (Eq. 3.61) will have the following dependencies.

$$\varepsilon \propto \frac{1}{\sqrt{\frac{1}{2}\dot{\gamma}:\dot{\gamma}^{T}}} \left(\frac{1}{ndL^2}\right) = (\dot{\gamma}_{II} ndL^2)^{-1} \tag{3.64}$$

Three factors are involved in the fiber orientation. Always present is the fluid motion, acting to align the fibers. Random mechanical fiber-fiber interactions will tend to disorient fibers, adding a mechanical dispersion, spreading the distribution function. As the concentration is increased, the magnitude of the mechanical interaction force will increase as fiber-fiber crossing becomes more frequent. Yet as the concentration is increased, variance in the interaction forces betweeen the fibers will decrease. This will tend to lessen the dispersive effect of mechanical interaction. Dispersion effects that increase and then decrease with concentration have been observed in the literature [26,44].

The spatial fiber distribution can be treated in the same fashion as the orientation. These calculations will reveal the effect of particle interactions on phenomenon such as fiber agglomeration or non-uniform dispersal. In this case we are concerned with a fiber number fraction which is a function of position $n(\mathbf{r})$. The Fokker-Planck equation in this case has the form

$$\frac{Dn}{Dt} = -\frac{\partial}{\partial \mathbf{r}} \cdot [\mathbf{A}_n(\mathbf{r}) n(\mathbf{r})] + \frac{1}{2}\frac{\partial^2}{\partial \mathbf{r}^2} : [\mathbf{D}_n(\mathbf{r}) n(\mathbf{r})] \tag{3.62}$$

The number fraction advection vector is the expected value of the centroid motion given in Eq. (3.44).

$$\mathbf{A}_n(\mathbf{r}) = \boldsymbol{\kappa} \cdot \mathbf{r} \tag{3.63}$$

The number fraction diffusion tensor is the variance of the centroid motion multiplied by the correlation time.

$$\mathbf{D}_n(\mathbf{r},\mathbf{p}) = \frac{\varepsilon n d}{2\zeta_a^2} \oint_{\mathbf{p}'} \int_{-L/2}^{+L/2} \int_{-L/2}^{+L/2} \psi(\mathbf{p}') \, |\mathbf{p}\times\mathbf{p}'| \, \{ \mathbf{f}_\parallel \cdot [\, s\boldsymbol{\kappa}:\mathbf{ppp} - s'\boldsymbol{\kappa}:\mathbf{p}'\mathbf{p}'\mathbf{p}' \,] \cdot (\boldsymbol{\delta} + \mathbf{pp}) \}^{II} ds \, ds' \, d\mathbf{p}' \tag{3.64}$$

Equations (3.58) and (3.62) are the governing equations for the macroscopic variables that are concerned with the microstructure of the composite suspension. The number fraction of fibers and the orientation of those fibers are critically important to the rheology of the suspension and to the mechanics of the solid composite. Therefore, transport equations are needed to describe the evolution of the microstructure during processing. Inspection of these equations (3.58) and (3.62) together with the momentum transport equation (3.54) reveals that they are all coupled. Kinematics produce stress which produces reorientation which alters kinematics, *etc.*.

3.10 Summary

This chapter details the governing equations for a fluid with an internal structure. Processing of fiber reinforced polymer composites is related to the rheology of concentrated fiber suspensions. Within a concentrated or non-dilute suspensions of long slender particles, particle-particle interactions are highly probable. The effects of these interactions are here incorporated into a theory for the evolution of the structure and the stress in the suspension.

Mechanical fiber-fiber interactions cause an increase in the normal stresses in the suspension. Mechanical fiber-fiber interactions induce dispersive fiber velocities resulting in a diffusive effect in the probability distribution function describing the orientation. Both of these phenomena have been witnessed experimentally and are reported in Chapter Two.

4. NUMERICAL SIMULATION OF CONCENTRATED SUSPENSION THEORY

This chapter describes numerical solutions to the theory for concentrated suspensions of interacting fibers. The equations for suspension stress and fiber orientation distribution typically have no analytical solution, therefore a numerical approximation is an appropriate means to determine the behavior of the governing equations. The numerical work detailed in this chapter is focused on a solution to the conservation equation for orientation, Eq. (3.58). This equation is solved for planar fiber orientation states where the orientation can be described by only a single Eulerian angle ϕ ($\theta = \pi/2$). (See Figure 2.1.)

The governing equations developed in Chapter Three are given in terms of the general 3D orientation vector $\mathbf{p}$, and by that virtue the theory is properly invariant under coordinate rotation. The simplified 2D planar equations in terms of ϕ are presented in Appendix C, and the orientation conservation equation is Eq. (C 6). These are *not* properly invariant in that they must rely on a specific plane of fiber orientation being known *a priori*. Even so, the restriction allows a significant simplification and economy in the numerical solution, as well as facilitating clearer visualization of the results.

The goal of the work described in this chapter is to calculate transient and steady state behavior of the advection-diffusion equation for orientation distribution function. Orientation results are given for planar flows in shear, elongation, and combinations thereof. Viscometric functions of the suspensions under strain are also presented.

4.1 Formulation of the Finite Difference Solution

4.1.1 Governing Equations

The equation of conservation of orientation is a special form of the advection-diffusion equation.

$$\frac{D\psi}{Dt} = -\frac{\partial}{\partial\phi}[A_\phi(\phi)\psi(\phi)] + \frac{1}{2}\frac{\partial^2}{\partial\phi^2}[D_\phi(\phi)\psi(\phi)] \tag{4.1}$$

The subscripts ϕ will be henceforth dropped from A and D for the sake of simplicity and clarity.

The harmonic character of the domain and the nature of the probability distribution function are well served by the flux-conservative form of this equation in the numerical solution. The change in the probability distribution or the fraction of fibers at ϕ is due only to orientation moving into or out of the differential volume about ϕ. The amount of orientation probability multiplied by the velocity with which it is carried is the *flux*.

$$\frac{D\psi}{Dt} = -\frac{\partial}{\partial\phi}\{\text{Flux}(\phi)\} \tag{4.2}$$

Transformation of Eq. (4.2) into this form gives

$$\frac{D\psi}{Dt} = -\frac{\partial}{\partial\phi}\left\{A(\phi)\psi(\phi) - \frac{1}{2}\frac{\partial}{\partial\phi}[D(\phi)\psi(\phi)]\right\} \tag{4.3}$$

It is elucidating to differentiate the second term on the right-hand-side of Eq. (4.3) into two parts.

$$\frac{D\psi}{Dt} = -\frac{\partial}{\partial\phi}\left\{A(\phi)\psi(\phi) - \frac{1}{2}D(\phi)\frac{\partial}{\partial\phi}[\psi(\phi)] - \frac{1}{2}\psi(\phi)\frac{\partial}{\partial\phi}[D(\phi)]\right\} \tag{4.4}$$

The right hand side of this equation has an advection term and a standard diffusion term similar to those seen in mass or heat transfer. The third term in the curly brackets is a second diffusion-derived term. Its existence is due to the fact that the interaction-driven diffusion term $D(\phi)$ is a function of the orientation. This creates a flux of oriented fibers due to the non-constant fiber dispersion effects of fiber-fiber interaction. To summarize, the flux in the curly bracket is comprised of three terms. By dividing each by the distribution function, an *orientation velocity* results.

Advective velocity: $A(\phi)$

Diffusion velocity: $D_v(\phi) \equiv \frac{D(\phi)}{\psi(f)} \frac{\partial}{\partial \phi}[\psi(\phi)]$

Interaction velocity: $I_v(\phi) \equiv \frac{\partial}{\partial \phi}[D(\phi)]$

The fully-explicit finite-difference form of Eq. (4.2) is written as follows

$$\frac{\psi_{i+1}^{m} - \psi_{i}^{m}}{\Delta t} = -\frac{1}{\Delta \phi}\left[\text{Flux}^{m+1/2}_{i} - \text{Flux}^{m-1/2}_{i}\right] \tag{4.5}$$

The superscript index ^{m} denotes position and the subscript index $_{i}$ denotes time within the finite difference scheme. The flux is derived from the terms in the curly brackets of Eq. (4.3). The flux out of the finite difference grid point is evaluated as follows.

$$\text{Flux}^{m+1/2}_{i} = \frac{[A^{m+1}_{i}\psi^{m+1}_{i} + A^{m}_{i}\psi^{m}_{i}]}{2} - \frac{1}{2}\frac{[D^{m+1}_{i}\psi^{m+1}_{i} - D^{m}_{i}\psi^{m}_{i}]}{\Delta \phi} \tag{4.6}$$

The flux into the grid point is

$$\text{Flux}^{m-1/2}_{i} = \frac{[A^{m}_{i}\psi^{m}_{i} + A^{m-1}_{i}\psi^{m-1}_{i}]}{2} - \frac{1}{2}\frac{[D^{m}_{i}\psi^{m}_{i} - D^{m-1}_{i}\psi^{m-1}_{i}]}{\Delta\phi} \tag{4.7}$$

Fully explicit time differencing of transient problems is prone to numerical instability problems, and small time steps are required to retain well mannered solutions. A two-step predictor-corrector method is used in this work to avoid such difficulties. This method requires making an initial calculation for the time derivative of the probability distribution function. Then, rather than using that number to move to *time* = i+1, the calculation is remade at *time* = i+1/2. The time derivative of ψ found at i+1/2 is used to step ψ from i to i+1.

In equations, this process first needs the probability distribution function at the intermediate time step.

$$\psi^{m}_{i+1/2} = \left(\frac{D\psi}{Dt}^{m}_{i}\right)\frac{\Delta t}{2} + \psi^{m}_{i} \tag{4.8}$$

Next, the temporary value of ψ is used to correct the derivative of the distribution function and calculate the new value of ψ.

$$\psi^{m}_{i+1} = \left(\frac{D\psi}{Dt}^{m}_{i+1/2}\right)\Delta t + \psi^{m}_{i} \tag{4.9}$$

This is also known as a second-order Runge-Kutta method. Higher order predictor-corrector methods exist which often provide more economical explicit time differencing. In spite of this fact the primary computing time requirement in this problem is the integration of the diffusion function $D(\phi)$, and integration must be performed with each prediction and each correction.

The diffusion term is integrated at each orientation over all possible orientations of the interacting fibers. The analytical diffusion integral is derived in Chapter Three and simplified for planar orientation in Appendix C.

$$D(\phi) = 4\varepsilon n d L^2 f_I^2 \zeta_a^{-2} \int_0^{\pi} \psi(\phi) \sin|\phi - \phi'| \left[\cos^2\phi' \frac{\partial v_x}{\partial x} + \sin^2\phi' \frac{\partial v_y}{\partial y} + \cos\phi' \sin\phi' \left(\frac{\partial v_x}{\partial y} + \frac{\partial v_y}{\partial x}\right)\right]^2 d\phi' \qquad (4.10)$$

This is the diffusion integral after integration over the lengths of the interaction and test fibers has been executed with a constant n (uniform spatial orientation). This equation for the diffusion function uses the scalar fiber-fiber interaction force coefficient, which is proportional to $[\sin(\phi - \phi')]^{-1}$. The sin(...) term accounts for the variation in area of interaction as the relative orientation between test fiber and interacting fiber changes. If $g(\phi,\phi',t)$ represents the integrand of Eq. 4.10, the numerical representation of the integrand is $g_i^{m\,n}$, where ^{n} signifies the grid points of the interacting fibers, we write the numerical integration as a sum. The numerical integration is performed over all ^{n} using the trapezoidal rule.

$$D_i^m = \sum_{n=0}^{\frac{\pi}{\Delta\phi}-1} \frac{1}{2}\left[g_i^{m\,n} + g_i^{m\,n+1}\right]\Delta\phi \qquad (4.11)$$

where $g_i^{m\,n}$ takes the form

$$g_i^{m\,n} = 4\varepsilon n d L^2 f_i^2 \zeta_a^{-2} \psi_i^m \sin|\phi^m - \phi^n|$$

$$\left[\cos^2\phi^n \frac{\partial v_x}{\partial x} + \sin^2\phi^n \frac{\partial v_y}{\partial y} + \cos\phi^n \sin\phi^n \left(\frac{\partial v_x}{\partial y} + \frac{\partial v_y}{\partial x}\right)\right]^2 \qquad (4.12)$$

Equations (4.6) and (4.11) make up the equations solved by the finite difference simulation.

4.1.2 Boundary and Initial Conditions

The domain of the equation for conservation of orientation in three dimensions is the surface of the unit sphere. For a planar orientation, the domain is the boundary of a unit circle; fibers may be oriented at any angle $0 \le \phi \le 2\pi$. Yet, fibers at π are indistinguishable from those at 0 or 2π. Therefore, it is useful to consider only the domain of orientation as $0 \le \phi < \pi$ where fibers at some angle ϕ^* are equivalent to those at $\phi^* + \pi$. Furthermore, the boundary conditions on $\psi(\phi)$ are harmonic. That is,

$$\psi(\pi) = \psi(0) \qquad (4.13a)$$

$$\frac{\partial}{\partial\phi}\psi(\pi) = \frac{\partial}{\partial\phi}\psi(0) \qquad (4.13b)$$

The initial conditions required for the numerical solution are simply a specification of $\psi(\phi)$ the orientation state at time equal zero, the onset of strain on the suspension. The orientation in polymer composite suspensions will often be random at the beginning of processing and thus while any initial orientation state is possible we will begin from a random-in-plane orientation. In that case, ψ is a constant equal to $\frac{1}{2\pi}$.

4.1.3 Problem Parameters

Solutions of the difference equations require certain suspension and kinematic data. Velocity gradients are the key to fiber rotation, and they must be specified. The theory and thus the numerical code requires the planar velocity gradients $\frac{\partial v_x}{\partial x}$, $\frac{\partial v_y}{\partial y}$, $\frac{\partial v_x}{\partial y}$, and $\frac{\partial v_y}{\partial x}$ in the input file. We will examine the behavior of the solutions for shear and stretching flows as well as combinations of each.

The fiber-fiber interaction force coefficient describes the magnitude of the hydrodynamic friction between two fibers at a separation distance of less than or equal to d. The strain rate in the fluid between the interacting fibers is therefore greater than or equal to $\frac{v^{relative}}{d}$. The suspending fluid viscosity is μ, and the area of interaction between the two fibers goes like $d^2\sin(\phi-\phi')$. Therefore, the interaction force coefficient can be expressed as $f_I \geq \frac{\mu d}{\sin(\phi-\phi')}$.

The hydrodynamic drag tensor is characterized by the axial drag coefficient ζ_a. Burgers [28] calculated $\zeta_a = L\mu$ in slender body theory. The correlation time ε is related to the inverse of the frequency of new interactions on the test fiber. The frequency of interactions must be proportional to the strain rate $\dot{g}_{II}$, the aspect ratio of the fibers L/d, and the number of fibers in the suspension near the test fiber nL^2d. At the same time, an increase in the number of interacting fibers on the test fiber will lessen the significance of each individual interaction thereby increasing the correlation time (from Eq. 2.49, number of interactions = $2nL^2d/\pi$). Therefore, in a concentrated suspension where the number of fiber crossings per fiber is greater than one, the time over which the interaction geometry is uncorrelated has the following form.

$$\varepsilon = O\left[\dot{\gamma}_{II}^{-1} \frac{d}{L} \frac{1}{nLd^2} \frac{2nL^2d}{\pi} \right] = O\left[\dot{\gamma}_{II}^{-1} \frac{2d}{\pi L} \right] \tag{4.14}$$

This relation is pleasantly simple but strictly an approximation of the size of the correlation time. The experimental work detailed in Chapter Five will in part be devoted to assessing this assertion about the correlation time.

4.2 Numerical Results

This section demonstrates the numerical behavior of the mechanistic-interaction fiber orientation model. Here we examine predictions for probability distribution function and the components of the its governing equation (Eq. 4.1) according to the suspension dynamics described in the previous chapters. Flows found during processing of short-fiber reinforced polymer composites can be generally considered to be combinations of shear and stretching. Therefore, the response of concentrated suspensions of fibers in shear and elongation are studied.

4.2.1 Shearing Flow

The numerical model described in the preceding sections of this chapter is exercised for an suspension described initially by a random-in-plane orientation distribution function in a planar shear flow. In this case the velocity field is

$$v_x = 0; \qquad v_y = \dot{\gamma}_{II} x \qquad v_z = 0 \tag{4.15}$$

The results shown in Figures 4.1-4.7 were generated using the parameters given in Table 4.1.

Figure 4.1 shows the evolution of the probability distribution function y. The distribution function is initially uniform for all orientation angles (i.e. random, in-plane orientation). The fibers in the suspension are rotated by the

Table 4.1 Input parameters for numerical simulation of flow and orientation of a concentrated suspension with fiber-fiber interactions

Parameter	Symbol	Value	Units
scalar strain rate	$\dot{\gamma}_{II}$	0.25	1/s
number density	n	6.82e9	$1/m^3$
fiber length	L	12.7e-3	m
fiber diameter	d	152.4e-6	m
suspending fluid viscosity	μ	1.0	Pa·s
interaction force coefficient	f_I	30.0e-3	Pa·s·m
hydrodynamic force coefficient	ζ_a	12.7e-3	Pa·s·m
interaction correlation time	ε	0.01	s
time step size	Δt	0.01	s
angular step size	$\Delta\phi$	$\pi/30$	radians

straining motion that has been imposed on the system. Soon the largest fraction of fibers are oriented primarily in the direction of the y axis where $\phi = \pi/2$.

The peak of the probability distribution function is skewed away from $\phi = \pi/2$ due to the fact that shearing flow has an asymmetric rotational component. While the slender fibers that lie perfectly in the streamline will experience zero hydrodynamic torque, the slightest alignment away from $\phi = \pi/2$ results in very different behaviors depending on the sign of the angular disturbance. The fiber whose orientation is displaced $-\Delta\phi$, or towards the direction of principle positive normal strain rate is rotated back towards the streamline. Meanwhile, fibers which are displaced $+\Delta\phi$ are rotated away from the streamline until the fiber has rotated 180°.

Figure 4.2 shows profiles of the distribution function at selected times during the simulation. For the flowing suspension in Figure 4.2, time equals four (4) seconds and 32 seconds are equivalent to the scaled times $\dot{\gamma}_{II}t$ of Figure 4.1 of one (1) and eight (8) respectively. Scaling the time by the magnitude of the

strain rate (in this case $\dot{\gamma}_{II} = 0.25\ s^{-1}$) gives an indication of the magnitude of the total strain in the suspension.

The orienting strength of the advective contribution to the probability distribution function is given in Figure 4.3. This is the fiber rotation that Jeffrey [28] calculated, given by Eq. (2.31). The angular velocity of fibers oriented at right angles to the streamlines is maximum, while fiber parallel to the streamlines experience no effect of the rotational component of the strain in the suspension.

The diffusion orientation velocity, shown in Figure 4.4, shows the disorienting effect of fiber-fiber interactions. While the fibers are aligned by the shearing motion, they are hindered and dispersed by the interaction forces between the fibers. Figure 4.5 shows the interaction orientation velocity. This term exists as a result of the fact that the strength of the diffusion changes with orientation.

In Figure 4.6 are displayed the simulation results for the diffusion function $D(\phi,t)$. The diffusion is used in the orientation calculations, and it is itself a function of the orientation and requires a numerical integration over every node, at every node, and at every time step. The result is a diffusion that is smallest in the direction aligned with highest orientation probability density. This distinctive shape is the result of a pair of factors. The interactions that create the diffusion effect are more numerous for fibers oriented away from the streamlines. Meanwhile, interaction forces *from* fibers oriented perpendicular to the streamlines will be largest, due to the fact that they have the largest advective angular velocity. The interaction velocity in the probability flux term is a result of the changing magnitude of the diffusion.

Orientation tensors are a compact means of describing the state of the fiber orientation in a suspension of fibers. The terms of the two-dimensional second

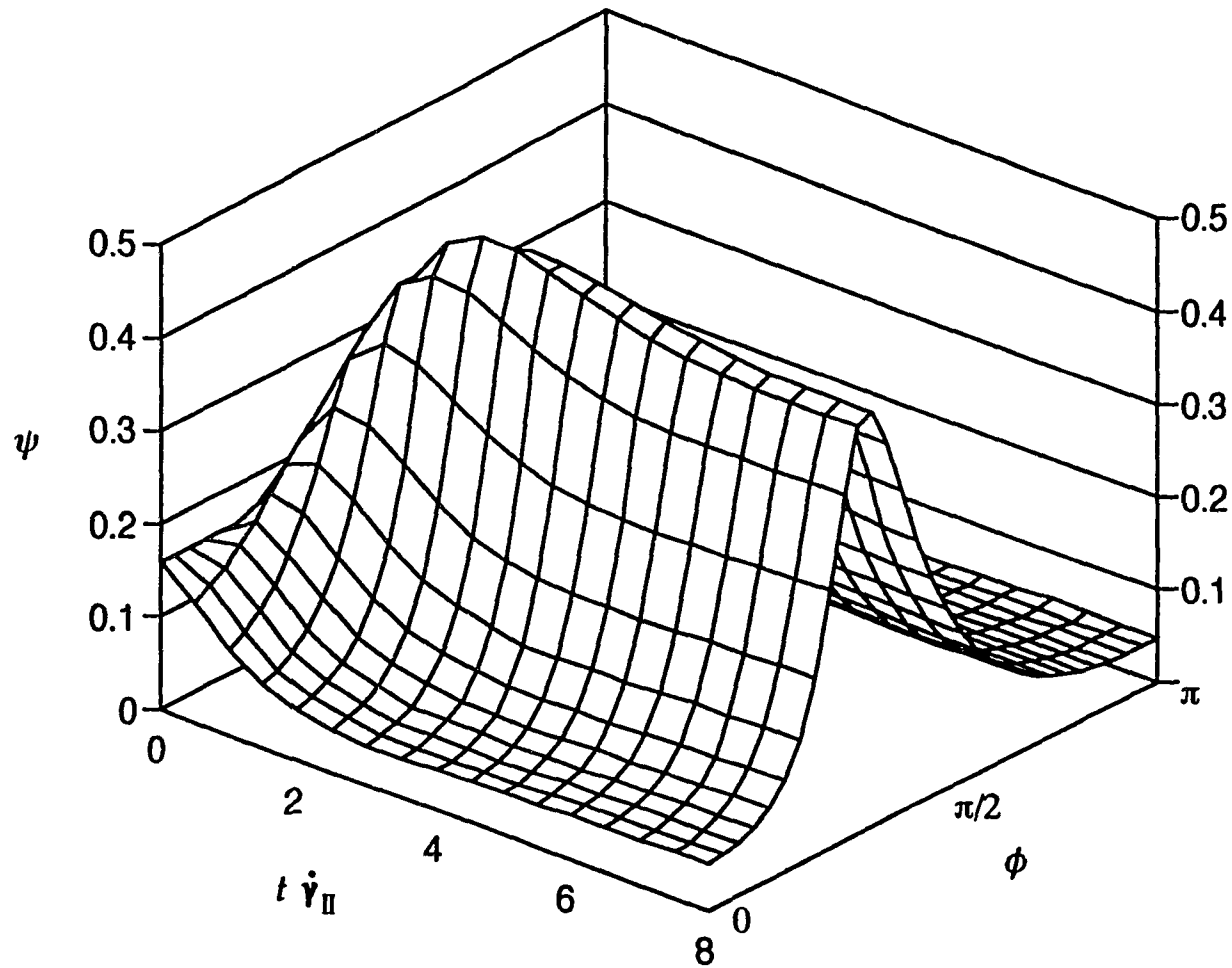

Figure 4.1 The probability distribution of fiber orientation ψ in a suspension of rigid rods undergoing planar shear flow. ψ is shown as a function of orientation angle and time scaled by the magnitude of the strain rate in the suspension. Suspension properties and other parameters used in the simulation are given in Table 4.1.

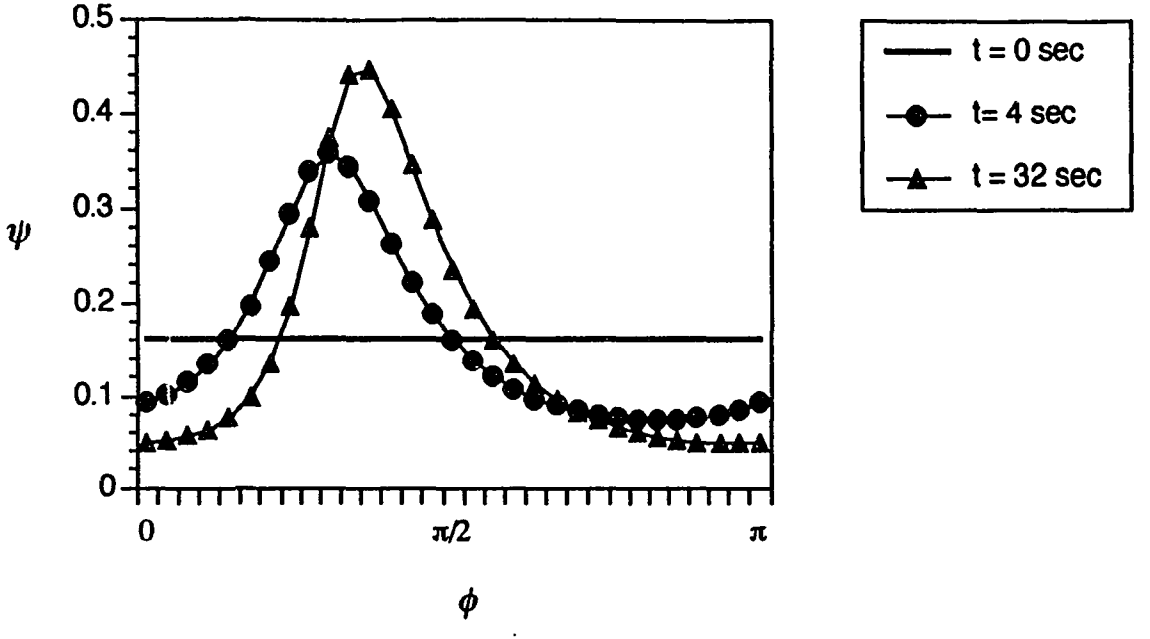

Figure 4.2 The probability distribution of fiber orientation ψ in a suspension of rigid rods undergoing planar shear flow. ψ is shown as a function of orientation angle for three different times. Suspension properties and other parameters used in the simulation are given in Table 4.1.

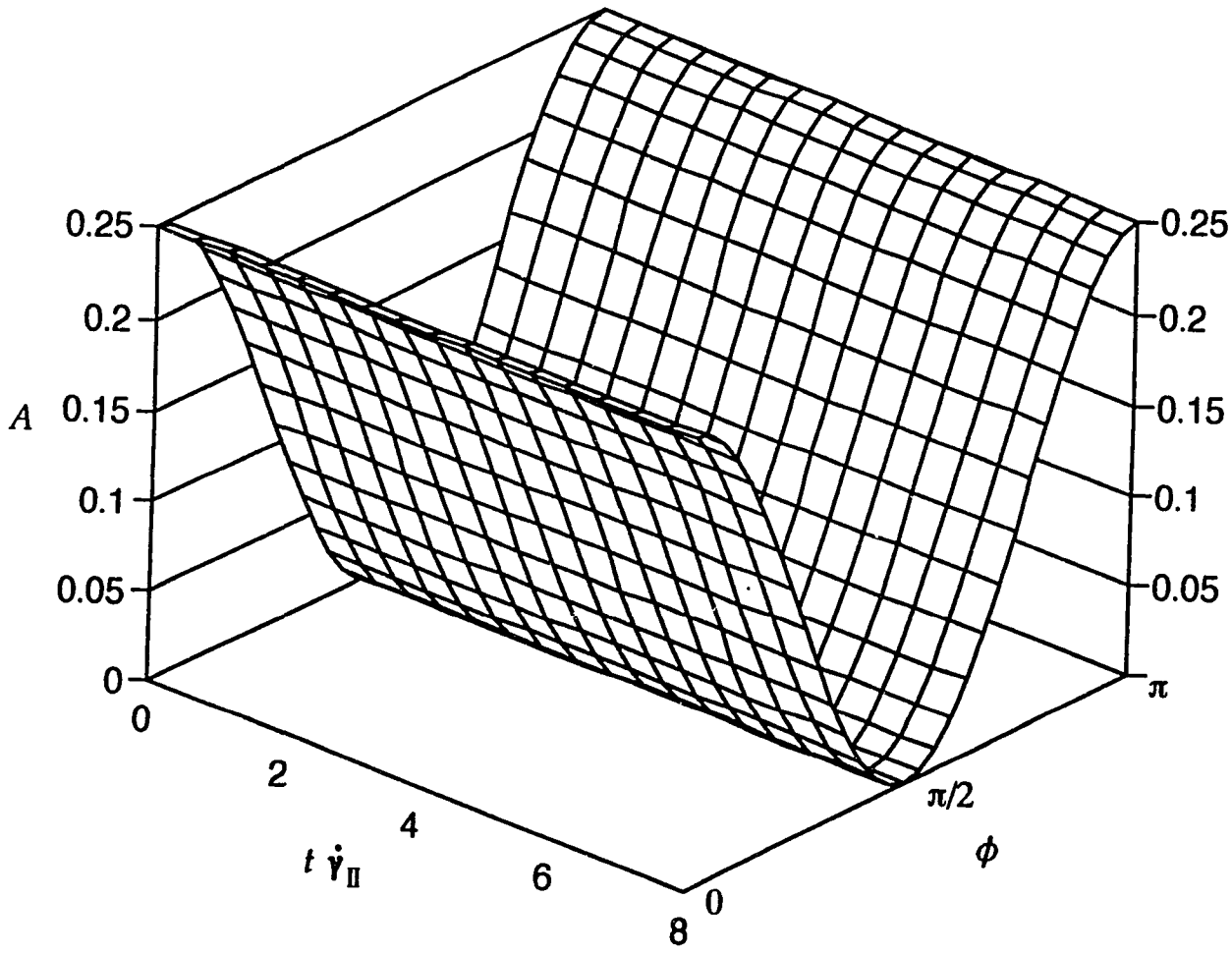

Figure 4.3 The convective orientation probability velocity A in a suspension of rigid rods undergoing planar shear flow. A is shown as a function of orientation angle and time scaled by the magnitude of the strain rate in the suspension. Suspension properties and other parameters used in the simulation are given in Table 4.1.

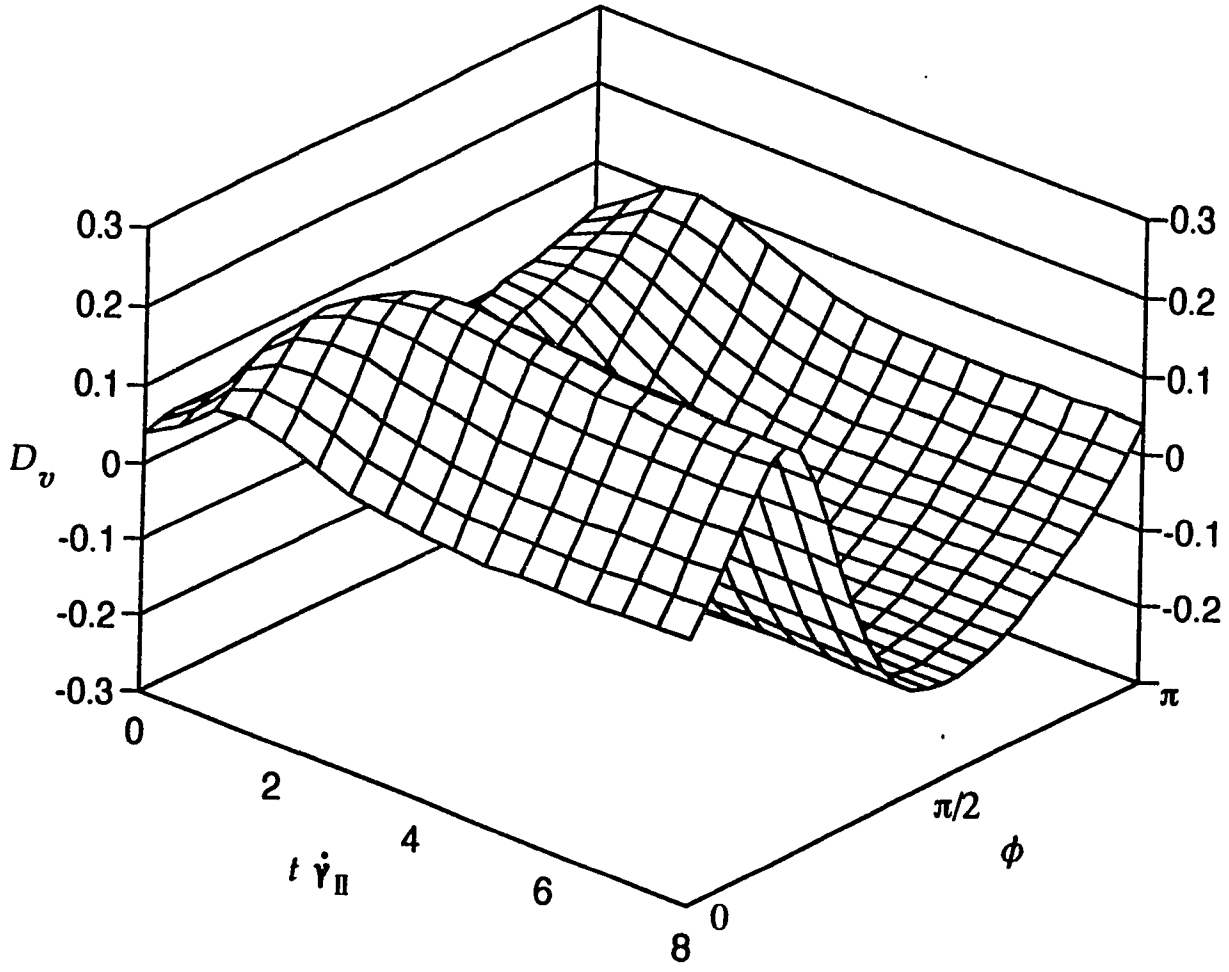

Figure 4.4 The diffusion orientation probability velocity D_v in a suspension of rigid rods undergoing planar shear flow. D_v is shown as a function of orientation angle and time scaled by the magnitude of the strain rate in the suspension. Suspension properties and other parameters used in the simulation are given in Table 4.1.

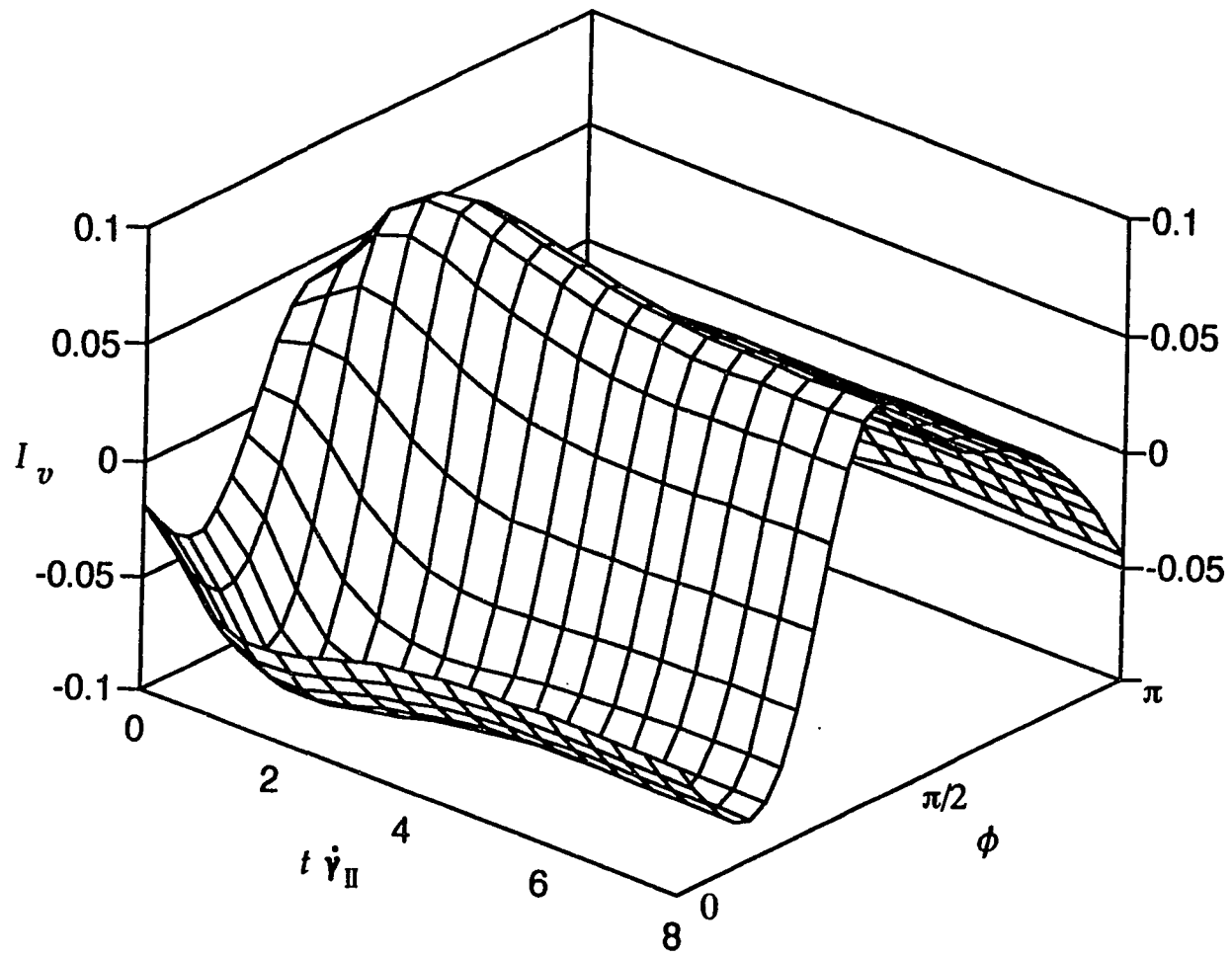

Figure 4.5 The interaction orientation probability velocity I_v in a suspension of rigid rods undergoing planar shear flow. I_v is shown as a function of orientation angle and time scaled by the magnitude of the strain rate in the suspension. Suspension properties and other parameters used in the simulation are given in Table 4.1.

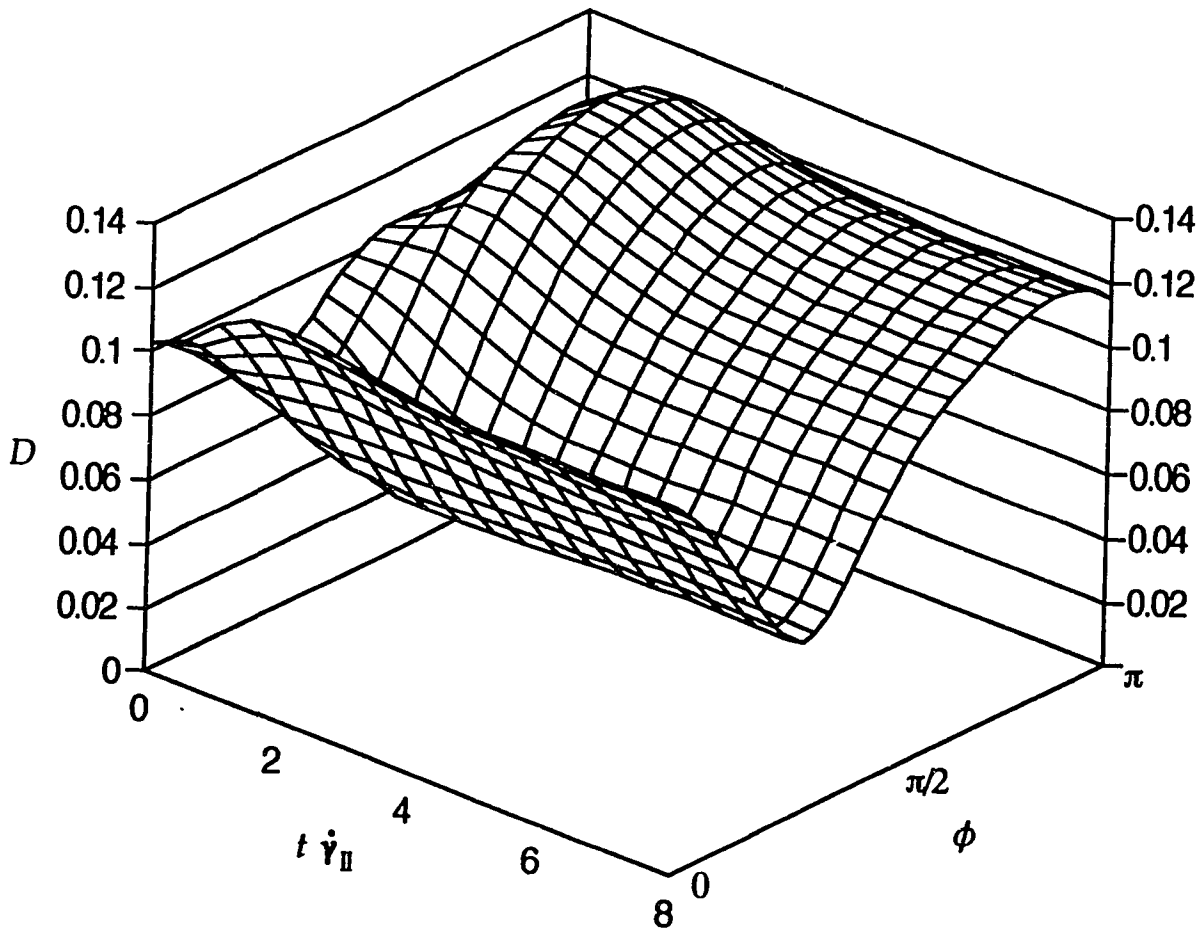

Figure 4.6 The mechanistic diffusion function D in a suspension of rigid rods undergoing planar shear flow. D is shown as a function of orientation angle and time scaled by the magnitude of the strain rate in the suspension. Suspension properties and other parameters used in the simulation are given in Table 4.1.

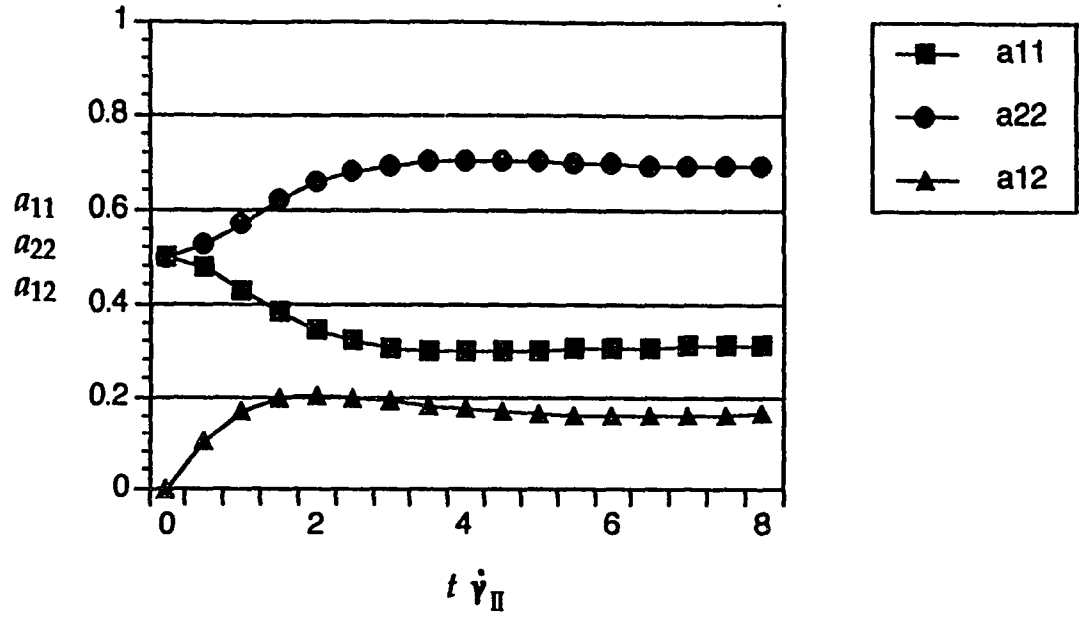

Figure 4.7 The orientation tensor components a_{11}, a_{22}, a_{12} for suspension of rigid rods undergoing planar shear flow. Tensor components are shown as a function of time scaled by the magnitude of the strain rate in the suspension. Suspension properties and other parameters used in the simulation are given in Table 4.1.

order orientation tensor are shown in Figure 4.7. At time equals zero, the diagonal terms a_{11} and a_{22} are equal indicating no preferential, or random-in-plane, orientation. As the fibers begin to line up along the streamlines, the a_{22} term grows at the expense of a_{11}. Meanwhile the growth of a_{12} indicates that the most probable orientation is tilted slightly away from the y-axis.

4.2.2 *Stretching Flow*

The behavior of a suspension of rods experiencing fiber-fiber interaction in a planar stretching flow is examined through the next set of figures. Planar stretching has a velocity field described by

$$v_x = -\frac{\dot{\gamma}_{II}}{2} x; \qquad v_y = \frac{\dot{\gamma}_{II}}{2} y; \qquad v_z = 0 \tag{4.16}$$

All other inputs for the simulation of planar stretching are the same as those for the planar shear simulation of §4.2.1 and are given in Table 4.1.

Figure 4.8 shows the evolution of the orientation probability distribution function for a concentrated suspension in planar stretching. The distribution function is presented for select times during the simulation in Figure 4.9. The initially random fibers are rotated towards the streamlines from both directions in stretching flow. Therefore, the planar elongational flow will result in a peaked distribution function that is symmetric about the streamline direction $\phi = \pi/2$.

The convective orientation velocity imparted to the fibers by the bulk straining motion in the suspension is shown in Figure 4.10. Fibers at angles less than $\pi/2$ have positive angular velocity while those at orientations greater than $\pi/2$ will be rotated in a negative direction towards the streamline.

The diffusive and interaction orientation velocities are shown in Figures 4.11 and 4.12 respectively. As heretofore shown in the simulation of shearing flow, the dispersive effect of fiber-fiber interaction produces terms that must change the overall orientation state of the suspension. Once again, the diffusion effect is not constant for fibers at all orientations.

The diffusion function $D(\phi, t)$, for planar elongation shown in Figure 4.13 is evidently not constant for suspensions with mechanical fiber-fiber interactions. $D(\phi, t)$ shows a marked dip in the region where the fibers are most highly aligned. This occurs because the fibers oriented at $\phi = \pi/2$ are least likely to experience crossings from other fibers in the suspension. Fewer crossings mean lower dispersive effect from fiber-fiber interactions.

The orientation tensor elements for a suspension in planar stretching are shown in Figure 4.14. The initially random suspension has a_{11} and a_{22} equivalent at 0.5, but the strain in the suspension orients the fibers in the y-axis direction. In the case of no dispersion effect from fiber-fiber interaction, the orientation tensor a_{22} would quickly attain a value of unity, all fibers aligned in the y direction. Fiber-fiber interaction precludes perfect alignment of the fibers. Since planar stretching is symmetric about the y axis, there will be no 'tilt' to the orientation distribution and the simulation shows that a_{12} remains zero throughout the test. A comparison of the tensorial results in Figures 4.14 and 4.7 reveals that, although the shear and stretching flows have equal magnitudes and the interaction parameters are equivalent, the stretching flow aligns the fibers more quickly and more strongly.

4.2.3 Viscometric Functions and Combination Flows

The introduction of fibers into the Newtonian solvent will produce a suspension with a viscosity that will be significantly larger than that of the

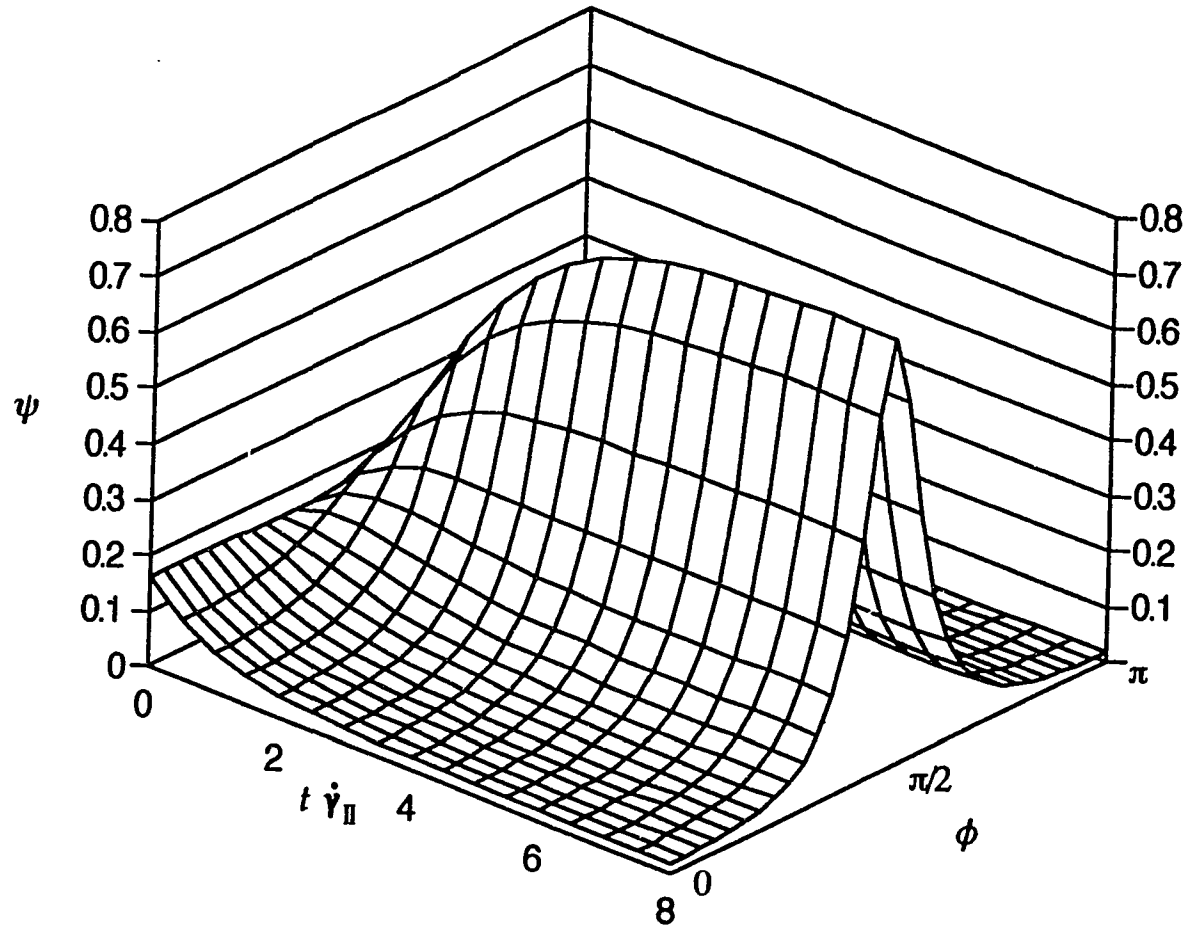

Figure 4.8 The probability distribution of fiber orientation ψ in a suspension of rigid rods in planar elongation. ψ is shown as a function of orientation angle and time scaled by the magnitude of the strain rate in the suspension. Suspension properties and other parameters used in the simulation are given in Table 4.1.

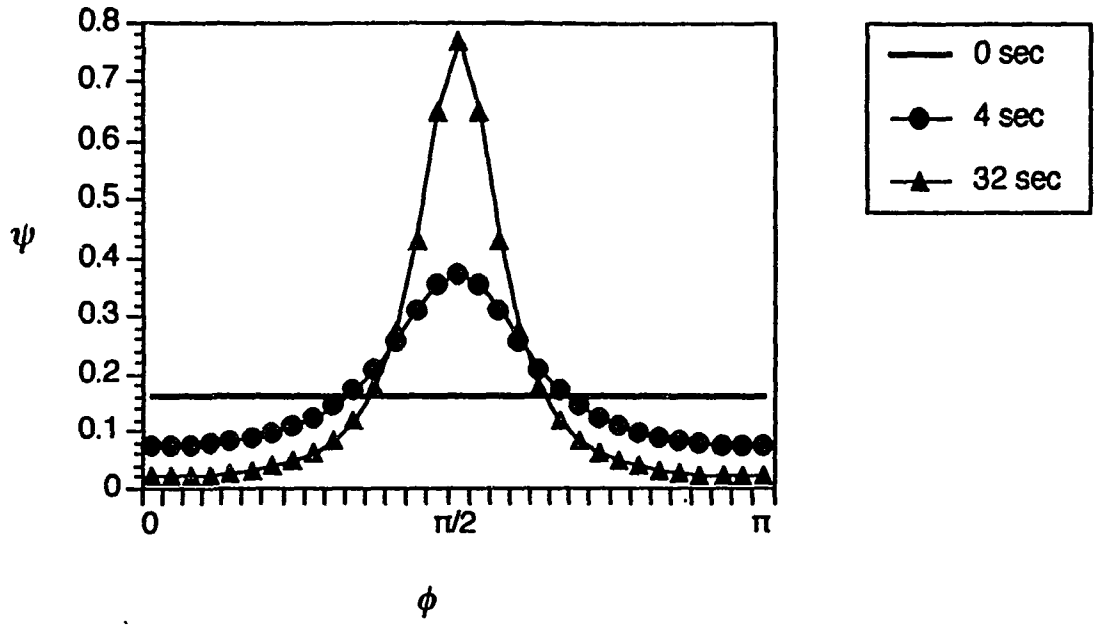

Figure 4.9 The probability distribution of fiber orientation ψ in a suspension of rigid rods undergoing planar shear flow. ψ is shown as a function of orientation angle for three different times. Suspension properties and other parameters used in the simulation are given in Table 4.1.

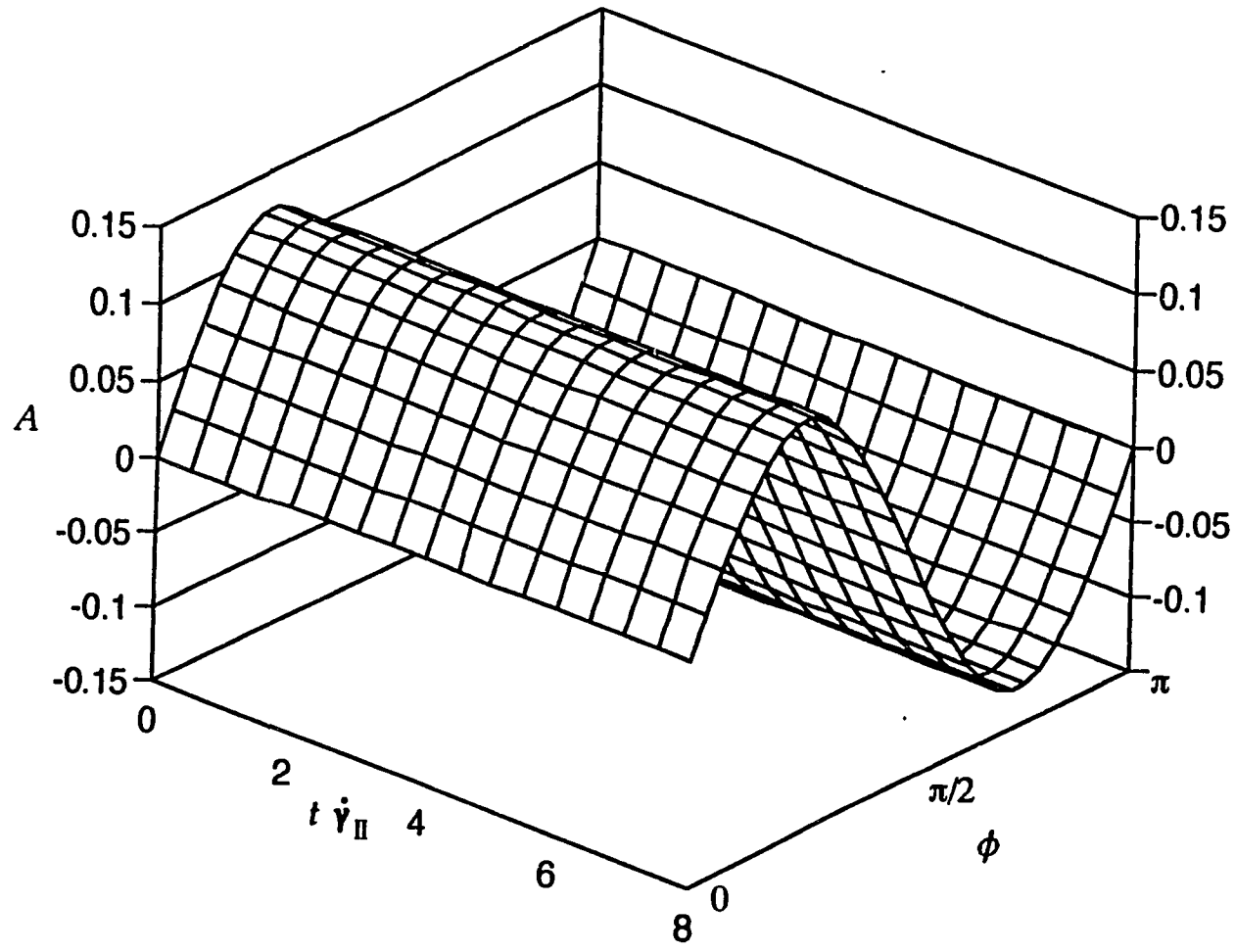

Figure 4.10 The convective orientation probability velocity A in a suspension of rigid rods in a planar elongation. A is shown as a function of orientation angle and time scaled by the magnitude of the strain rate in the suspension. Suspension properties and other parameters used in the simulation are given in Table 4.1.

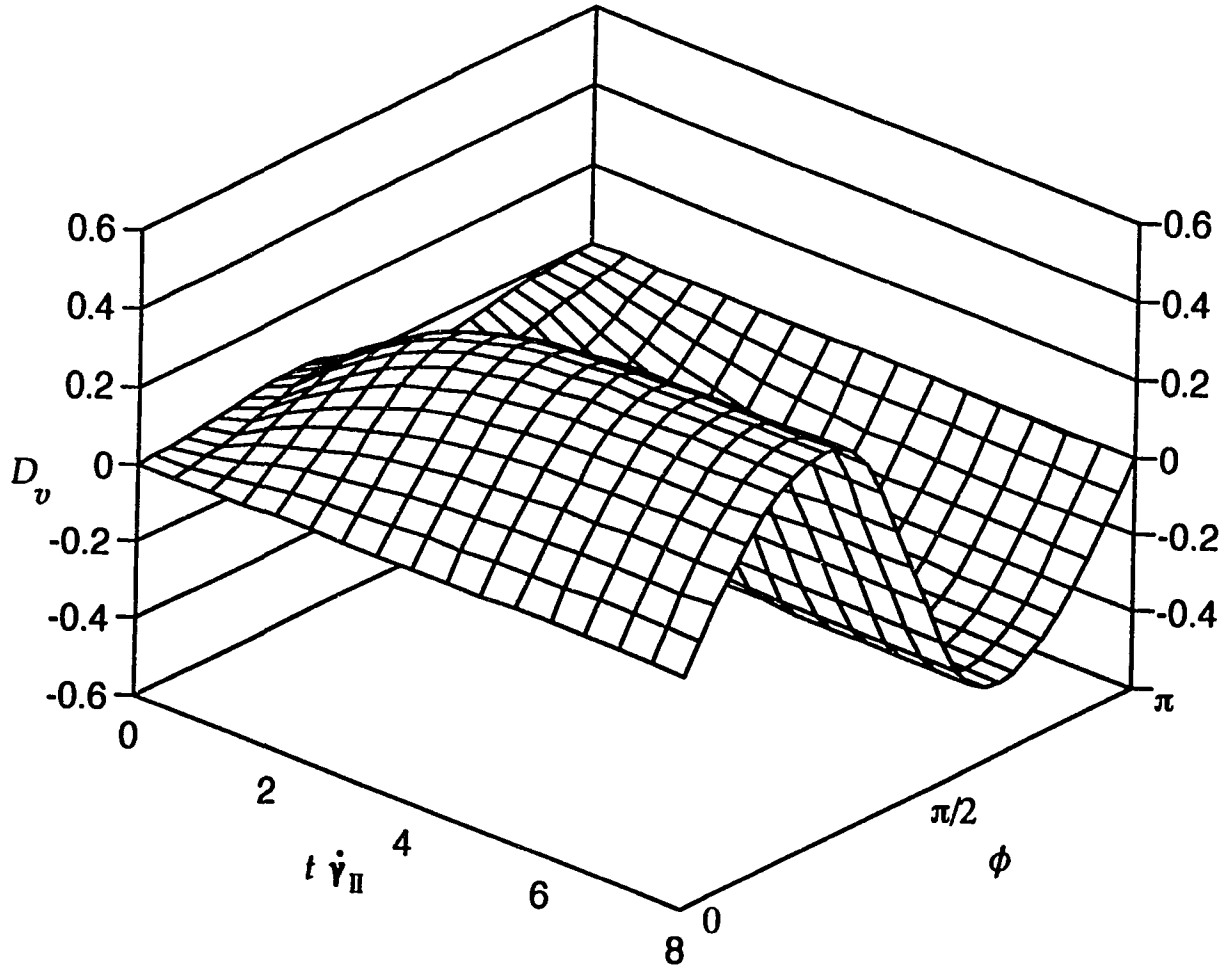

Figure 4.11 The diffusion orientation probability velocity D_v in a suspension of rigid rods undergoing planar elongation. D_v is shown as a function of orientation angle and time scaled by the magnitude of the strain rate in the suspension. Suspension properties and other parameters used in the simulation are given in Table 4.1.

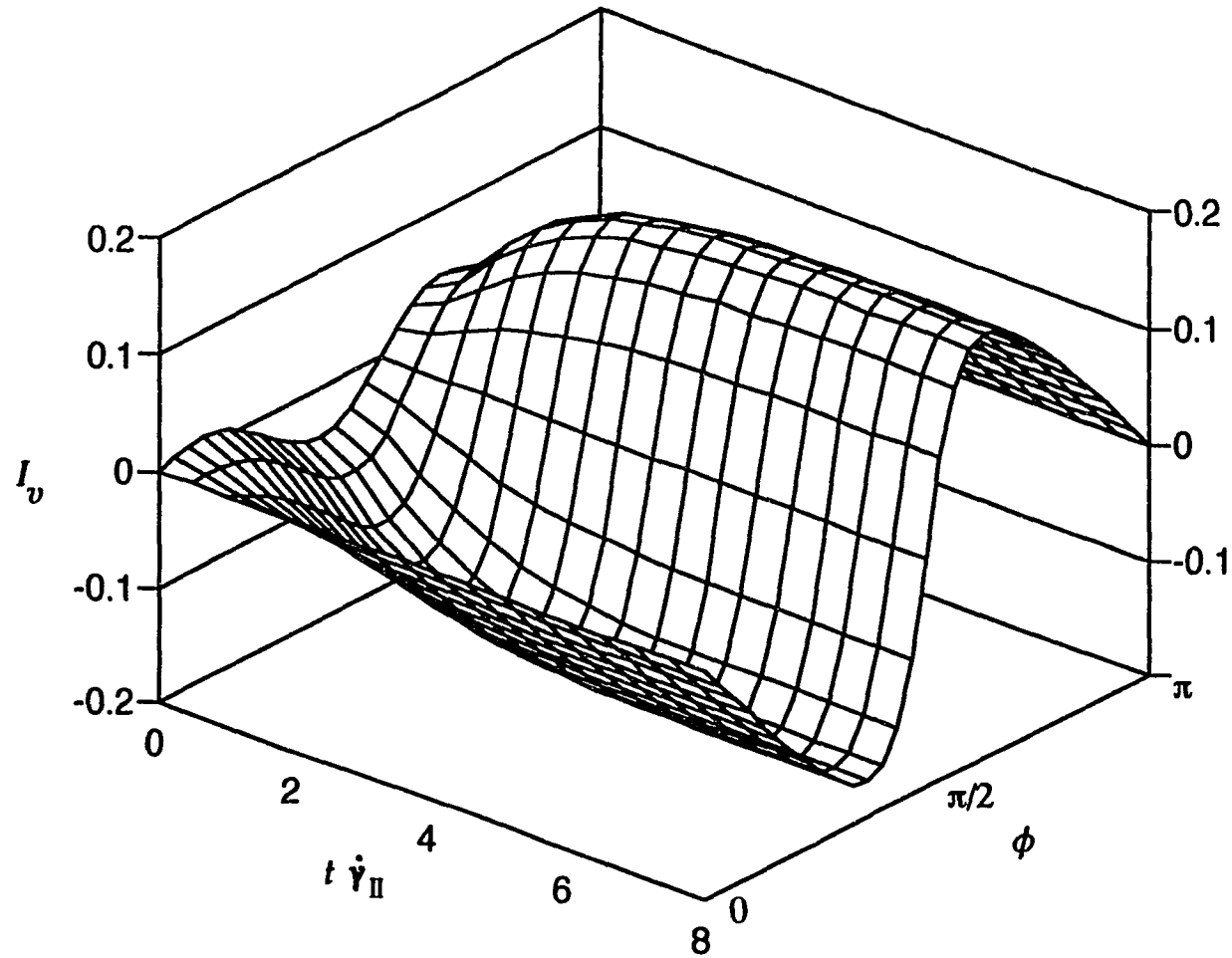

Figure 4.12 The interaction orientation probability velocity I_v in a suspension of rigid rods in planar elongation. I_v is shown as a function of orientation angle and time scaled by the magnitude of the strain rate in the suspension. Suspension properties and other parameters used in the simulation are given in Table 4.1.

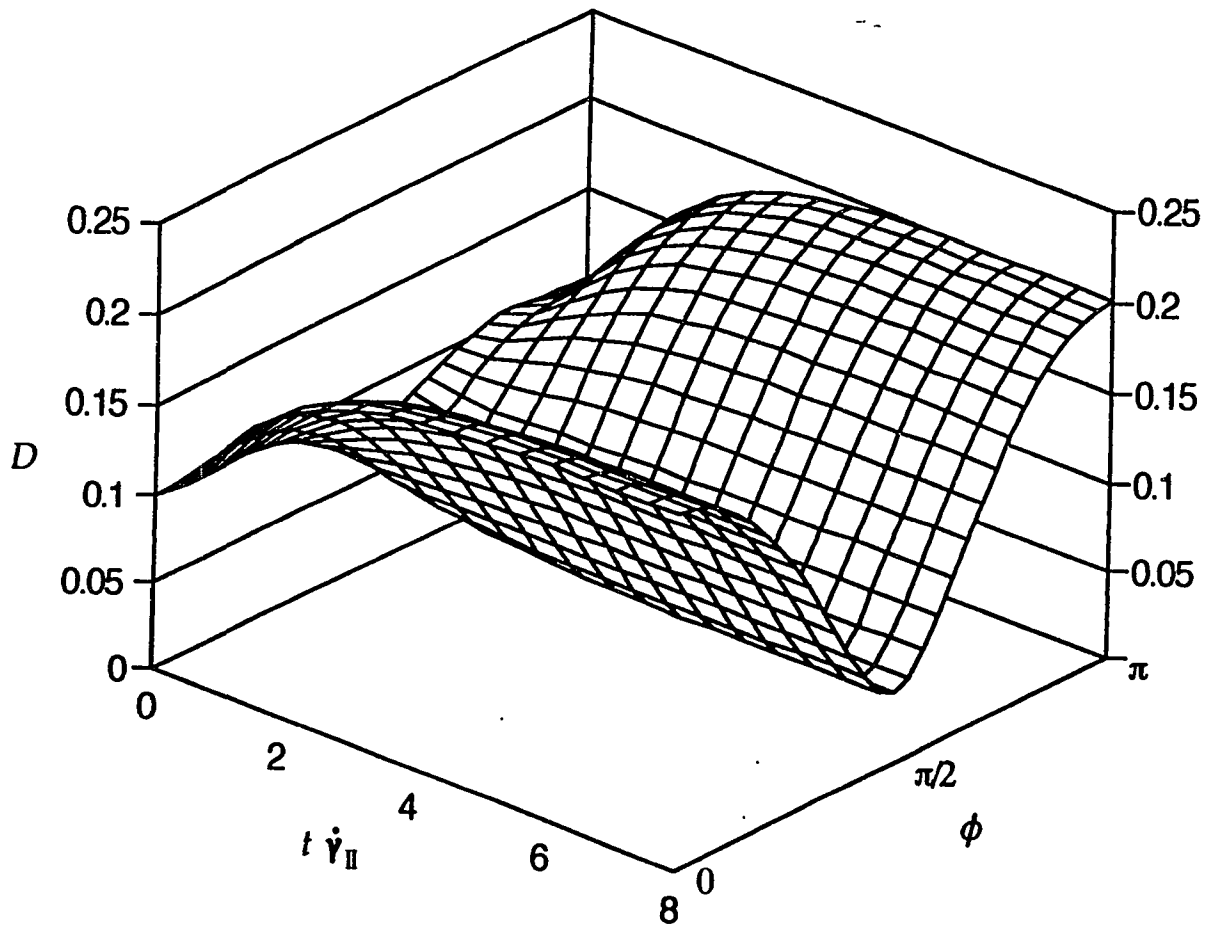

Figure 4.13 The mechanistic diffusion function D in a suspension of rigid rods undergoing planar elongation. D is shown as a function of orientation angle and time scaled by the magnitude of the strain rate in the suspension. Suspension properties and other parameters used in the simulation are given in Table 4.1.

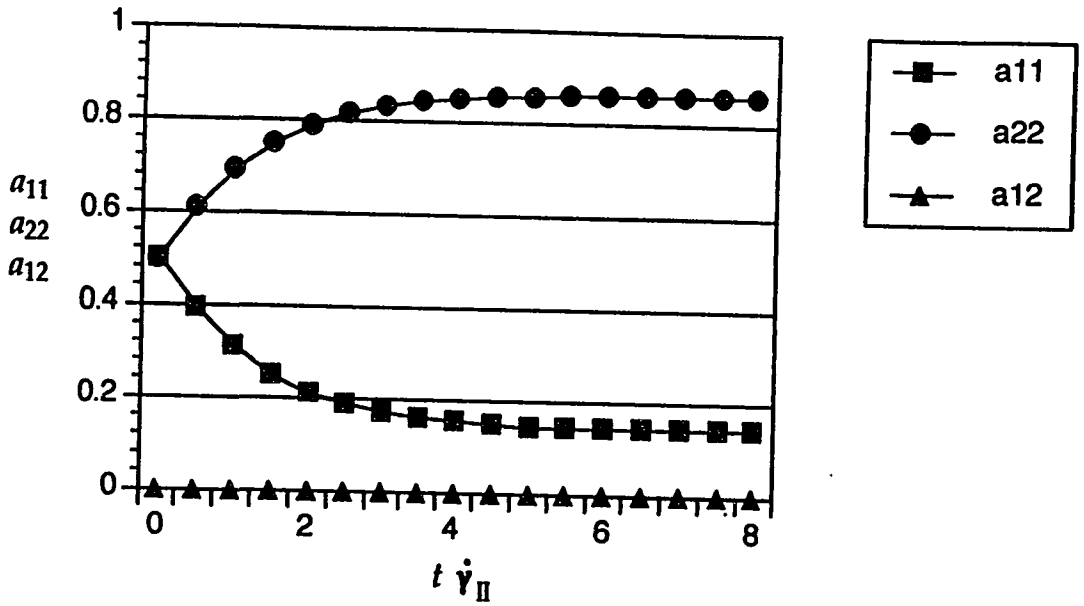

Figure 4.14 The orientation tensor components a_{11}, a_{22}, a_{12} for suspension of rigid rods undergoing planar elongation. Tensor components are shown as a function of time scaled by the magnitude of the strain rate in the suspension. Suspension properties and other parameters used in the simulation are given in Table 4.1.

solvent alone. Furthermore, since the fibers are anisometric, they create viscosity increases that are anisotropic. The viscosity of the suspension is a function of the straining in the Newtonian solvent viscosity and the resistance of the fibers to stretching along their axes. The simple shear viscosity in a fluid is defined as

$$\eta = \frac{\tau_{xy}}{\dot{\gamma}_{xy}} \tag{4.17}$$

The shear stress is given in the expression in Eq. (3.55). After substituting the expressions for the hydrodynamic drag coefficient (Eq. (2.40)) the shear stress the shear stress for any orientation state results.

$$\tau_{xy} = \mu \dot{\gamma}_{xy} + \frac{nL^2}{12} \zeta_a \dot{\gamma}_{xy} \langle p_x p_y p_x p_y \rangle + \frac{n^2 d L^4 f_1}{12} \dot{\gamma}_{xy} \langle p_x p_y p_x p_y \rangle \tag{4.18}$$

The terms in the angle brackets are elements of the fourth order orientation tensor, $\langle p_x p_y p_x p_y \rangle = a_{1212}$. The shear viscosity is therefore

$$\eta = \mu + \left[\frac{nL^2 \zeta_a}{12} + \frac{n^2 d L^4 f_1}{12} \right] a_{1212} \tag{4.19}$$

The orientation tensor a_{1212} can be calculated from the probability distribution function shown in Figure 4.1, the orientation in planar shear. Using this and the values given in Table 4.1, the shear viscosity for the suspension is calculated and shown in Figure 4.15. From Table 4.1, the size of the first term in the square brackets of Eq. (4.19) is $O(10^3)$, and the second term in the square

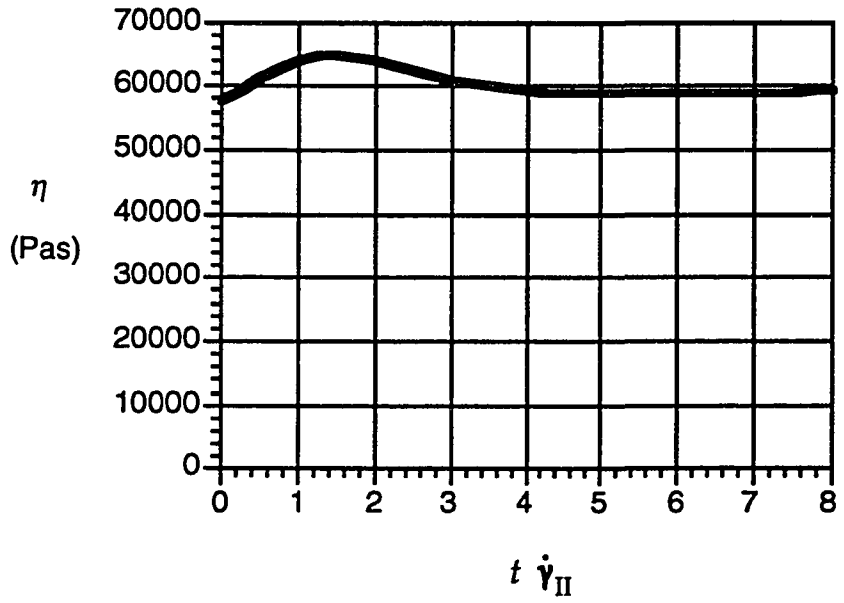

Figure 4.15 The simple shear viscosity as a function of time scaled by the magnitude of the strain rate tensor for a suspension of rigid rods initially oriented randomly in-plane.

brackets is $O(10^4)$. The presence of the fibers will certainly increase the viscosity of the suspension. Rheological experiments can assist in properly quantifying the parameters that govern the effect of the fiber orientation such as the interaction force coefficient. The fourth order orientation tensor component a_{1212} is non-zero for the duration of the shearing, therefore the suspension shear viscosity (shown in Figure 4.15) is predicted to be significantly higher than the solvent viscosity.

A slight increase in the predicted shear viscosity near $t\dot{\gamma}_{II} = 1.5$ shows in Figure 4.15 as result of fibers moving through an orientation colinear with the direction of the positive principle strain rate in the suspension $\phi = \pi/4$. In a shear flow of slender fibers that experience no dispersive interactions, all fibers will lie along the streamline and would make no contribution to the shear viscosity. The inclusion of the fiber-fiber interactions causes an increase in the

shear viscosity for two reasons: one, the diffused distribution of fibers away from the streamlines and particularly towards the direction of positive normal strain rate allows the fibers to resist stretching along their axes. And two, the forces between the fibers create another resistance to straining of the suspension with a resulting increase in viscosity.

Another common viscometric function is the first normal stress coefficient, Ψ_1. Many suspensions, polymer melts and polymer solutions show normal stresses arising in simple shear flow. This is due to elongated molecules that are trying to regain a higher entropy state or aligned fibers that resist the stretching component of the strain. The first normal stress coefficient is defined as

$$\Psi_1 \equiv \frac{\tau_{yy} - \tau_{xx}}{\dot{\gamma}_{xy}^2} \tag{4.20}$$

The normal stresses τ_{yy} and τ_{xx} are also both functions of particular terms in the fourth order orientation tensor $\mathbf{a}_4$.

$$\tau_{yy} = \dot{\gamma}_{xy}\left[\frac{nL^2\zeta_a}{12} + \frac{n^2dL^4f_I}{12}\right]a_{1222} \tag{4.21}$$

$$\tau_{xx} = \dot{\gamma}_{xy}\left[\frac{nL^2\zeta_a}{12} + \frac{n^2dL^4f_I}{12}\right]a_{1211} \tag{4.22}$$

The first normal stress coefficient is shown in Figure 4.16. As the fibers in the suspension are oriented from random to a preferred direction near $\phi = \pi/2$, the normal stresses grow from zero as a result of the changing orientation state. The slender fibers will resist only stretching along their axes and as the peak of

the distribution function approaches the direction of maximum elongation at $\phi = \pi/4$, so will the normal stress follow. The steady state orientation distribution retains a significant fraction of fibers pointing in the neighborhood of $\pi/4$ so therefore the steady state value of Ψ_1 will remain quite large in steady state.

The elongational viscosity of the suspension is also a function of the orientation state of the fibers in the suspension. As a fiber in the stretching suspension is oriented towards the direction of greatest stretching, it will resist that straining motion along its axis, changing the apparent viscosity of the suspension as the orientation state changes. The elongational viscosity for a suspension during start up of planar elongation is defined as

$$\bar{\eta}^+ = \frac{\tau_{yy} - \tau_{xx}}{\frac{1}{2}\dot{\gamma}_{II}} \tag{4.23}$$

The normal stresses in the suspension undergoing a planar elongation will be

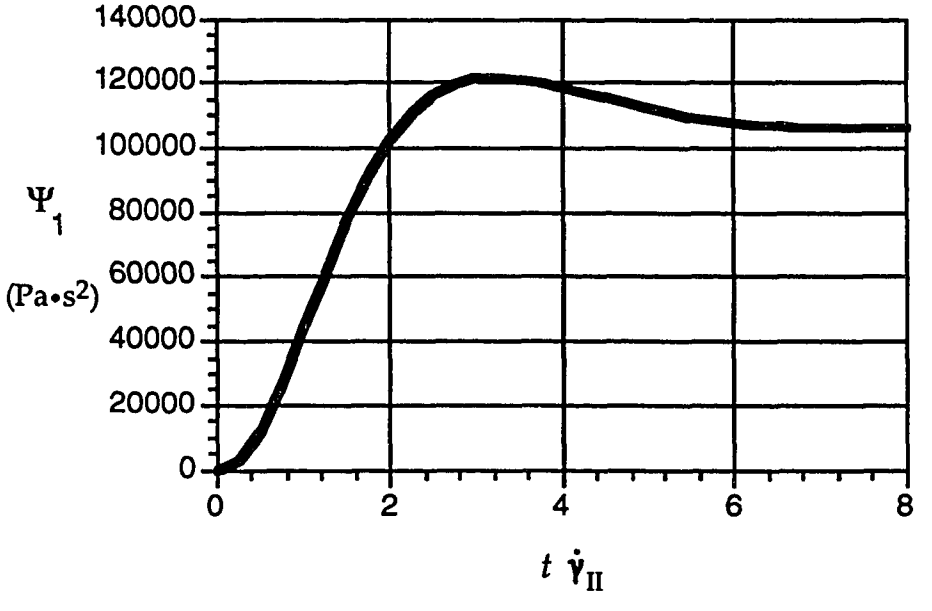

Figure 4.16 The first normal stress coefficient Ψ_1 during start up of steady planar shear of a concentrated suspension of rigid rods.

$$\tau_{yy} = \mu_2^1 \dot{\gamma}_{II} + \frac{1}{2}\dot{\gamma}_{II}\left[\frac{nL^2\zeta_a}{12} + \frac{n^2 dL^4 f_I}{12}\right](a_{2222} - a_{1122}) \tag{4.24}$$

$$\tau_{xx} = -\mu_2^1 \dot{\gamma}_{II} - \frac{1}{2}\dot{\gamma}_{II}\left[\frac{nL^2\zeta_a}{12} + \frac{n^2 dL^4 f_I}{12}\right](a_{1111} - a_{2211}) \tag{4.25}$$

In this case, the orientation tensor components are calculated from the distribution function for a suspension in stretching flow. Figure 4.17 shows the growth of the elongational viscosity in planar elongation of a concentrated suspension of fibers. The elongational viscosity grows in the suspension as the fibers are aligned such that the majority are pointed in the direction of the largest positive strain rate.

Often in polymer processing flows one will find combinations of shearing and stretching flows. Numerical simulations are well suited to experimentation

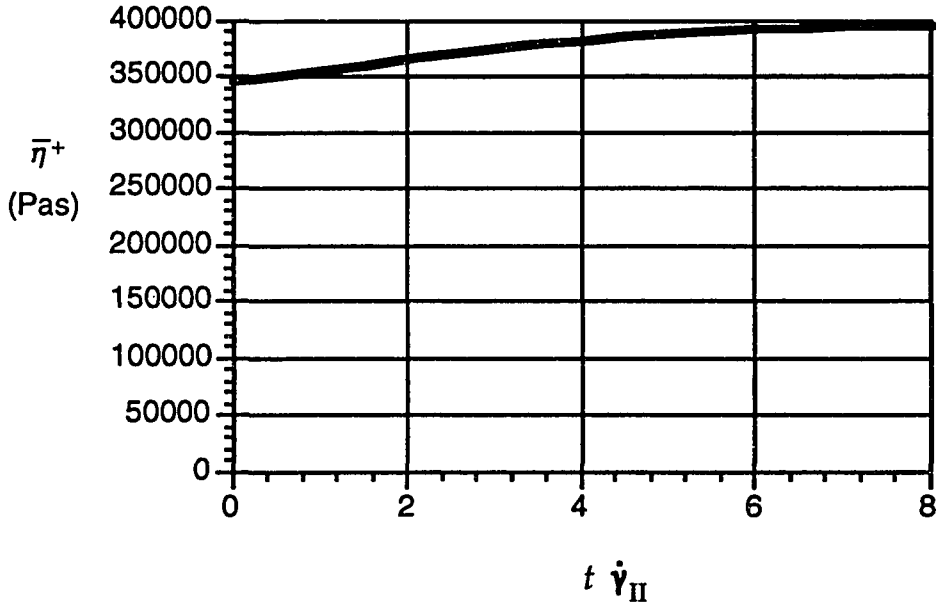

Figure 4.17 The elongational viscosity of a suspension of initially random fibers subject to planar elongation. Viscosity is plotted as a function of time scaled by the magnitude of the strain rate in the suspension.

with the input parameters such as the velocity gradients. Therefore, the shearing flow field of §4.2.1 can be combined with the stretching flow field of §4.2.2. In earlier discussion it was noted that the stretching flow was more effective at orienting fibers. Apparently, a flow could orient the fibers in the suspension more quickly and more thoroughly. A combination simulation could verify these observations.

Figure 4.18 shows the results of an equal combination of shearing and stretching flow. The velocity field for this simulation is

$$v_x = -\frac{\Gamma}{2}x + \Gamma y; \quad v_y = \frac{\Gamma}{2}y; \qquad v_z = 0; \qquad \Gamma = 0.25\,s^{-1} \tag{4.26}$$

Figure 4.18 shows the orientation tensor values a_{11}, a_{22}, and a_{12} for an equal combination of shear and stretching. The results confirm that the stretching flow will align the fibers more quickly and more effectively in the y-axis direction. This is shown by the preeminence of a_{22}. The shearing flow does act to reduce the stretching alignment, which results in an orientation state which is nearly random with some tilt ($a_{12} \neq 0$) with a few extra fibers pointing in the stretching direction at steady state.

If we increase the strength of the shearing portion of the combination flow, the simulation reveals more about the orientation behavior of stretching versus shearing flow. In this experiment, the velocity field is input as

$$v_x = -\frac{\Gamma}{4}x + \Gamma y; \quad v_y = \frac{\Gamma}{4}y; \qquad v_z = 0; \qquad \Gamma = 0.25\,s^{-1} \tag{4.27}$$

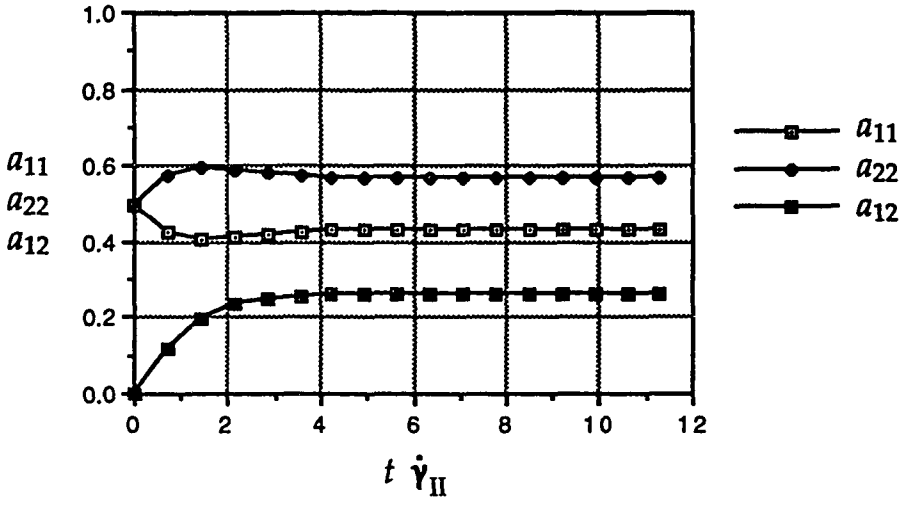

Figure 4.18 Orientation tensors as a function of strain for a concentrated suspension in an equal combination of shear flow in the 1 direction and stretching in the 2 direction.

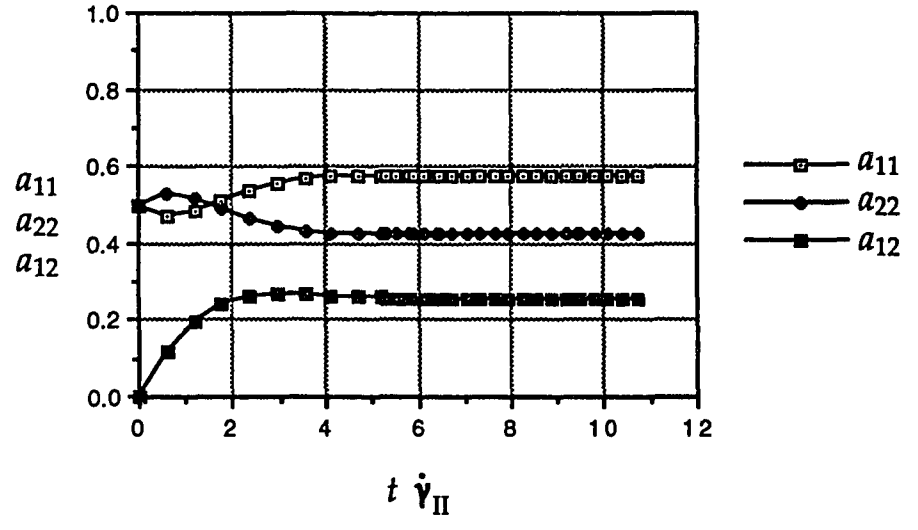

Figure 4.19 Orientation tensors as a function of strain for a concentrated suspension in a combination of shear and stretching flow. The shear flow in the 1 direction is twice the magnitude of the stretching flow in the 2 direction.

The orientation tensor data of Figure 4.18 reveals a stretching action that although handicapped, can still orient fibers more quickly than shear. Note that the a_{22} component briefly starts to grow larger than a_{11}. Eventually, the larger strength of the shear flow forces the greater fraction of the fibers to orient in the 1 direction. Here again, the overall orientation is still only partially oriented, and there is notable tilt in the distribution maximum away from the x axis.

4.2.4 Numerical Convergence Tests

The numerical calculations presented in this chapter are only numerical *approximations* to the actual solution of the governing equation for fiber orientation. Refinement of the finite difference grid will typically increase the accuracy of a properly formulated finite difference scheme.

In this section, we investigate the behavior of the orientation simulations for a succession of increasingly finer finite difference grids. The parameters used in this study of numerical convergence in planar elongation are given in Table 4.2

The results of the four cases are shown in Figure 4.20. In this figure are the steady state probability distribution functions for simulations using 18, 30, 60, and 90 nodes in the finite difference grid of the orientation space for the fibers. The calculations with 30, 60, and 90 nodes all look very similar while the results of the simulation using 18 nodes show a marked decrease in accuracy.

Figure 4.21 shows the convergence more clearly. Here the a_{11} component of the orientation tensor is plotted for each simulation. Clearly, mesh refinement beyond 90 nodes will achieve little reward. The 30-node simulation shows a barely discernible decrease in numerical accuracy. Due to nature of the computations involved in this finite difference model, increases in the number of nodes in the orientation domain are computationally expensive. The choice of

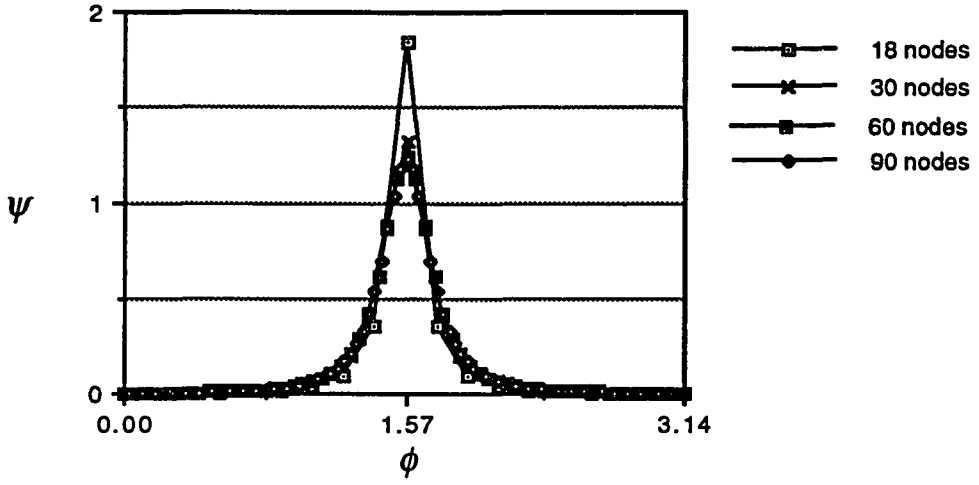

Figure 4.20 Steady state probability distribution functions as a function of orientation for successively finer finite difference grids.

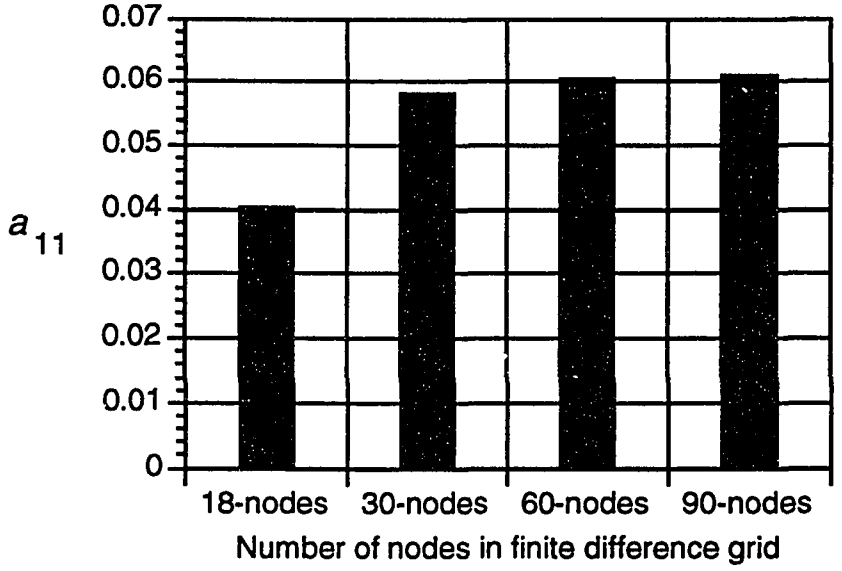

Figure 4.21 Steady state orientation tensor component a_{11} as a function of number of nodes in the orientation domain of the finite difference model for fiber orientation.

30 nodes therefore is optimum when computational resources need conservation, and this is the choice used to create the bulk of this results in this work of research.

Table 4.2 Finite difference simulation input parameters for convergence tests with elongational flow of a concentrated suspension.

Parameter	Symbol	Value	Units
scalar strain rate	$\dot{\gamma}_{II}$	0.25	1/s
number density	n	6.82e9	$1/m^3$
fiber length	L	12.7e-3	m
fiber diameter	d	152.4e-6	m
suspending fluid viscosity	μ	1.0	Pa·s
interaction force coefficient	f_I	152.4e-6	Pa·s·m
hydrodynamic force coefficient	ζ_a	12.7e-3	Pa·s·m
interaction correlation time	ε	0.5	s
time step size	Δt	0.01	s
angular step size – four cases	$\Delta\phi$	$\pi/18$, $\pi/30$, $\pi/60$, $\pi/90$	radians

4.3 Summary

Chapter Four has described a numerical solution to the distribution function calculation for suspensions that experience mechanical fiber-fiber interaction. These interactions create a dispersive effect in the fiber rotations that acts like a diffusion in the governing equation for the probability distribution function. In dilute particle suspensions, fibers would freely rotate into the directions of the streamline. The resulting distribution function is a Dirac delta function at the orientation in the flow direction. However in concentrated suspensions, fibers are hindered and bumped as they rotate. This factor creates a material that is rheologically dependent on the the fiber orientation and the forces that the fibers impart to one another.

The numerical simulations given in this chapter can be used to ascertain the validity of the assumptions involved in creating a model of fiber orientation in concentrated suspensions. Given results that are sound, the numerical methods used here to solve the distribution function are necessary to experiment and analyze the behavior of different suspensions under various flow conditions. Furthermore since the distribution function calculations have proved to be computationally intensive, the comprehensive solutions to the distribution function must be used to validate solutions to the governing equations for the orientation tensor.

5. EXPERIMENTS WITH FIBER ORIENTATION IN STRETCHING FLOW

This chapter details an experimental program meant to check the results of the numerical solution and to provide greater insight into the physical phenomena present in flows of concentrated fiber suspensions. In these experiments, concentrated suspensions of high aspect ratio fibers with planar orientation are forced to undergo planar stretching flow. Here *planar orientation* means that the fibers are oriented all in a single plane. Meanwhile, the stretching flow is to take place all in the same plane as the plane of fiber orientation.

5.1 Description of Experiments

5.1.1 Kinematics of Planar Stretching

The term *planar stretching* implies a deformation in which the velocities and velocity gradients in the material lie wholly in a single plane. We shall call this the x-y plane. In these experiments with suspensions of orientable fibers, the fibers shall have negligible component of orientation lying outside of the x-y If the magnitude of the strain rate in the material is $\dot{\gamma}$, the velocity field in the material will be

$$v_x = \frac{\dot{\gamma}}{2} x \tag{5.1}$$

$$v_y = -\frac{\dot{\gamma}}{2} y \tag{5.2}$$

The total strain will be a function of position.

$$\gamma = 2 \ln \frac{x}{x_o} = -2 \ln \frac{y}{y_o} \tag{5.3}$$

x_o and y_o describe the initial position of the material element in the stretching flow. The strain on a particular element of the material is a linear function of the time that it remains in the flow.

$$\gamma = \dot{\gamma} t \tag{5.4}$$

The streamlines in the bulk material are described by the equation, $xy = C$. The product of x and y is a constant.

5.1.2 Materials – Fibers and Fluid

The suspension used in the experiments is comprised of glycerin and clear fibers of nylon monofilament. Tracer fibers of the same nylon monofilament colored black were included to indicate the orientation state of the fibers in the suspension.

Nylon monofilament of two different diameters was used to create suspensions with different fiber aspect ratios. The filaments were provided by E.I. DuPont de Nemours & Co. in diameters of 0.006" and 0.0016". The measured diameters of the filaments were 0.0059" ± 0.000025 and 0.00152" ± 0.000031". The hanks were chopped to half inch fibers, measured to be 0.51" ± 0.017". The viscosity of the glycerin was measured at 24.8° C. The Newtonian viscosity of the glycerin, $\eta = 2.99$ (lb_f/in^2)·s ± 0.039 (lb_f/in^2)·s = 0.994 Pa·s ± 0.013 Pa·s.

Silicone oil was used as a lubricant for the walls of the apparatus. The low viscosity silicone (200 centistokes) had two important qualities that allowed it to lubricate the flow of the glycerin/nylon fiber suspension. One, the silicone was

immiscible with the glycerin fluid. Two, the silicone would wet the Plexiglas walls of the experiment more readily than the glycerin. This results in a layer of low viscosity silicone adhering to the walls of the experiment, lubricating the flow of the glycerin. The majority of the out-of-plane shearing ($\frac{\partial v_x}{\partial z}, \frac{\partial v_x}{\partial z}$) would therefore occur in the thin layer of silicone. The silicone was spread thinly on all interior surfaces of the channel momentarily prior to the start of the elongational flow. Several other researchers have used similar lubricated flows to successfully establish and analyze stretching flows in polymers [58-60].

5.1.3 Apparatus for Planar Stretching

The planar stretching apparatus used in the experiment is shown schematically in Figure 5.1. The test section whose sides are described by the hyperbola $xy = \pm 4$ in^2 was fed with suspension from two material loading zones. The $\frac{1}{4}$ " deep channel was fed from the extreme opposite ends of the material loading zones by an unfilled glycerin pumping fluid. The pumping fluid was driven by an Instron Model 8501 tensile testing machine (100 kN rated maximum force) using a hydraulic piston. The top of the apparatus was made of one inch thick Plexiglas that allowed visualization of the suspension flowing in the channel.

The Plexiglas top of the apparatus was removable so that the randomly oriented suspension could be poured into the prelubricated channel momentarily prior to the start of the experiment. The channel height of one quarter inch insured that the fibers would be forced to find an orientation in the x-y plane of the apparatus. The channel was slightly overfilled to insure that no air would be trapped with the suspension as the silicone oil-lubricated top was lowered and secured in place.

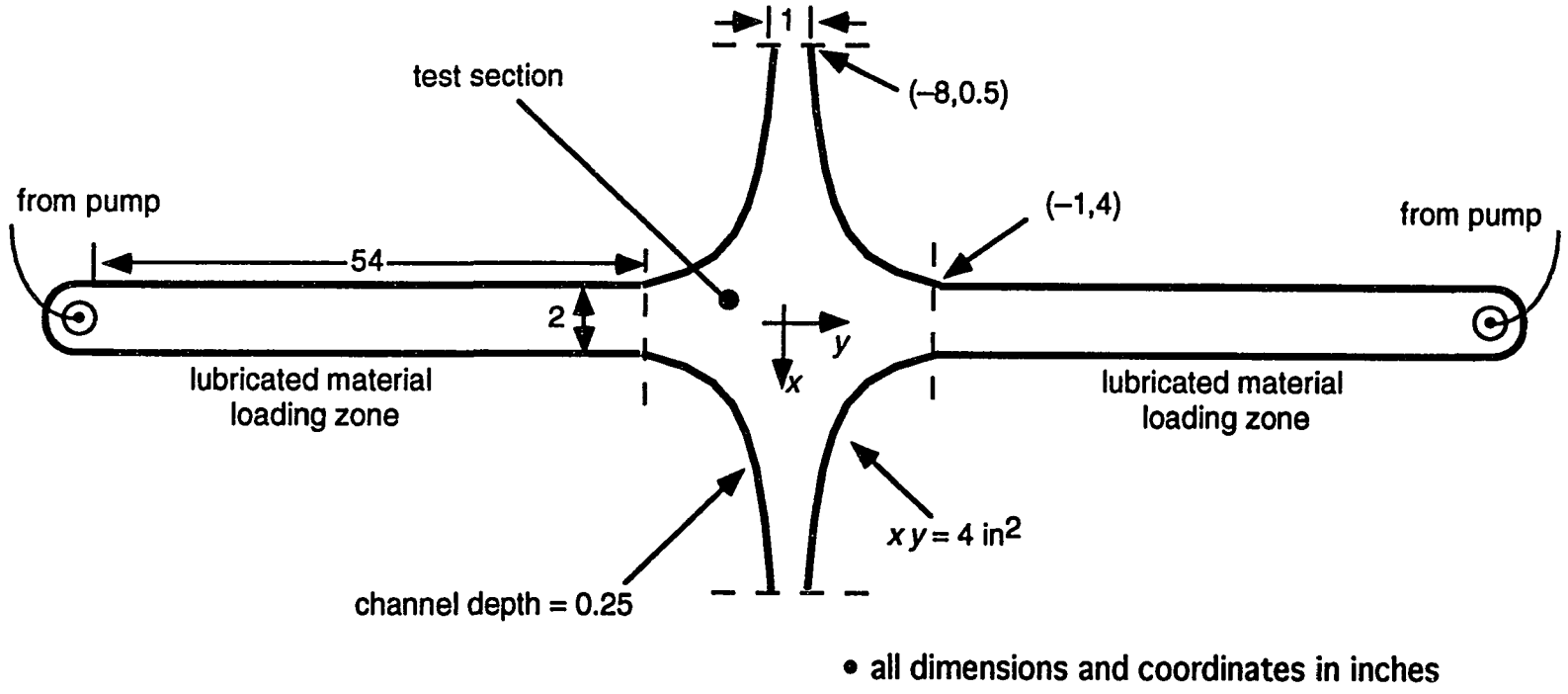

Figure 5.1 Schematic drawing of the planar elongation device

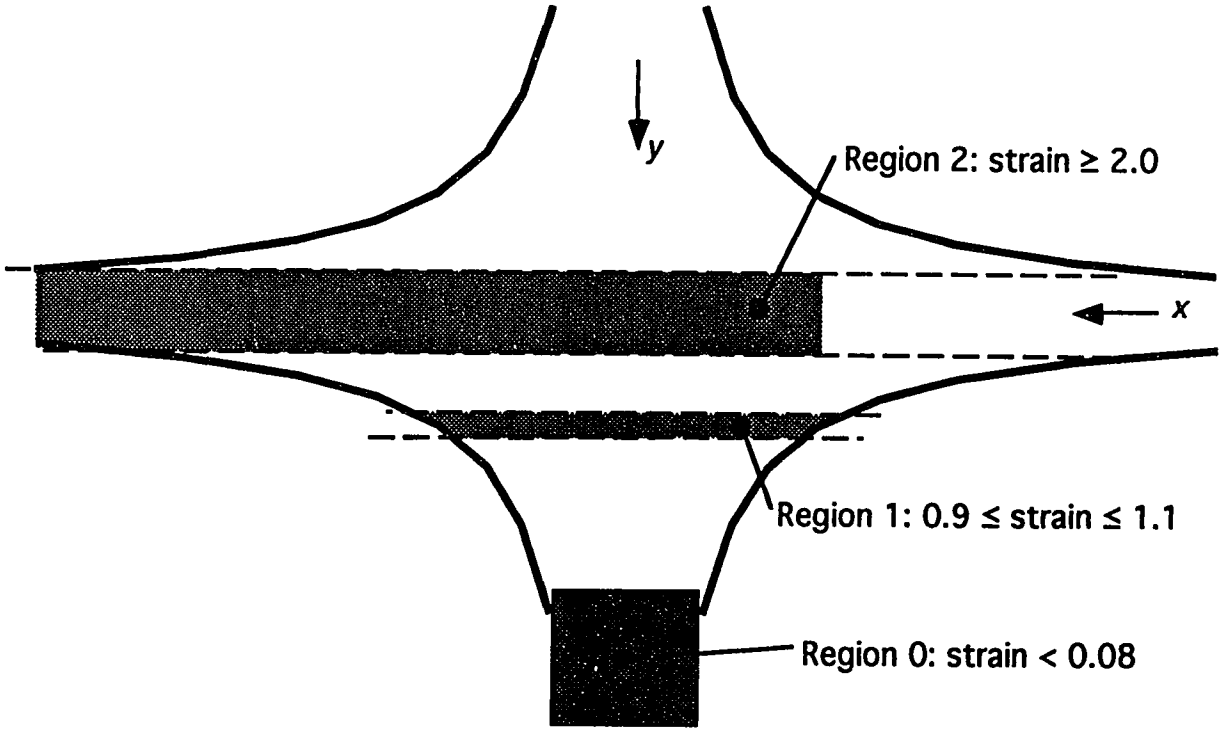

Figure 5.2 Test section detailing the regions from which orientation data is taken.

5.1.4 *Data Acquisition and Processing*

The clear Plexiglas top of the apparatus allowed observation of the fibers in the stretching flow. After a period equal to 10 times the inverse of the strain rate magnitude, photographs were taken of the suspension in the first quadrant of the test section at a rate of 2.2 exposures per second. Three photographs were selected across each experimental set. The selections were spaced widely over the set so that the orientation state of each would be statistically independent.

After enlargement, the black tracer fibers in the suspension show clearly in the photographs and their orientations were digitized using a HP-Apollo model 730 workstation and a HP digitizing tablet. The fibers were grouped according the position of their centroid. Centroid position in this experiment indicates the amount of total strain the fiber has experienced in the stretching flow (as per Eq. (5.3)). Fibers were sorted into three groups in which the total strain was less than 0.08, between 0.9 and 1.1, and greater than 2.0. The orientation tensor components a_{11}, a_{22}, and a_{12} were calculated for each of these groups from each photo. Figure 5.2 shows the test section and the regions in which the suspension strain fell into these bins.

5.2 Experimental Results

The 0.006" and 0.0015" fibers were each combined with glycerin in five different concentrations for elongational flow experiments. These combinations are shown in Table 5.1. The concentrations are comparable across the two diameters. For random planar orientation, each row of Table 5.1 will have an equal number of fiber crossings according to Eq. (2.49).

The magnitude of the strain rate in each experiment was $\dot{\gamma} = 2.828\ s^{-1}$. This yields a velocity at the entrance of the test section $v_x = 2.827$ in/s. The

particle Reynolds number for this flow is $O(10^{-3})$, and the Reynolds number for the bulk flow is $O(10^{-1})$.

A sample photograph capturing the fiber suspension moving through the test section is shown in Figure 5.3. In this experiment, the fibers are 0.015" in diameter and 0.5" in length. The suspension concentration is 5.33%; this is a concentrated suspension for fibers of this aspect ratio. The concentration level is larger than the square of the inverse aspect ratio. The black tracer fibers evident in the photo make up $\frac{1}{8}$ of the fibers in the suspension and will be used to characterize the orientation state.

The orientation tensors measured from in the latest stages of strain in the experiments (Region 3 of Figure 5.2) are given as a function of suspension concentration in Figures 5.4 and 5.5 for 0.006" diameter fiber suspensions and 0.015" diameter fiber suspension respectively. This shall be called the steady state result. These data indicate that an increase in fiber concentration brings about a decrease in the stretching direction alignment. This is an apparent diffusion effect due to the fiber-fiber interactions in the straining suspension. The error bars on the data are taken from the standard deviations in the data divided by the square root of the number of fibers digitized (typically 100 per region per photo) over the group of three photographs

Table 5.1 Suspension concentrations used in the planar elongation experiment.

fiber diameter = 0.006		fiber diameter = 0.015"	
concentration, c	number density, n	concentration, c	number density, n
%	$1/in^3 - 1/m^3$	%	$1/in^3 - 1/m^3$
0.25	13.9e3 -- 8.49e8	0.67	5.93e3 -- 3.61e8
0.50	27.8e3 --1.70e9	1.33	11.9e3 -- 7.23e8
1.00	55.6e3 -- 3.39e9	2.66	23.7e3 -- 1.45e9
2.00	11.1e4 -- 6.78e9	5.33	47.4e3 -- 2.89e9
3.00	16.7e4 -- 10.2e9	8.00	71.1e3 -- 4.34e9

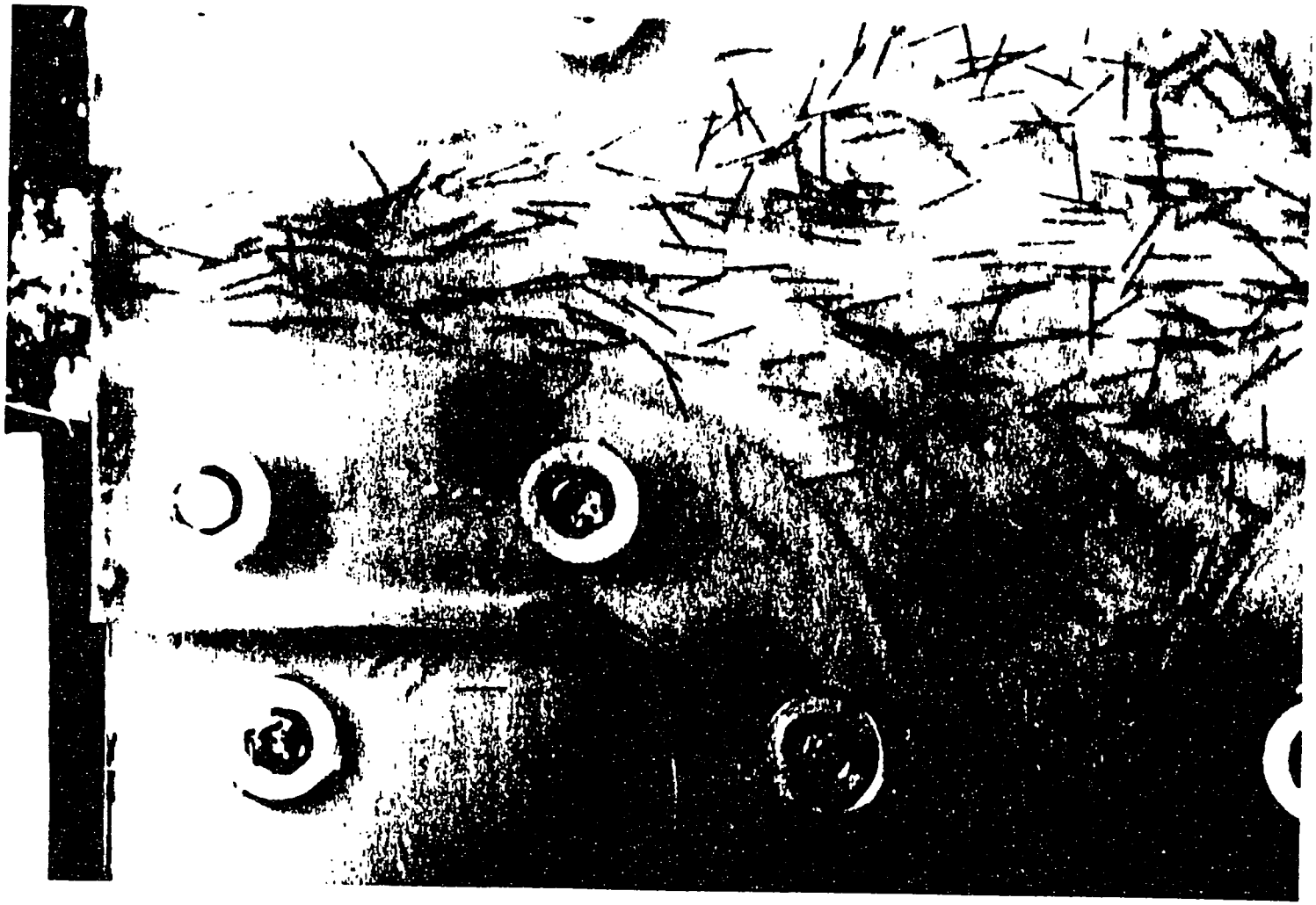

Figure 5.3 Photograph of a suspension of fibers of 0.015" diameter at a concentration of 2.66% by volume in glycerin. The suspension is flowing in at the bottom and top and out to the left and right.

Figures 5.7-5.16 give the evolution of the orientation tensors in the test section. They show the orientation as a function of strain, or time multiplied by the magnitude of the strain rate. These figures show results for each suspension given in Table 5.1. In many of these figures at strain equal to zero, i.e. the entrance to the test section, the fibers begin the experiment preoriented in the y direction. The fibers had been loaded in the channel in an initially random state, and flow and shear in the loading zone orients the fibers. This is altered to a principally x-direction orientation in the stretching flow. The data from the more concentrated suspensions of the 0.015" diameter fibers (Figures 5.12-15) show a quicker approach to a steady state value for any value of the initial orientation.

5.3 Discussion

This chapter has described a simple look at the behavior of concentrated suspensions of fibers in planar elongation flow. The fibers in these suspensions experience numerous fiber-fiber contacts (approach to within a diameter distance). These contacts cause the orientation of the fibers to exhibit a diffusion effect; perfect streamline orientation is impeded by the inter-fiber forces.

In all of the experiments, the fiber-fiber contacts would often form clumps, i.e. groups of fibers that traveled, rotated, and strained together. Figure 5.16 shows a photograph of an experiment with fibers of 0.0006" diameter at 3.0% concentration by volume. The wave-like orientation structure through the middle of the test section in this figure is a result of macro-scale changes to the bulk flow due to persistent clumping effects. The clumps are located under the crest of each wave; their existence forces the other fibers and fluid to find a new path. Therefore in the framework of this observation, fiber-fiber interactions do

not cause a dispersive orientation velocity that results in a diffusion in the overall orientation state, but rather a hindrance to the tangled fibers.

Whether the fibers are dispersed or impeded by interactions makes a difference in the rheology of the suspension. This difference changes the orientation state of the fiber in a different fashion, it alters the fiber forces from interactions, and clumps indicate a wholly different flow field around the fibers leading to macro-scale changes to the flow field in the suspension. While the theory that is presented in this work assumes that the interactions create a dispersion rather than a hinderance, the resulting orientation states are often indistinguishable.

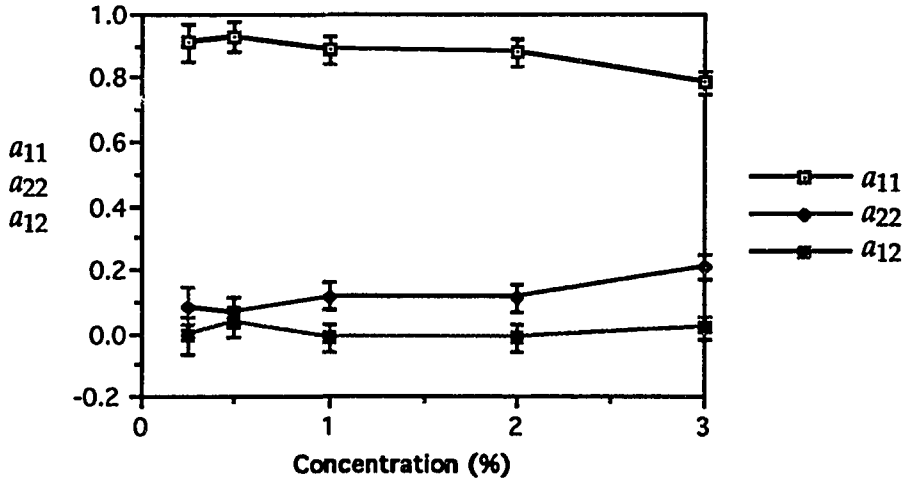

Figure 5.4 Steady state orientation tensors for suspensions of 0.006" diameter fibers in planar stretching as a function of concentration.

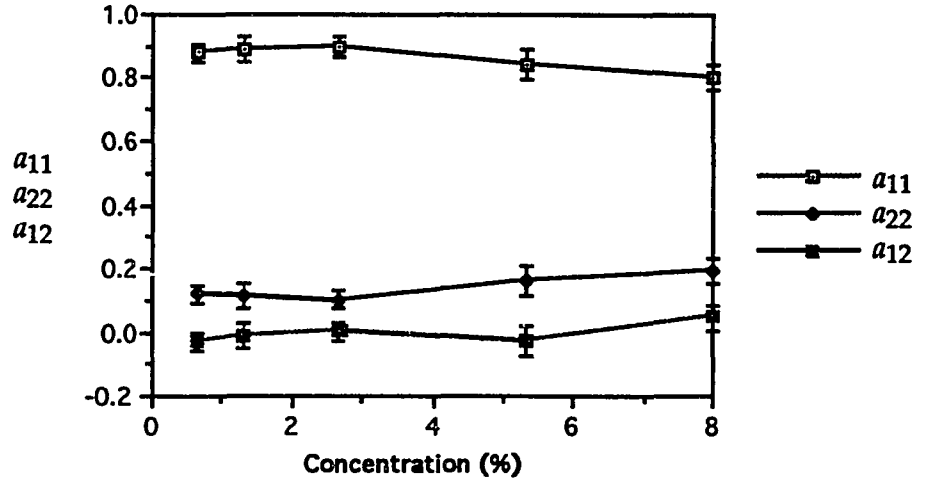

Figure 5.5 Steady state orientation tensors for suspensions of 0.015" diameter fibers in planar stretching as a function of concentration.

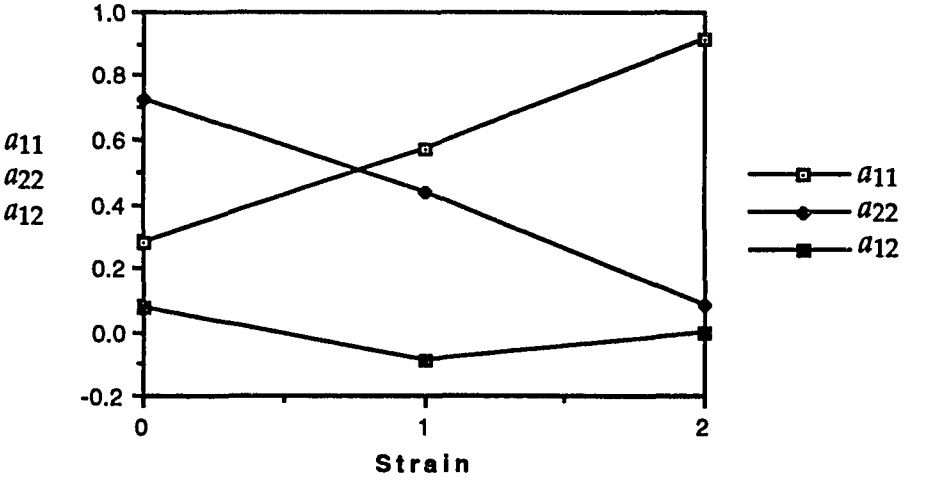

Figure 5.6 Orientation tensors for 0.25% concentration suspensions of 0.006" diameter fibers in planar stretching as a function of strain.

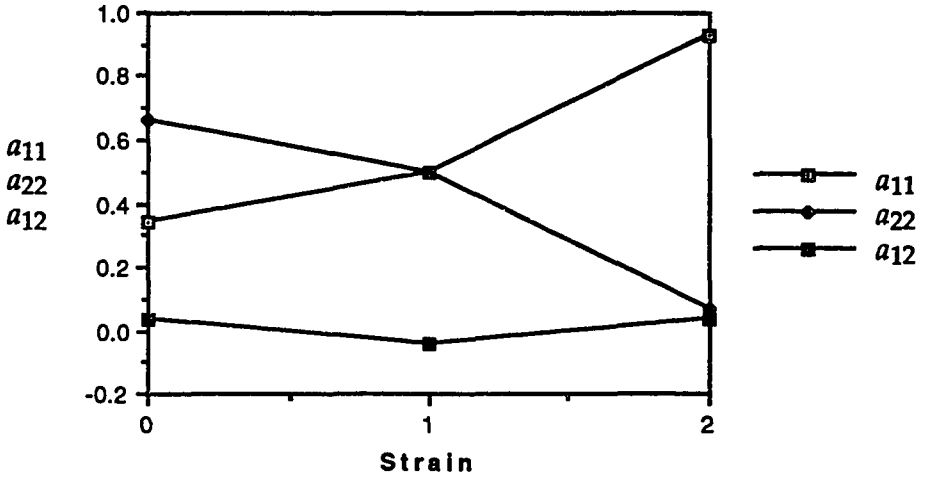

Figure 5.7 Orientation tensors for 0.50% concentration suspensions of 0.006" diameter fibers in planar stretching as a function of strain.

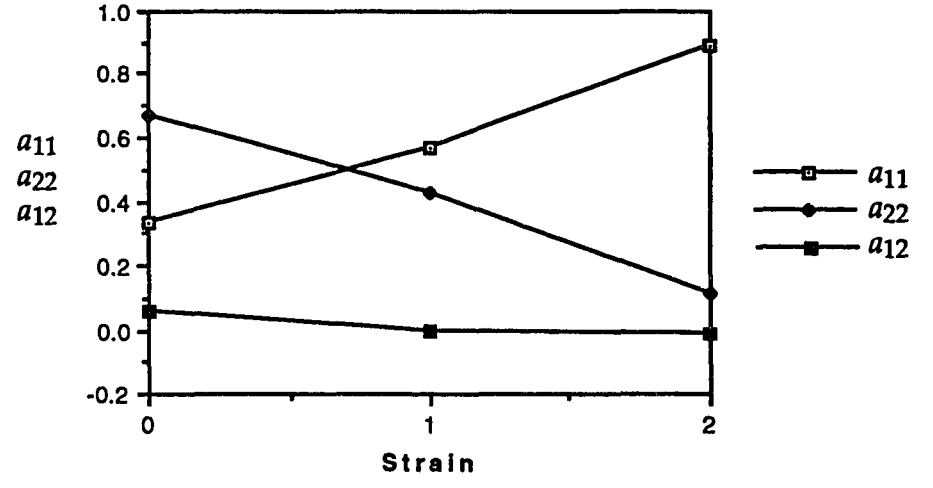

Figure 5.8 Orientation tensors for 1.0% concentration suspensions of 0.006" diameter fibers in planar stretching as a function of strain.

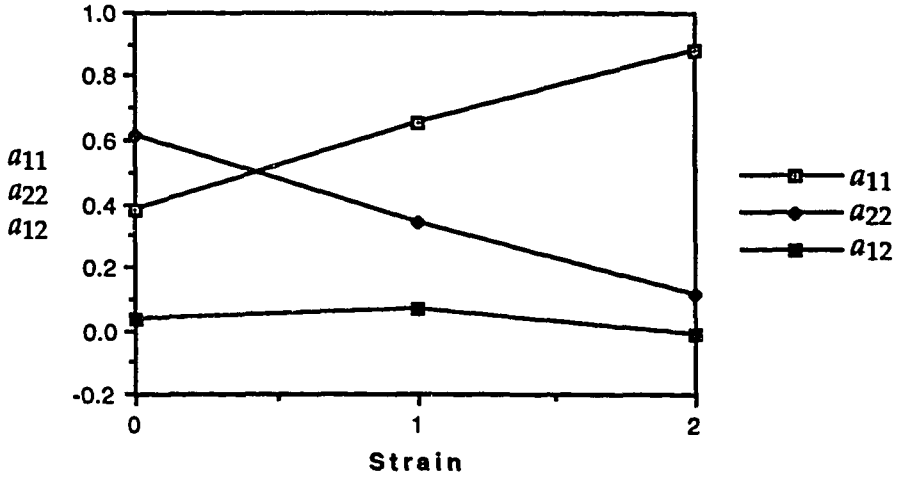

Figure 5.9 Orientation tensors for 2.0% concentration suspensions of 0.006" diameter fibers in planar stretching as a function of strain.

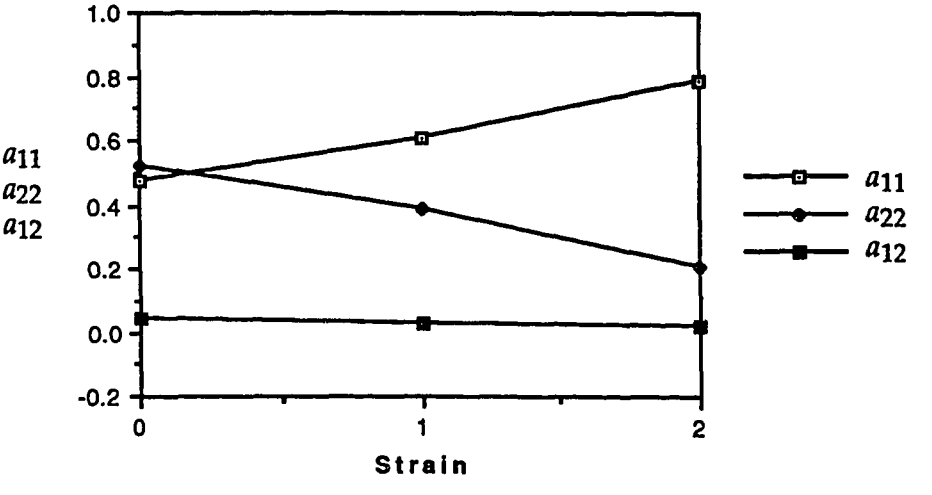

Figure 5.10 Orientation tensors for 3.0% concentration suspensions of 0.006" diameter fibers in planar stretching as a function of strain.

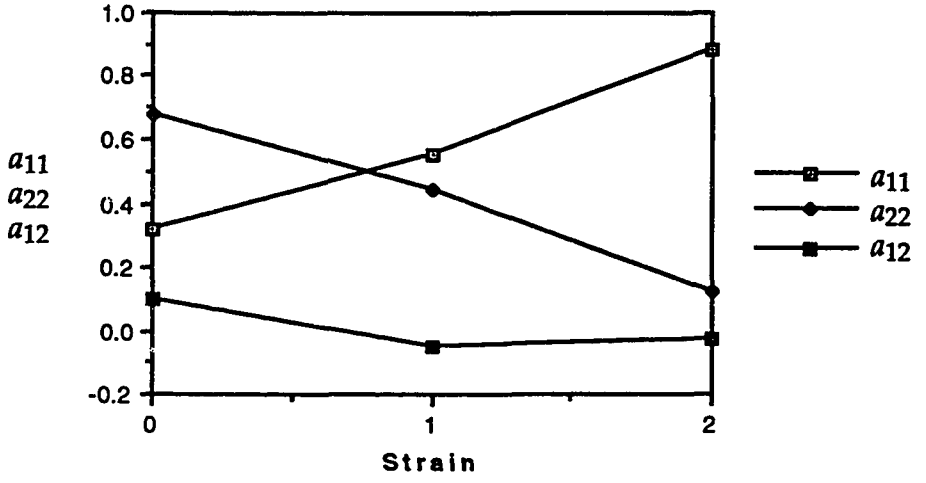

Figure 5.11 Orientation tensors for 0.667% concentration suspensions of 0.015" diameter fibers in planar stretching as a function of strain.

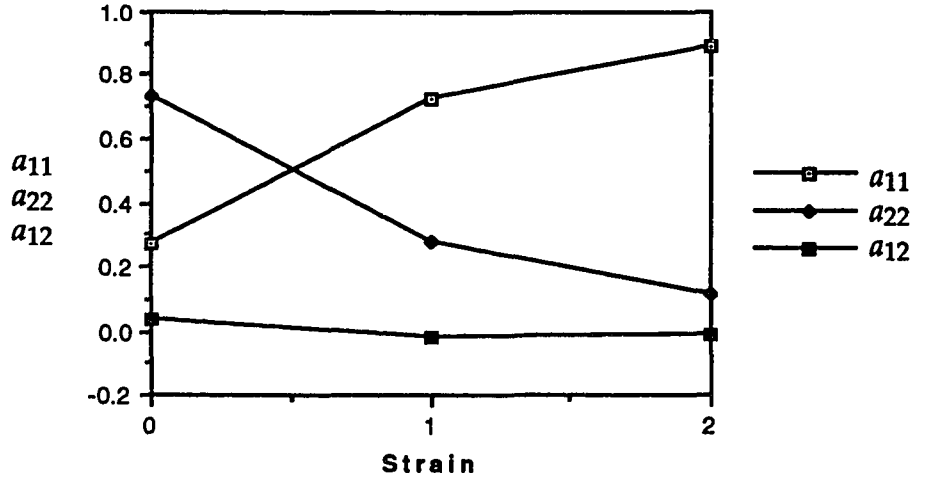

Figure 5.12 Orientation tensors for 1.33% concentration suspensions of 0.015" diameter fibers in planar stretching as a function of strain.

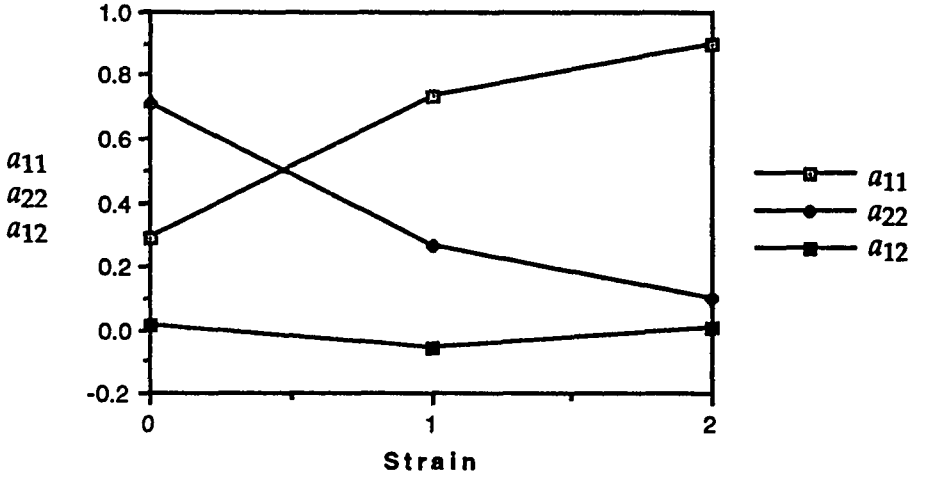

Figure 5.13 Orientation tensors for 2.66% concentration suspensions of 0.015" diameter fibers in planar stretching as a function of strain.

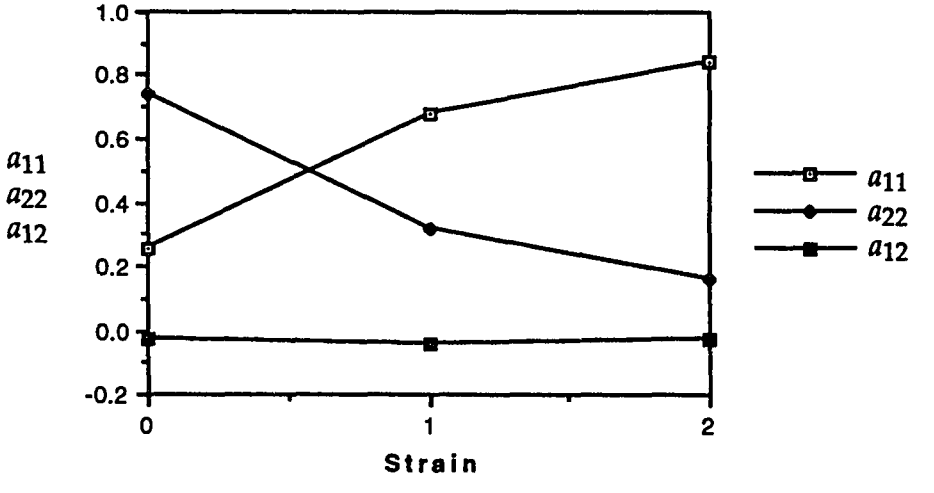

Figure 5.14 Orientation tensors for 5.33% concentration suspensions of 0.015" diameter fibers in planar stretching as a function of strain.

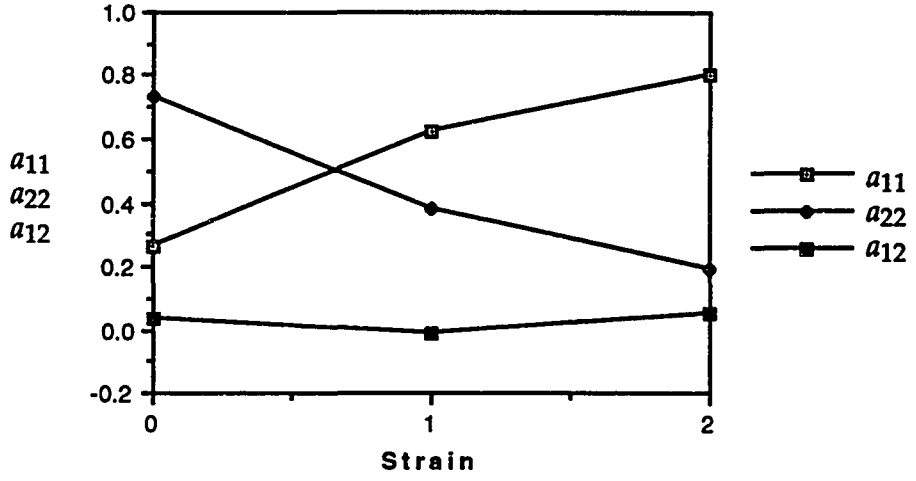

Figure 5.15 Orientation tensors for 8.0% concentration suspensions of 0.015" diameter fibers in planar stretching as a function of strain.

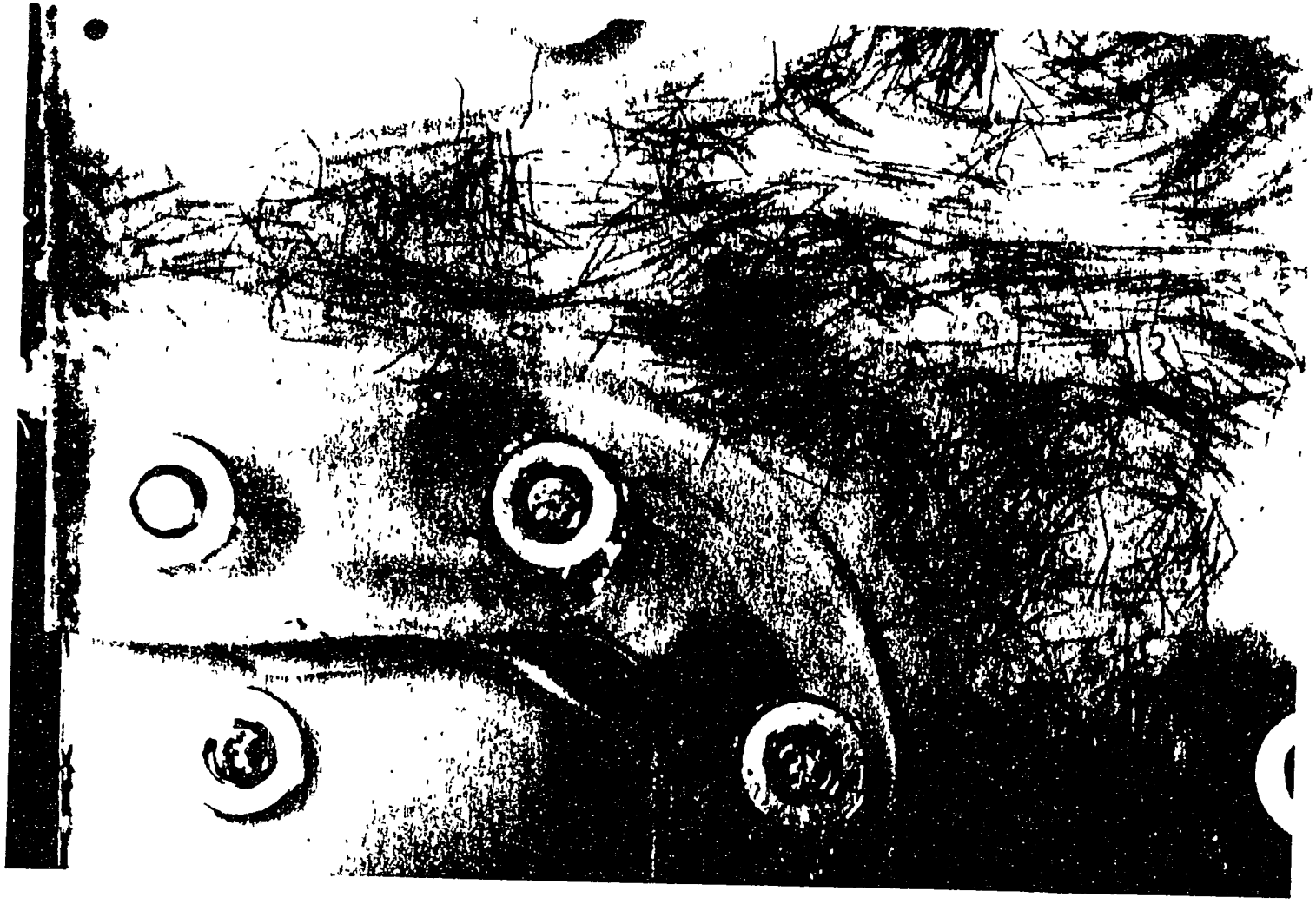

Figure 5.16 Photograph of a suspension of fibers of 0.006" diameter at a concentration of 3.0% by volume in glycerin. The suspension is flowing in at the bottom and top and out to the left and right. Note the wave patterns of fiber orientation and the clumps of fibers near the center of the hyperbola.

6. DISCUSSION OF RESULTS

The numerical model exercised in Chapter Four and the experimental results of Chapter Five are gathered together here to analyze the effectiveness of the mechanical fiber-fiber interaction model. Numerical simulations of suspension behavior including interactions have shown themselves to be quite computationally intensive. Therefore, simplified versions of the mechanistic diffusion are also discussed.

6.1 Comparison of Numerical Results and Experiments

The experimental results from Chapter Five are presented in the following figures against numerical results of the simulation of the orientation model. The goal of any simulation of a physical process such as fiber orientation in a concentrated suspension is to predict behaviors under a range of conditions with a minimum required amount of parameter adjustment. The parameters of

Table 6.1 Input parameters for numerical simulation of flow and orientation of three concentrated suspensions of 0.006" diameter fibers

Parameter	Symbol	Value	Units
scalar strain rate	$\dot{\gamma}_{II}$	2.828	1/s
number density	n	3.39e9 6.78e9 10.2e9	$1/m^3$
fiber length	L	12.7e-3	m
fiber diameter	d	152.4e-6	m
suspending fluid viscosity	m	1.0	Pa·s
interaction force coefficient	f_I	23.62e-3	Pa·s·m
hydrodynamic force coefficient	ζ_a	12.7e-3	Pa·s·m
interaction correlation time	ε	0.001	s
time step size	Δt	0.001	s
angular step size	$\Delta\phi$	$\pi/30$	radians

Table 6.2 Input parameters for numerical simulation of flow and orientation of three concentrated suspensions of 0.015" diameter fibers

Parameter	Symbol	Value	Units
scalar strain rate	$\dot{\gamma}_{II}$	2.828	1/s
number density	n	1.45e9 2.89e9 4.34e9	$1/m^3$
fiber length	L	12.7e-3	m
fiber diameter	d	381.0e-6	m
suspending fluid viscosity	m	1.0	Pa·s
interaction force coefficient	f_I	15.75e-3	Pa·s·m
hydrodynamic force coefficient	ζ_a	12.7e-3	Pa·s·m
interaction correlation time	ε	0.0025	s
time step size	Δt	0.001	s
angular step size	$\Delta\phi$	$\pi/30$	radians

this model include the interaction force coefficient and the correlation time. Other terms such as the hydrodynamic force coefficient and the carrier fluid viscosity are well defined and understood.

The input data to the simulation are given in Table 6.1 for the 0.006" diameter fiber suspensions and Table 6.2 for the 0.015" diameter fibers suspensions. The orientation tensors calculated from the finite difference solutions of the probability distribution function are given in Figures 6.1-6.8.

Figure 6.1 shows the steady state values of the x direction orientation tensor for concentrated suspensions of 0.006" diameter fibers, and Figure 6.2 shows the same data for the 0.0015" diameter fibers. Each of these figures gives the calculated steady state value for a_{11} against the experimental results. Results from the numerical solution indicate that a steady configuration had been established at strain equal to three (3), $\dot{\gamma}_{II}t = 3$. At that point, the slope of the

orientation as a function of strain decreased below 0.02, and at strain equal to five (5), the orientation would change by 0.7% per unit strain. Data on these figures, 6.1 and 6.2, was taken from each condition at strain equals five.

In each figure, all model parameters remain the same; only the input concentration level is varied once a suitable number for the interaction force coefficient is determined by trial an error for each fiber diameter. The experimental and numerical data indicate that a true steady state was not measured in the experiments. Therefore, an interaction force coefficient was chosen such that the numerical steady state value was slightly higher than the last data point in each experiment. The numerical results do show the same linear decrease in the equilibrium orientation state as the experimental data. The favorable results in these figures indicate that the model does a good job of calculating the suspension orientation state for the range of suspension concentrations examined in these experiments (i.e. semi-concentrated to concentrated).

The interaction force coefficient is discussed in Chapters Three and Four. There the interaction force is presumed to behave like hydrodynamic friction. In that case, the magnitude of the interaction force coefficient f_I is governed by the viscosity of the suspending fluid μ, the nominal area of interaction d^2, and the separation distance $h \leq d$.

$$f_I = O\left(\frac{d^2\mu}{h}\right) \tag{6.1}$$

From this, the separation distance in each suspension is calculated to be 1.5 μm for the 0.0015" diameter fibers and 1.0 μm for the 0.006" diameter fibers. Therefore, fitting f_I confirms that fiber centers in the concentrated suspensions

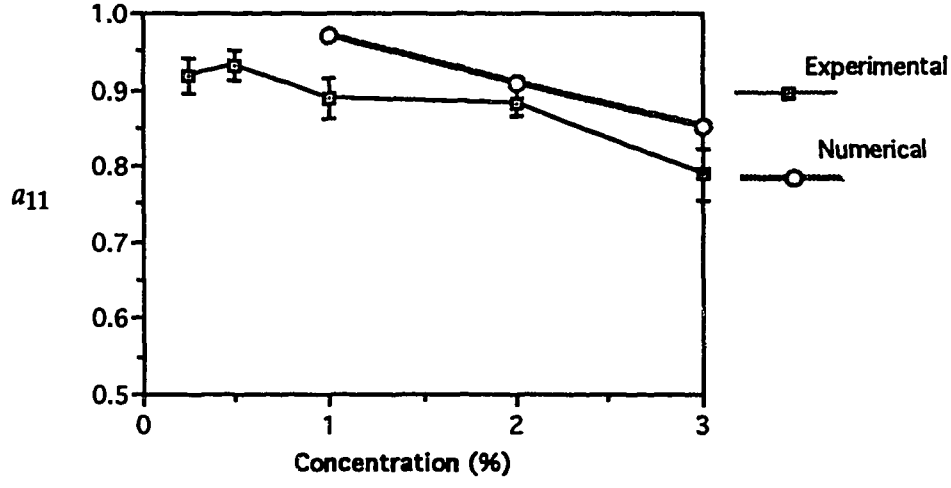

Figure 6.1 The stretching direction orientation tensor a_{11} from experiment and from numerical simulations of suspension of 0.006" diameter fibers in planar stretching flow.

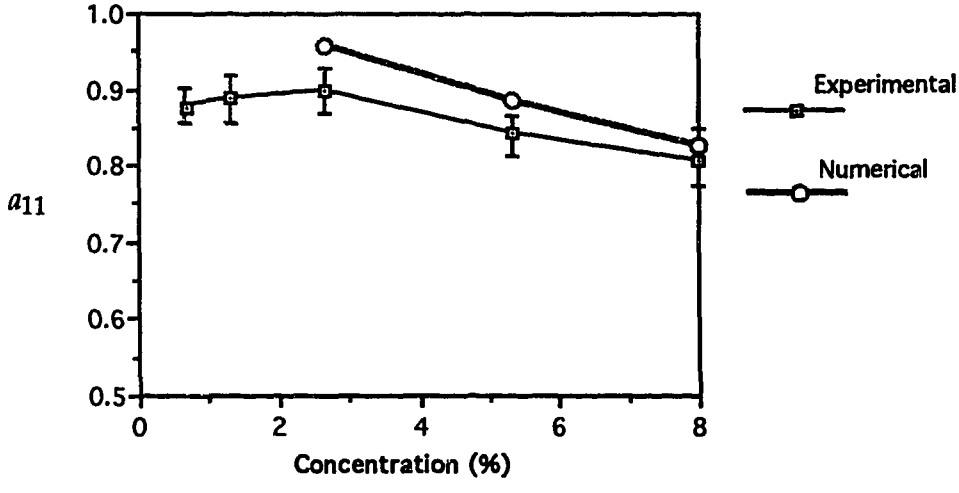

Figure 6.2 The stretching direction orientation tensor a_{11} from experiment and from numerical simulations of suspensions of 0.015" diameter fibers in planar stretching flow.

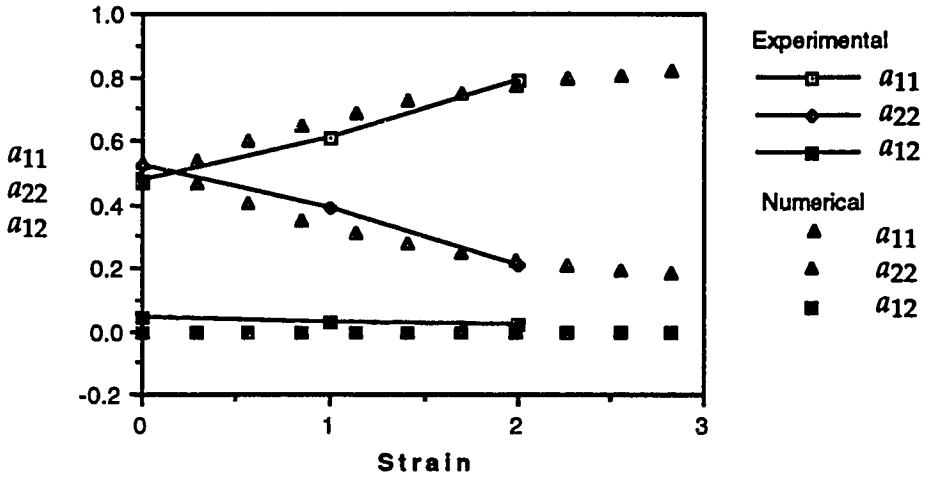

Figure 6.3 Orientation tensors from stretching experiment and from numerical simulation of an 3.0% concentration suspension of 0.006" diameter fibers in planar stretching flow.

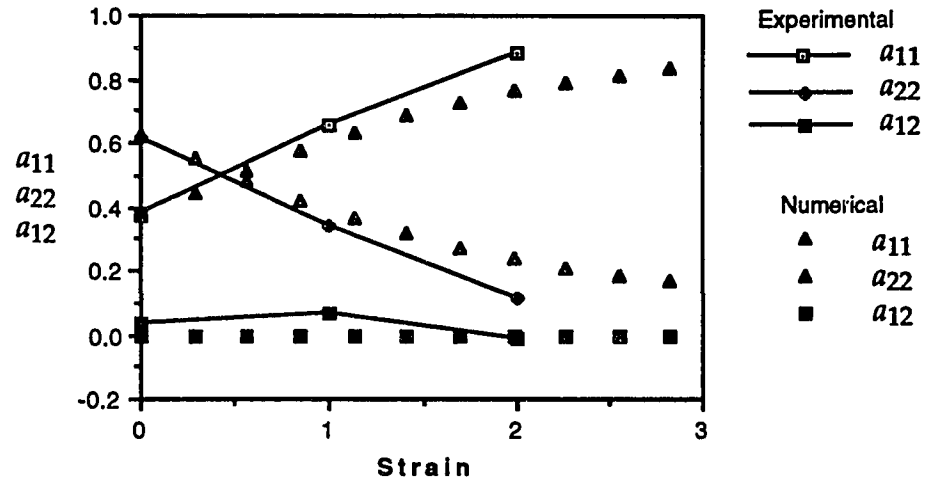

Figure 6.4 Orientation tensors from stretching experiment and from numerical simulation of an 2.0% concentration suspension of 0.006" diameter fibers in planar stretching flow.

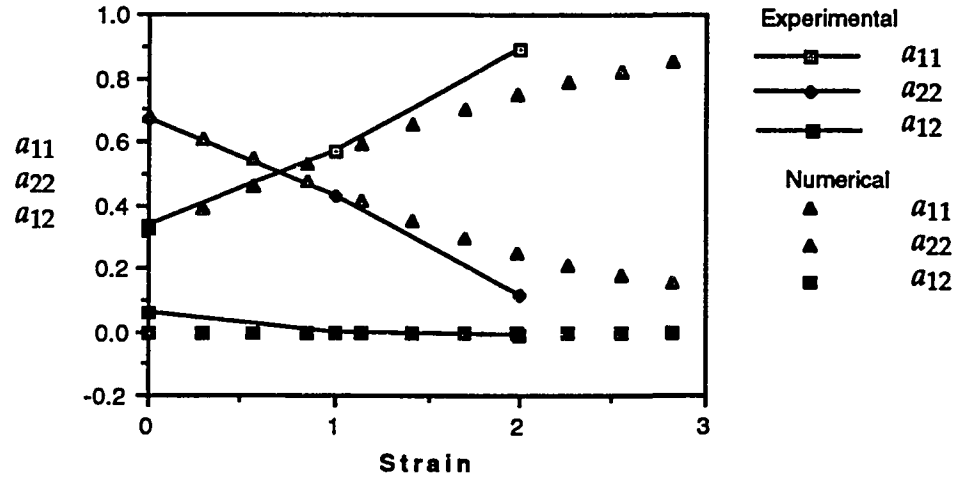

Figure 6.5 Orientation tensors from stretching experiment and from numerical simulation of an 1.0% concentration suspension of 0.006" diameter fibers in planar stretching flow.

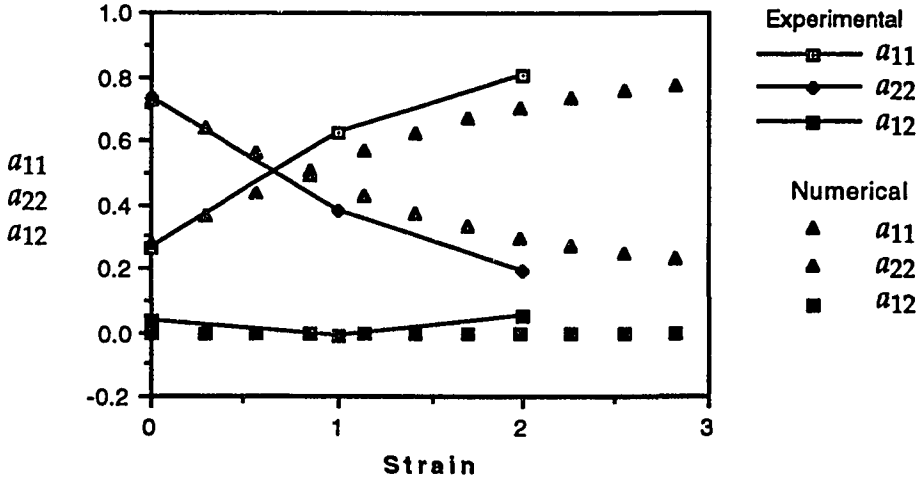

Figure 6.6 Orientation tensors from stretching experiment and from numerical simulation of an 8.0% concentration suspension of 0.015" diameter fibers in planar stretching flow.

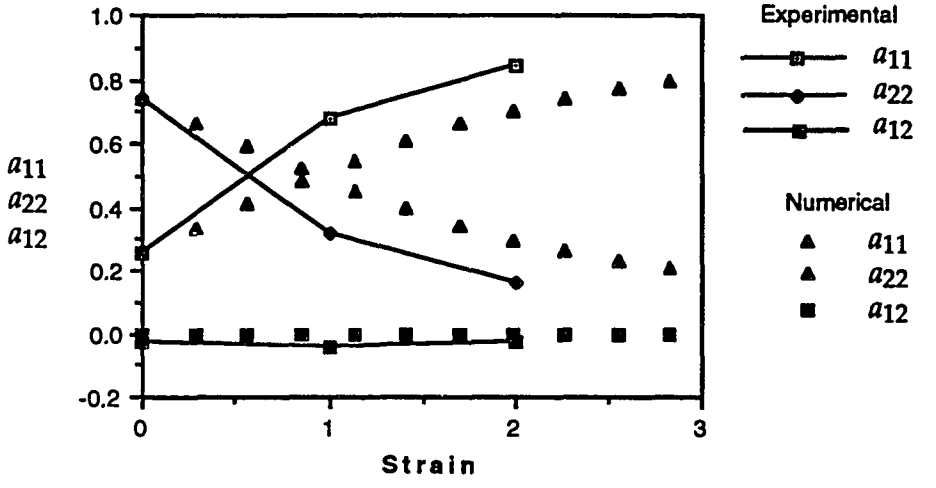

Figure 6.7 Orientation tensors from stretching experiment and from numerical simulation of an 5.33% concentration suspension of 0.015" diameter fibers in planar stretching flow.

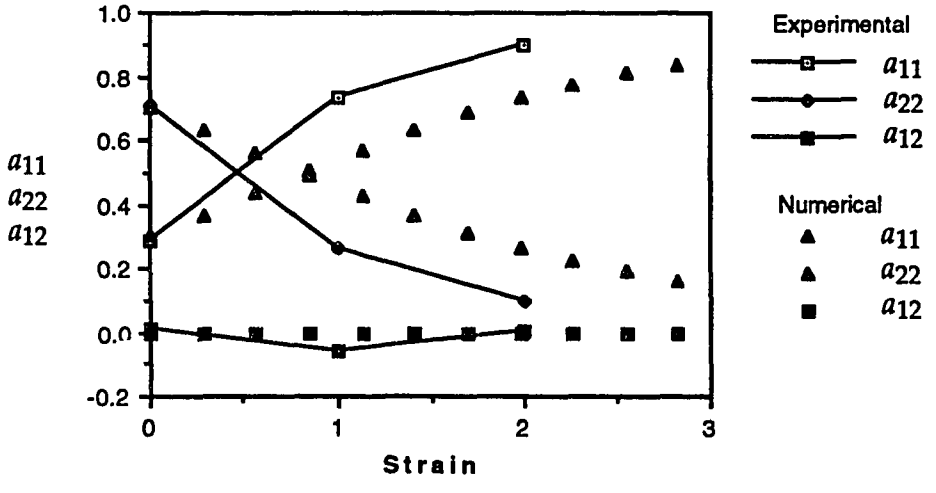

Figure 6.8 Orientation tensors from stretching experiment and from numerical simulation of an 2.66% concentration suspension of 0.015" diameter fibers in planar stretching flow.

must lie nearly one diameter apart and the surfaces are lubricated by a thin film of fluid.

The time evolution of the orientation in concentrated suspensions is shown in Figures 6.3-6.8. The orientation tensors are again calculated from the probability distribution function, whose behavior is determined via the interaction-based diffusion theory. In each of these cases the orientation tensors appear to qualitatively follow the behavior of the experimental data, but the time scale appears to be too long in the majority of the simulations. i.e. the orientation show equilibriums in the experimental data more quickly than predicted. This may be due in to overly large sampling areas in the experiments (see Figure 5.2), to a sampled fiber population that is too small, or possibly to an inability to sustain a random fiber orientation state at the entrance to the test section.

6.2 Isotropic Diffusion and Governing Equations for Orientation Tensors

While the fiber interaction-based diffusion function is a sensible approach to the problem of prediction of fiber orientation in concentrated suspensions, it is computationally prohibitive. Integration over the entire planar orientation domain at each node in the orientation space and at each time step requires a significant number of calculations. Other more frugal techniques exist for the simulation of concentrated suspension behavior. This section examines the possibility of using such techniques in conjunction with the fiber-fiber interaction model to economize the process of simulating flow and orientation of fiber suspensions.

One such technique includes adding an isotropic orientational (or rotational) diffusion term to the dilute solution to the governing equation for

the probability distribution function [44]. In this case, the equation is simply a specialized version of Eq. (4.1).

$$\frac{D\psi}{Dt} = -\frac{\partial}{\partial\phi}[\dot{\phi}\psi] + D_r\frac{\partial^2}{\partial\phi^2}[\psi] \tag{6.2}$$

Folgar and Tucker postulate that the rotational diffusion due to interactions is likely to be proportional to the strain rate in the material. Only fiber motion can cause fiber dispersion.

$$D_r = C_I\,\dot{\gamma}_{II} \tag{6.3}$$

Equation (6.1) can be evaluated very efficiently in comparison to Eq. (4.1). The diffusion function of the fiber-fiber interaction theory does indeed turn out to be proportional to $\dot{\gamma}_{II}$. When Eq. (6.2) is evaluated with the interaction coefficient C_I adjusted to match the steady state results of the mechanistic diffusion equation, we arrive at the results shown in Figures 6.9 and 6.10 for two different suspensions respectively. These figures show that the isotropic diffusion results do not vary significantly from the results of the interaction-based diffusion calculations.

This process of matching the results of the isotropic diffusion calculation to those of the mechanistic diffusion equation is repeated for several conditions, and in Figure 6.11 are shown the data. The isotropic interaction coefficient is plotted as a function of the terms that appear in the diffusion function Eq. (3.61). The data fall convincingly onto a straight line, and ignoring a constant that is non-physical and negligible, the interaction coefficient C_I has the following form.

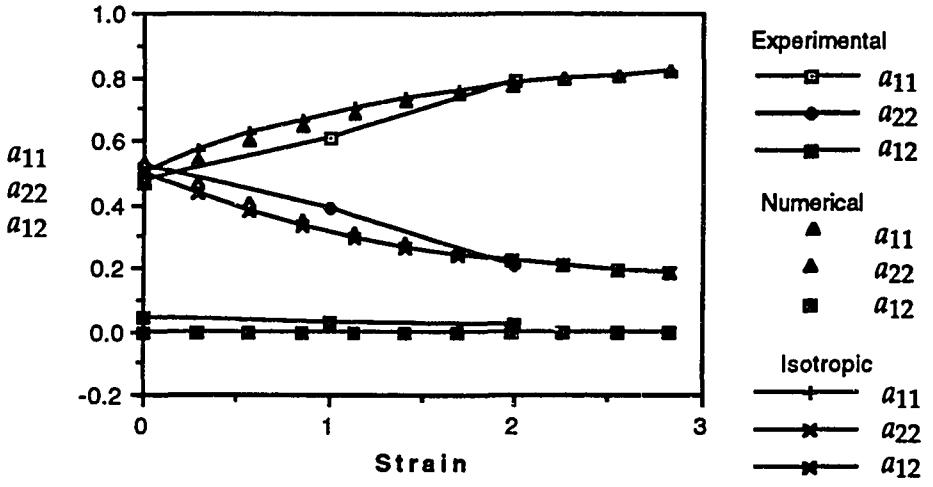

Figure 6.9 Orientation tensors from stretching experiment, and mechanistic diffusion and isotropic diffusion simulations for a suspension of 0.006" fibers at 3.0% concentration by volume.

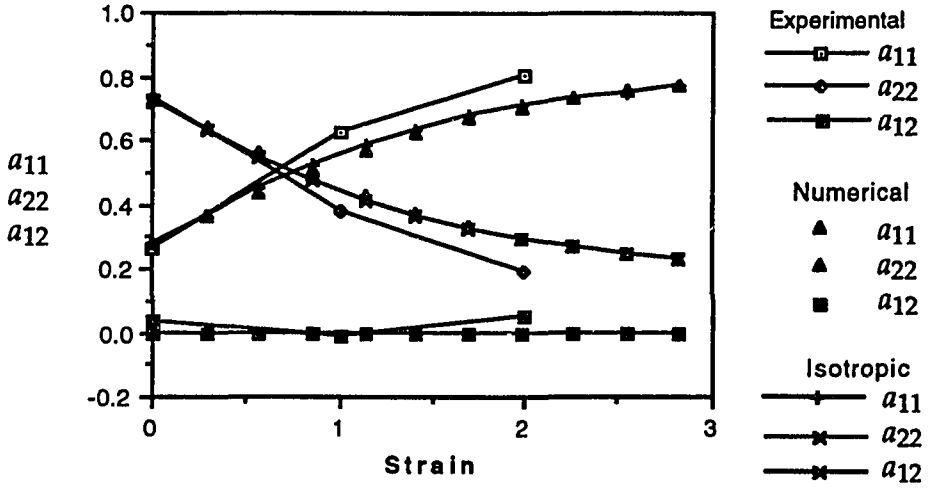

Figure 6.10 Orientation tensors from stretching experiment, and mechanistic diffusion and isotropic diffusion simulations for a suspension of 0.015" fibers at 8.0% concentration by volume.

$$C_I \propto \varepsilon n d L^2 f_I^2 \zeta_a^{-2} \tag{6.3}$$

The constant of proportionality in this case is 0.422.

Another technique that provides an even greater computational savings over the mechanistic diffusion calculations is a direct evaluation of the governing equation for the orientation tensors.

$$\frac{D\mathbf{a}_2}{Dt} = -\frac{1}{2}(\boldsymbol{\omega}\cdot\mathbf{a}_2 - \mathbf{a}_2\cdot\boldsymbol{\omega}) + \frac{1}{2}(\dot{\boldsymbol{\gamma}}\cdot\mathbf{a}_2 - \mathbf{a}_2\cdot\dot{\boldsymbol{\gamma}} - 2\dot{\boldsymbol{\gamma}}:\mathbf{a}_4) + 2D_r\,(\boldsymbol{\delta} - 2\mathbf{a}_2) \tag{6.4}$$

$\boldsymbol{\omega} = \nabla\mathbf{v} - \nabla\mathbf{v}^T$ is the vorticity and $\dot{\boldsymbol{\gamma}} = \nabla\mathbf{v} + \nabla\mathbf{v}^T$ is the rate of strain tensor. In this governing equation is the rotational diffusivity D_r. This term is identical to that found in the governing equation for the probability distribution function. Advani [23] shows how (6.4) can be derived from (6.2). A problematic term in the

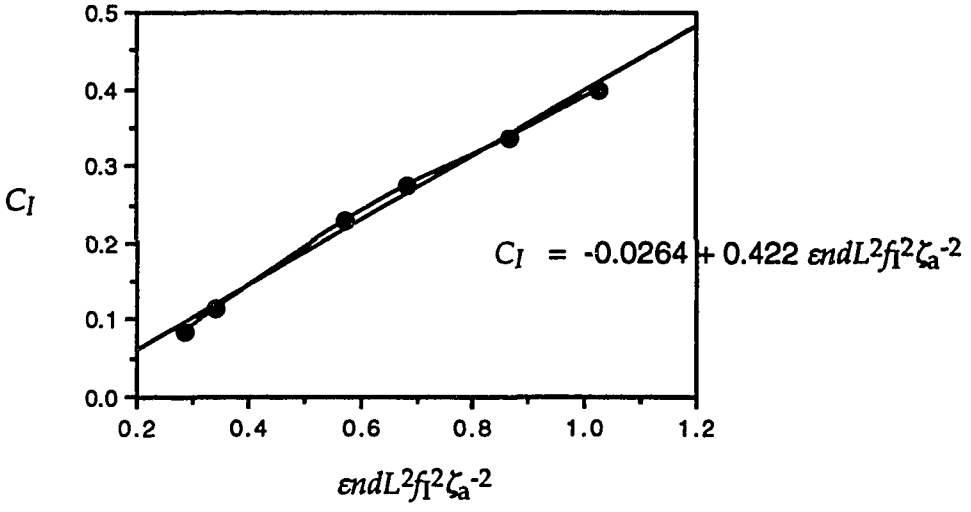

Figure 6.11 Isotropic diffusion coefficient C_I required to match steady state results from mechanistic diffusion calculations as a function of the variables that govern the magnitude of the diffusion function.

equation of change for the second order orientation tensor is the fourth order orientation tensor $\mathbf{a}_4$. In that the orientation tensors are incomplete descriptors of the full probability distribution function, the savings in variables comes with a necessary approximation of the higher order tensor. This closure problem is discussed by Advani [23] as well as others [26, 61].

6.3 Summary

The model for fiber-fiber interaction that describes that dispersion of fibers in concentrated suspensions can be used to successfully model the increase in the diffusion observed in concentrated suspensions of slender fibers. The numerical simulations of the experimental suspensions required hundreds of minutes of CPU time on a modern workstation. This was for an experiment were the strain rate was uniform and constant throughout. Modeling a more complicated flow field or three dimensional orientation states would certainly be prohibitively time-consuming.

In answer to this need, the governing equation to the probability distribution function for fiber orientation and the orientation tensor equation of change can include an isotropic rotary diffusion term and possess a definite advantage in economy. This chapter has shown how the use of an isotropic diffusion whose magnitude is proportional to the strain rate can be matched to the results of the interaction diffusion model for planar orientation and flow. The scalar interaction coefficient C_I has shown a simple proportional relationship to the suspension variables that appear in the mechanistic equation of change for the probability distribution function in a suspension with strong fiber-fiber interaction.

7. CONCLUSIONS AND RECOMMENDATIONS

Slender stiff fibers added to polymers create composite materials that have the processability of the polymer matrix and the strength of the fiber reinforcement. The mechanical properties of these composites are highly dependent on the orientation of the fibers. Processing fiber reinforced polymer composites determines to a large extent the orientation state of the reinforcement in the material. In commercially viable composites, the reinforcing fibers are added to thermoses or thermoplastics to volume concentrations of 5-40%. In these concentrated suspensions each fiber will experience numerous fiber-fiber interactions. The orientation and rheology in the composite during processing will be influenced by the restraining nature of the interaction forces.

The interaction forces are incorporated in a model based on classical slender body theory to predict the orientation and rheology of concentrated suspensions of fibers. The interaction force between particles is modeled as a hydrodynamic friction; the force is proportional to the relative velocity at the point of contact. The addition of the interfiber forces creates additional terms in the stress response of the material that are second order in concentration. The addition of the interfiber forces create a diffusion in the behavior of the probability distribution function. This diffusion term is proportional to the number of fibers and the rate of strain in the suspension.

Numerical solution of the advection-diffusion equation verifies the diffusive nature of the interfiber forces. The perfect alignment of the fibers in shear or stretching is moderated. More fibers in the suspension mean greater total interaction forces and subsequently a larger diffusion effect. The rheological responses calculated from the numerical simulations show normal stresess in steady shear, variation during start-up of shear flow and extensional viscosity that is

several orders of magnitude larger that the carrier fluid viscosity. These characteristics are all typical of suspension of slender fibers.

Experiments with semi-concentrated and concentrated suspension of fibers in a glycerin simulate the flow of composite materials during processing. The fibers were oriented initially in a random-in-plane orientation and subject to a stretching flow in the plane of the fiber orientation. The experiments conducted during this research lead to two important conclusions.

- Concentrated suspensions do show a diffusive effect in their orientation states, and this effect increases with increasing concentration levels. That is, higher concentration results in lower fiber alignment in the flow direction.
- The nature of the interaction force in concentrated suspensions does not actually produce a dispersive effect in the fiber rotation velocity, but rather it produces a hindrance to the fiber rotation. Observed fibers would travel in the suspension in clumps of the size of the fiber length and larger. These clumps apparently possessed a viscosity higher than the mean, and the suspension would set up flow fields that curved around the groups of 10-50 fibers. This indicates that the simple hydrodynamic approximation for the interfiber force used in the theory is not strictly correct.

The results of the experiments were compared to numerical simulations of the suspension behavior using the interaction-based diffusion model. Simulation and experiment concur that, in the concentrated regime, increases in the fiber volume fraction increase the spread in the probability distribution function. Comparison of simulation and experiment show also that future experiments must be able to capture orientation behavior at strains greater than two (2), and that the theory predicts an approach to steady state that is too slow in stretching flow.

In spite of the complexity of the diffusion function that results from including an interaction force in the fiber dynamics of a concentrated suspension, the theoretical predictions can be effectively mimicked by an isotropic rotary diffusion. This rotary diffusion was shown to be proportional to the strain rate in the material and proportional to the combination of variables ($\epsilon n d L^2 f_1^2 \zeta_a^{-2}$) that govern the magnitude of the mechanistic diffusion function. This fact allows significant economy in solving for the fiber orientation in suspensions of slender fibers.

Inclusion of the fiber-fiber contact forces is an important and necessary component of prediction of concentrated suspension orientation and rheology. Future work must be targeted at better describing the relative motion between crossed fibers and the force between them. Furthermore, the current model requires a more accurate prediction of the time over which fiber-fiber contact geometry is uncorrelated. Future work must also include experiments that allow observation of fiber behavior at large (>2) strains.

LIST OF REFERENCES

[1] Darlington, M.W., P. L. McGinley, and G. R. Smith, "Structure and Anisotropy of Stiffness in Glass Fibre-Reinforced Thermoplastics," *J. Mat. Sci., 11,* 877 (1976).

[2] Pipes, R. B., R. L. McCullough and D. G. Taggart, "Behavior of Discontinuous Fiber Composites: Fiber Orientation," *Polym. Comp., 3,* 34-39 (1982).

[3] Goettler, L. A., "Mechanical Property Enhancement in Short-Fiber Composites Through the Control of Fiber Orientation During Fabrication," *Polym. Compos., 1,* 60 (1984).

[4] Denton, D. L., "Effects of Processing Variables on the Mechanical Properties of Structural SMC-R Composites," *Proc., 36th Ann. Tech. Conf., SPI RP/C Div., Sect. 16-A* (1981).

[5] Curtis, P. T., M. G. Bader, and J. E. Bailey, "The Stiffness and Strength of a Polyamide Thermoplastic Reinforcedwith Glass and Carbon Fibers," *J. Mat. Sci., 13,* 377-390 (1978).

[6] Schwartz, P., G. Fischer, and P. Eyerer, "Elastic Properties and Thermal Expansions of Short Fiber Composites with Varying Fiber Content, Length and Orientation," *SPE Tech. Papers, 49,* 592-594 (1991).

[7] Hill, R., "Elastic Properties of Reinforced Solids: Some Theoretical Principles,"*J. Mech. Phys. Solids, 11,* 357-372 (1963).

[8] Halpin, J. C. and J. L. Kardos, "The Halpin-Tsai Equations: A Review," *Polym. Eng. Sci., 16,* 344-352 (1976).

[9] Halpin, J. C. and N. J. Pagano, "The Laminate Approximation for Randomly Oriented Fibrous Composites," *J. Comp. Mat., 3,* 720-?? (1969).

[10] McCullough, R. L., "Anisotropic Elastic Behavior of Crystalline Polymers," *Treatise on Materials Science and Technology, 10B,* 453 Academic Press, Inc., NewYork (1977).

[11] Advani, S. G. and C. L. Tucker, "The Use of Tensors to Describe and Predict Fiber Orientation in Short Fiber Composites," *J. Rheology, 31,* 751 (1987).

[12] Owen, M. J., D. H. Thomas, and M. S. Found, "Flow, Fibre Orientation and Mechanical Property Relationships in Polyester DMC," *Proc. 33rd Ann. Tech. Conf., SPI RP/C Div., Sect. 20-B* (1978).

[13] Owen, M. J. and K. Whybrew, "Fiber Orientation and Mechanical Properties in Polyester Dough Molding Compound (DMC)," *Plastic and Rubber, 1(6),* 231 (1976)

[14] Gandhi, K. S. and R. Burns, "Rheological Properties of Glass Fiber-Reinforced Dough Molding Compounds," *Trans. Soc. of Rheo., 20,* 489-502 (1976).

[15] Darlington, M. W. and P. L. McGinley, "Fibre Orientation Distribution in Short Fibre Reinforced Plastics," *J. Mat. Sci., 10,* 906 (1975).

[16] Darlington, M. W. and G. R. Smith, " Some Features of the Injection Molding of Short Fiber Reinforced Thermoplastics in Center Sprue-Gated Cavities," *Polym. Comp., 8,* 16 (1987).

[17] Bright, P. F., R. J. Crowson, and M. J. Folkes. "A Study of the Effect of Injection Speed on Fibre Orientation in Simple Moldings of Short Glass Fibre-Filled Polypropylene," *J. Mat. Sci., 13,* 2497 (1978).

[18] Bay, R. S. and C. L. Tucker, "Fiber Orientation in Simple Injection Moldings. Part II: Experimental Results," *Polym. Comp., 13(4),* 332 (1992).

[19] Tucker, C. L., "Flow Regimes for Fiber Suspensions in Narrow Gaps," *J. Non-Newtonian Fluid Mech., 39,* 239-268 (1991).

[20] Dinh, S. M., "On the Rheology of Concentrated Suspensions," Sc.D. Thesis, Chem. Eng., M.I.T. (1982).

[21] Barone, M. R., D. A. Caulk, "Kinematics of Flow in Sheet Molding Compounds," *Polym. Comp., 6,* 105-109 (1985).

[22] Onat, E. T. and F. A. Leckie, "Representation of Mechanical Behavior in the Presense of Changing Internal Structure," *J. Appl. Mech., 55,* 1 (1988).

[23] Advani, S. G., "Prediction of Fiber Orientation During Processing of Short Fiber Composites," Ph.D. Thesis, Mech. Eng., U. of Illinois (1987).

[24] Hand, G. L., "A Theory of Anisotropic Fluids," *J. Fluid Mech., 13,* 33 (1962).

[25] Hinch, E. J. and L. G. Leal, "Constitutive Equations in Suspension Mechanics. Part 2. Approximate Forms for a Suspension of Rigid Particles Affected by Brownian Rotations," *J. Fluid Mech., 76,* 187-208 (1976)

[26] Bay, R. S. "Fiber Orientation in Injection Molded Composites: A Comparison of Theory and Experiement," Ph.D. Thesis, Mech. Eng., U. of Illinois (1991).

[27] Einstein, A., "Eine Neue Bestimmung der Molukul-dimensionen," *Annalen der Physic, 19,* 289 (1906).

[28] Jeffery, G. B., "The Motion of Ellipsoidal Particles in Dilute Suspensions," *Proc. Roy. Soc., Series A, 102,* (1922).

[29] Burgers, J. M. "On the Motion of Small Particles of Elongated Form. Suspended in a Viscous Liquid," *Akad. Von Wet. Verhand., 16,* Sec. 1, 113 (1938).

[30] Karnis, A., H. L. Goldsmith, and S. G. Mason, "The Kinetics of Flowing Dispersions. I. Concentrated Suspensions of Rigid Particles," *J. Colloid Interface Sci., 22,* 531 (1966).

[31] Anczurowski, E. and S. G. Mason, "Particle Motion in Sheared Suspensions. XXIV. Rotations of Rigid Sheroids and Cylinders," *Trans. Soc. of Rheo., 12(2),* 209 (1968).

[32] Anczurowski, E., R. G. Cox, and S. G. Mason, "The Kinetics of Flowing Dispersions. III. Equilibrium Orientations of Rods and Discs (Experimental)," *J. Colloid Interface Sci., 22,* 533 (1967).

[33] Okagawa, A., and S. G. Mason, "Suspensions: Fluids with Fading Memories," *Science, 181,* 159 (1973).

[34] Mason, S. G., R. St. J. Manley, "Particle Motions in Sheared Suspensions: Orientations and Interactions of Rigid Rods," *Proc. Roy. Soc., Series A, 238,* 117-131 (1957).

[35] Cox, R. G. "The Motion of Suspended Particles Almost in Contact," *Int. J. of MultiPhase Flow, 1,* 343 (1974).

[36] Shaqfeh, E. S. G. and D. L. Koch, "The Effect of Hydrodynamic Interactions on the Orientation of Axisymmetric Particles Flowing Through and Fixed Bed of Spheres or Fibers," *Phys. Fluids, 31(4),* 728 (1988).

[37] Kamal, M. R. and A. T. Mutel, "The Prediction of Flow and Orientation Behavior of Short Fiber Reinforced Melts in Simple Flow Systems," *Polym. Comp., 10,* 337 (1989).

[38] Dinh, S. M. and R. C. Armstrong, "A Rheological Equaiton of State for Semi-Concentrated Fiber Suspensions, " *J. Rheology, 28,* 207 (1984).

[39] Maschmeyer, R. O. and C. T. Hill, "Rheology of Concentrated Suspensions of Fibers. I. Review of the Literature, " *Adv in Chem. Series,* No. 134, 95, Am. Chem. Soc., Washington, D. C. (1974).

[40] Kulichikhin, V. G., A Ya. Malkin, and S. P. Papkov, "Rheological Properties of Liquid Crystalline Polymer Systems. Review," *Polym. Sci. U.S.S.R., 26(3),* 499 (1984).

[41] Marrucci, G., "Rheology of Liquid Crystal Polymers," *Pure Appl. Chem., 57(11),* 1545 (1985).

[42] Lipscomb, G. G., M. M. Denn, D. U. Hur, and D. V. Boger, "The Flow of Fiber Suspensions in Complex Geometries," *J. Non-Newtonian Fluid Mech., 26,* 297-325 (1988).

[43] Stover, C. A., D. L. Koch, and C. Cohen, "Observations of Fibre Orientation in Simple Shear Flow of Semi-Dilute Suspensions," *J. Fluid Mech., 238,* 277 (1992).

[44] Folgar, F. P. and C. L. Tucker, "Orientation Behavior of Fibers in Concentrated Suspensions," *J. Reinf. Plast. Compos., 3,* 98 (1984).

[45] Frisch, H. L. and R. Simha, "The Viscosity of Colloidal Suspensions and Macromolecular Solutions," *Rheology: Theory and Applications,* F. R. Eirich, ed., *1(14),* Academic Press, New York (1956).

[46] Mutel, A. T., "Rheological Behavior and Fiber Orientation in ZSimple Flows of Glass Fiber Filled Polypropylene Melts," Ph.D. Thesis, Dept. Chem. Eng., McGill U. (1989).

[47] Ericksen, J. L., "Transversely Isotropic Fluids," *Kolloid Z.., 173,* 117- (1960).

[48] Barthés-Biesel, D. and A. Acrivos, "The Rheology of Suspensions and its Relation to Phenomenological Theories for Non-Newtonian Fluids," *Int. J. Multiphase Flow, 1,* 1 (1973).

[49] Batchelor, G. K., "The Stress Generated in a Non-Dilute Suspension of Elongated Particles by Pure Straining Motion,' *J. Fluid Mech., 46,* 813 (1971).

[50] Dinh, S. M. and R. C. Armstrong, "A Rheological Equaiton of State for Semi-Concentrated Fiber Suspensions, " *J. Rheology, 28,* 207-227 (1984).

[51] Hinch, E. J. and L. G. Leal, "The effect of Brownian motion on the rheological properties of a suspension of non-spherical particles," *J. Fluid Mech,, 52(4),* 683 (1972).

[52] Doi, M. and S. F. Edwards, "Dynamics of Rod-like Molecules in Concentrated Solution; Part II," *J. of Chem. Soc. Faraday Trans. II, 74(3),* 918, (1978).

[53] Wedgewood, L. E. and H. C. Öttinger, " A Model of Dilute Polymer Solutions with Hydrodynamic Interaction and Finite Extensibility. II. Shear Flows," *J. Non-Newtonian Fluid Mechanics 27*, 245-264 (1988).

[54] Bay, R. S., C. L. Tucker and R. B. Davis, "Effect of Processing on Fiber Orientation in Simple Injection Moldings," *SPE ANTEC Conference*, 539-542 (1989).

[55] Kallmes, O., H, Corte, and G. Bernier, "The Structure of Paper: II. The Statistical Geomtry of a Multiplanar Fiber Network," *Tappi, 44(7)*, 519 (1961).

[56] Kallmes, O., H, Corte, and G. Bernier, "The Structure of Paper: II. The Statistical Geomtry of a Multiplanar Fiber Network," *Tappi, 44(7)*, 519 (1961).

[57] Reif, F., *Fundementals of Statistical and Thermal Physics*, Chapter 15, McGraw-Hill Book Co. (1965).

[58] van Aken, J. A. and H. Janeschitz-Kriegl, "New Apparatus for the Simultaneous Measurement of Stresses and Flow Birefringence in Biaxial Extension of Polymer Melts," *Rheol. Acta, 19*, 744 (1980).

[59] Macosko, C. W., M. A. Ocansey, and H. H. Winter, "Steady Planar Extension with Lubricated Dies," *J. Non-Newt. Fluid Mech., 11*, 301 (1982).

[60] Papanastasiou, A. C., C. W. Macosko, and L. E. Scriven, "Analysis of Lubricated Squeezing Flow," *Int. J. Num. Meth. Fluids, 6*, 819 (1986).

Appendix A. **Proof of** $\boldsymbol{\zeta}^{-1} = \frac{1}{2\zeta_a}(\boldsymbol{\delta} + \mathbf{pp})$

Prove that

$$\boldsymbol{\zeta}^{-1} = \frac{1}{2\zeta_a}(\boldsymbol{\delta} + \mathbf{pp}) \quad \text{(A.1)}$$

If A.1 is true then

$$\boldsymbol{\zeta} \cdot \boldsymbol{\zeta}^{-1} = \zeta_a(2\boldsymbol{\delta} - \mathbf{pp}) \cdot \frac{1}{2\zeta_a}(\boldsymbol{\delta} + \mathbf{pp}) = \boldsymbol{\delta} \quad \text{(A.2)}$$

Gibbs index notation is often more convenient for proofs.

$$\boldsymbol{\zeta} \cdot \boldsymbol{\zeta}^{-1} = \zeta_a(2\delta_{ij} - p_i p_j) \frac{1}{2\zeta_a}(\delta_{jk} + p_j p_k) = \delta_{ij} \quad \text{(A.3)}$$

$$= \frac{1}{2}(2\delta_{ij} - p_i p_j)(\delta_{jk} + p_j p_k) \quad \text{(A.4)}$$

$$= \frac{1}{2}(2\delta_{ij}\,\delta_{jk} + 2\delta_{ij}\,p_j p_k - p_i p_j\,\delta_{jk} - p_i p_j\,p_j p_k) \quad \text{(A.5)}$$

Recall that

$$\delta_{ij}\,\delta_{jk} = \delta_{ik}$$

$$\delta_{ij}\,p_j p_k = p_i p_k$$

$$p_j p_j = 1$$

Equation (A.5) simplifies to

$$\boldsymbol{\zeta} \cdot \boldsymbol{\zeta}^{-1} = \frac{1}{2}(2\delta_{ik} + 2p_i p_k - p_i p_k - p_i p_k) \quad \text{(A.6)}$$

$$\boldsymbol{\zeta} \cdot \boldsymbol{\zeta}^{-1} = \frac{1}{2}(2\delta_{ik}) = \boldsymbol{\delta} \quad \text{(A.7)}$$

Q.E.D.

Appendix B. Derivation of Diffusion Tensor $\mathbf{D(p)} = \varepsilon \mathrm{Var}(\dot{\mathbf{p}})$

The diffusion tensor was defined in Chapter Three as the expected value of the square of the angle change $\Delta\mathbf{p}$ achieved in a small time τ.

$$\mathbf{D(p)} = \lim_{\tau \to 0} \frac{E(\Delta \mathbf{p}^2)}{\tau} \tag{B.1}$$

More precisely, this is an integral over all possible values of the dyadic product $\Delta\mathbf{p}\Delta\mathbf{p}$.

$$\mathbf{D(p)} = \lim_{\tau \to 0} \oint_{\Delta p} \Delta\mathbf{p}\Delta\mathbf{p}\, P(\mathbf{p}+\Delta\mathbf{p},\tau \mid \mathbf{p})\, d\Delta\mathbf{p} \tag{B.2}$$

The weighting function in the integrand $P(\mathbf{p}+\Delta\mathbf{p},\tau \mid \mathbf{p})$ is a transition probability density. It is the normalized probability that a fiber initially at $\mathbf{p}$ will move to $\mathbf{p}+\Delta\mathbf{p}$ in time τ. The work detailed in this appendix is concerned primarily with finding this function. For the reasons of simplicity, $P(\mathbf{p}+\Delta\mathbf{p},\tau \mid \mathbf{p})$ shall be referred to as $P(\Delta\mathbf{p})$ henceforth.

The angle change $\Delta\mathbf{p}$ is comprised of a large number (N) of smaller angle changes $\delta\mathbf{p}$.

$$\Delta\mathbf{p} = \sum_{i=1}^{N} \delta\mathbf{p}_i \tag{B.3}$$

Then $P(\Delta\mathbf{p})$ is a comprised of the probabilities $w(\delta\mathbf{p}_i)$ of the the small angle changes $\delta\mathbf{p}_i$.

$$P(\Delta p)\, d\Delta p = \int_{\delta p_1} \int_{\delta p_2} \cdots \int_{\delta p_N} w(\delta p_1) d\delta p_1 w(\delta p_2) d\delta p_2 \ldots w(\delta p_N) d\delta p_N \quad \text{(B.4)}$$

The integration limits on each of the small angle changes must be restricted to include only the combinations of the angle changes δp_i, $i = 1...N$ such that

$$\Delta p < \sum_{i=1}^{N} \delta p_i < \Delta p + d\Delta p \quad \text{(B.5)}$$

This restriction is difficult to apply within the limits of the integral. The Dirac delta function can be used to selectively eliminate combinations of δp_i that do not sum to Δp. The analytical form of the Dirac delta function must be used in the expression to transfer this responsibility to the integrand.

$$\delta\left(\Delta p - \sum_{i=1}^{N} \delta p_i\right) = \frac{1}{2\pi} \int_{-\infty}^{+\infty} e^{-ik\left(\Delta p - \sum \delta p_i\right)} dk \quad \text{(B.6)}$$

Inserting this expression into Eq. (B.4), each integral may now be performed over *all* possible values of δp_i. The delta function selects only the values that combine to yield an angle change of Δp.

$$P(\Delta p)\, d\Delta p = \oint_{\delta p_1} \oint_{\delta p_2} \cdots \oint_{\delta p_N} w(\delta p_1) w(\delta p_2) \ldots w(\delta p_N)$$
$$\frac{1}{2\pi} \int_{-\infty}^{+\infty} e^{-ik\left(\Delta p - \delta p_1 - \delta p_2 - \ldots \delta p_N\right)} dk\, d\delta p_1\, d\delta p_2 \ldots d\delta p_N$$

(B.7)

The integrals can be rearranged to a more meaningful form.

$$P(\Delta p)\,d\Delta p = \frac{1}{2\pi}\int_{-\infty}^{+\infty}\Big[\oint_{\delta p_1} w(\delta p_1)\; e^{ikdp_1}\,d\delta p_1 \oint_{\delta p_2} w(\delta p_2)\, e^{ikdp_2}\,d\delta p_2 \ldots$$

$$\oint_{\delta p_N} w(\delta p_N)\; e^{ikdp_N}\,d\delta p_N\Big] e^{-ikDp}\,dk \qquad (B.8)$$

This can be regrouped again with the understanding that the small angle changes are due to interaction geometries that are statistically independent. Therefore, each small change δp is statistically independent and statistically equivalent.

$$P(\Delta p)\,d\Delta p = \frac{1}{2\pi}\int_{-\infty}^{+\infty} e^{-ik\Delta p}\Big[\oint_{\delta p} w(\delta p)\; e^{ikdp}\,d\delta p\Big]^N dk \qquad (B.9)$$

The term in square brackets can be substituted with a Taylor's series expansion for small δp.

$$\oint_{\delta p} w(\delta p)\; e^{ikdp}\,d\delta p = \oint_{\delta p} w(\delta p)\Big(1 + ik\delta p - \frac{1}{2}k^2\delta p^2 + \ldots\Big)d\delta p \qquad (B.10)$$

Evaluation of each of the terms in the integral in the right can now be easily accomplished.

$$\oint_{\delta p} w(\delta p)\; e^{ikdp}\,d\delta p = 1 + ik\overline{\delta p} - \frac{1}{2}k^2\,\overline{\delta p^2} + \ldots \qquad (B.11)$$

where

$$\overline{\delta p^n} = \oint_{\delta p} w(\delta p)\, \delta p^n\, d\delta p \tag{B.12}$$

This is the usual definition of the n^{th} moment of the random variable δp.

Equation (B.10) now has the form

$$P(\Delta p)\, d\Delta p = \frac{1}{2\pi}\int_{-\infty}^{+\infty} e^{-ik\Delta p}\, [1 + ik\overline{\delta p} - \frac{1}{2}k^2\,\overline{\delta p^2} + \ldots]^N\, dk \tag{B.13}$$

The term in the square brackets can be simplified by taking the natural logarithm and expanding that for small $ik\overline{\delta p}$

$$\ln [1 + ik\overline{\delta p} - \frac{1}{2}k^2\,\overline{\delta p^2} + \ldots]^N = N \ln [1 + ik\overline{\delta p} - \frac{1}{2}k^2\,\overline{\delta p^2} + \ldots] \tag{B.14}$$

$$= N [ik\overline{\delta p} - \frac{1}{2}k^2\,\overline{\delta p^2} - \left(ik\overline{\delta p}\right)^2 - \ldots] \tag{B.15}$$

$$= N [ik\overline{\delta p} - \frac{1}{2}k^2\,\overline{(\Delta\delta p)^2} - \ldots] \tag{B.16}$$

where the usual definition of the variance is used

$$\mathrm{Var}(\delta p) = \overline{\delta p^2} - (\overline{\delta p})^2 \tag{B.17}$$

Once the exponential of (B.16) is taken it may be returned to its place in Eq. (B.13), giving

$$P(\Delta p)\, d\Delta p = \frac{1}{2\pi}\int_{-\infty}^{+\infty} e^{-ik\Delta p}\left[e^{ikN\overline{\delta p} - \frac{1}{2}k^2 N\,\overline{(\Delta\delta p)2}}\right] dk \qquad \text{(B.18)}$$

Regrouping once more yields

$$P(\Delta p)\, d\Delta p = \frac{1}{2\pi}\int_{-\infty}^{+\infty} e^{ik(N\overline{\delta p} - Dp) - \frac{1}{2}k^2 N\,\overline{(\Delta\delta p)^2}} dk \qquad \text{(B.19)}$$

The solution to this integral is the familiar Gaussian form.

$$P(\Delta p)\, d\Delta p = \frac{1}{\sqrt{2\pi\, N\overline{(\Delta\delta p)^2}}}\, e^{(N\overline{\delta p} - \Delta p)^2 / 2N\,\overline{(\Delta\delta p)^2}} \qquad \text{(B.20)}$$

The diffusion tensor may now be calculated through substitution of this transition probability density into Eq. (B.2).

$$D(p) = \lim_{\tau\to 0}\frac{1}{\tau}\oint_p \Delta p \Delta p\, P(\Delta p)\, d\Delta p \qquad \text{(B.21)}$$

Equation (B.21) can be expressed in terms of the mean and the variance

$$D(p) = \lim_{\tau\to 0}\frac{1}{\tau}\oint_p \Delta p \Delta p\, P(\Delta p)\, d\Delta p \qquad \text{(B.21)}$$

$$= \lim_{\tau \to 0} \frac{1}{\tau} \left[N \overline{(\Delta \delta \mathbf{p})^2} + N^2 (\overline{\delta \mathbf{p}})^2 \right] \tag{B.22}$$

The diffusion tensor has been expressed in terms of the minute angle changes caused by the application of random interation forces over a finite but small period of time, and the average of those angle changes. The summed angle change $\Delta \mathbf{p}$ is a composite of numerous independent interaction geometries during the time period τ.

In order to put (B.21) into useful terms we must specify the time scale over which the interaction geometries change. The *correlation time* is the expected period over which interaction geometries are uncorrelated and shall be given the symbol ε. The correlation time was discussed in Chaper 2, Section 8. The distance that the orientation changes due to one interaction geometry is equal to the correlation time multiplied by the rotation rate imparted by the interaction forces.

$$\delta \mathbf{p} = \varepsilon \dot{\mathbf{p}} \tag{B.23}$$

Furthermore, N is the number of different interaction geometries in the period τ. Therefore,

$$\tau = N\varepsilon \tag{B.24}$$

Substitution of (B.23) into (B.22) gives

$$\mathbf{D}(\mathbf{p}) = \lim_{\tau \to 0} \frac{1}{\tau} \left[N\varepsilon^2 \overline{(\Delta \dot{\mathbf{p}})^2} + N^2 \varepsilon^2 (\overline{\dot{\mathbf{p}}})^2 \right] \tag{B.25}$$

Substitution of (B.24) into (B.25) simplifies to

$$\mathbf{D(p)} = \lim_{\tau \to 0} [\varepsilon \overline{(\Delta \dot{\mathbf{p}})^2} + N\varepsilon (\bar{\dot{\mathbf{p}}})^2] \tag{B.26}$$

Since Eq. (B.26) is taken as τ goes to zero $N\varepsilon$ must go to zero also and finally the result is

$$\mathbf{D(p)} = \varepsilon \overline{(\Delta \dot{\mathbf{p}})^2} \tag{B.27}$$

$$= \varepsilon \overline{(\dot{\mathbf{p}} - \bar{\dot{\mathbf{p}}})^2} = \varepsilon \mathrm{Var}(\dot{\mathbf{p}}) \tag{B.28}$$

Appendix C. Governing Equations for the Planar Suspension

When the orientation of the fibers in suspension are limited to only a single plane, for example the plane a compression mold, significant simplifications are possible in the governing equations. Planar orientation means that the Eulerian angle $\theta = \pi/2$, a constant, and that the single orientation variable remaining is ϕ. Figure 2.1 shows the physical relationship of the orientation descriptors θ and ϕ as well as the orientation vector for a single fiber **p**.

The first result to present is the rotation rate of a single fiber in a straining fluid. This is Jeffrey's equation in terms of ϕ for planar strains and planar orientation, and for fibers of infinite aspect ratio. The hydrodynamic component of the rotation is

$$\dot{\phi}_h = \sin\phi\cos\phi\left[\frac{\partial v_y}{\partial y} - \frac{\partial v_x}{\partial x}\right] + \cos^2\phi\frac{\partial v_y}{\partial x} - \sin^2\phi\frac{\partial v_x}{\partial y} \tag{C.1}$$

The total rotation of the fiber includes aggregate effect of the interactions on the test fiber oriented at ϕ.

$$\dot{\phi} = \sin\phi\cos\phi\left[\frac{\partial v_y}{\partial y} - \frac{\partial v_x}{\partial x}\right] + \cos^2\phi\frac{\partial v_y}{\partial x} - \sin^2\phi\frac{\partial v_x}{\partial y}$$
$$+ \sum_{i=1}^{N}\frac{6f_{fss_i}}{\zeta_a L^2}\left[\cos^2\phi_i'\frac{\partial v_x}{\partial x} + \sin^2\phi_i'\frac{\partial v_y}{\partial y} + \cos\phi_i'\sin\phi_i'\left(\frac{\partial v_x}{\partial y} + \frac{\partial v_y}{\partial x}\right)\right]\sin|\phi - \phi_i'| \tag{C.2}$$

The number of contacts N, their orientation ϕ', and their placement s, ands' are all random variables in the suspension and the theory. Eq. (C.2) and others used in the

theory that depend on the aggregate effects of the random variables are all evaluated as an integral over the probability space rather than a discrete sum.

The diffusion in the planar theory is a scalar function of ϕ. According to the analysis of Appendix B the diffusion will be

$$D(\phi) = \varepsilon \, \mathrm{Var}(\dot{\phi}) \tag{C.3}$$

This expression is evaluated as an integral over the probability space of the interactions, the lengths of the interacting and test fiber and over all possible orientations of the interacting fibers.

$$D_{\phi}(\phi) = \varepsilon \, 2\int_0^{\pi} \int_{-L/2}^{+L/2} \int_{-L/2}^{+L/2} 2nd\psi(\phi) \sin|\phi - \phi'| \, [\dot{\phi} - \dot{\phi}_h]^2 ds \, ds' \, d\phi' \tag{C.5}$$

Substituting (C.2) and (C.1) in Eq. (C.5) gives the following.

$$D_{\phi}(\phi) = \varepsilon \, 2\int_0^{\pi} \int_{-L/2}^{+L/2} \int_{-L/2}^{+L/2} 2nd\psi(\phi) \sin|\phi - \phi'| \left[\frac{12 f_l s s'}{L^2 \zeta_a} \sin(\phi - \phi')\right]^2$$
$$\left[\cos^2\phi' \frac{\partial v_x}{\partial x} + \sin^2\phi' \frac{\partial v_y}{\partial y} + \cos\phi' \sin\phi' \left(\frac{\partial v_x}{\partial y} + \frac{\partial v_y}{\partial x}\right)\right]^2 ds \, ds' \, d\phi' \tag{C.6}$$

Equation (C.6) can be integrated over the fiber lengths and the rearranged.

$$D_{\phi}(\phi) = 4\varepsilon ndL^2 f_l^{\,2} \zeta_a^{-2} \int_0^{\pi} \psi(\phi) \sin|\phi - \phi'| \, [\sin(\phi - \phi')]^2$$
$$\left[\cos^2\phi' \frac{\partial v_x}{\partial x} + \sin^2\phi' \frac{\partial v_y}{\partial y} + \cos\phi' \sin\phi' \left(\frac{\partial v_x}{\partial y} + \frac{\partial v_y}{\partial x}\right)\right]^2 d\phi' \tag{C.5}$$

This expression is evaluated numerically as described in Chapter Four and used in the Fokker-Planck equation, a generalized advection-diffusion equation that governs the behavior of the orientation distribution function of interacting fibers in a concentrated suspension.

$$\frac{D\psi}{Dt} = -\frac{\partial}{\partial\phi}[A_{\phi}(\phi)\psi(\phi)] + \frac{1}{2}\frac{\partial^2}{\partial\phi^2}[D_{\phi}(\phi)\psi(\phi)] \qquad (C.6)$$

VITA

Chad Sandstrom was born on August 10, 1966 in St. Paul Minnesota. He moved to Rockford, Illinois and completed his secondary education. From there he moved on to the University of Illinois where with the help of the Gannett Foundation and the General Motors Scholarship Fund he completed his Bachelor of Science degree. At this time he had the good fortune to meet his future thesis advisor, Dr. Charles Tucker and the divine grace to meet his future wife, Julia Grace Johnston. Over the course of his graduate studies he was supported by research assistantships and was granted a Teaching Fellowship by the Department of Mechanical and Industrial Engineering of the University of Illinois for the Academic year of 1990-1991. Also during the course of his graduate studies, he guided a fine group of young men and women through three hugely successful seasons of soccer action, while he himself played defense with the Illinois Hockey Club. Chad has accepted a job with the 3M Corporation in the Optical Recording Laboratory and has returned to the Land of 10,000 Lakes.